

ref
FAA 10-06

DOT/FAA/AAR-00/16
DOT-VNTSC-FAA-00-06

Office of Aviation Research
Washington, DC 20591

Motion of Aircraft Wake Vortices in Ground Effect

David C. Burnham
James N. Hallock

Research and Special Programs Administration
John A. Volpe National Transportation Systems Center
Cambridge, MA 02142-1093

Final Report
April 2000

This document is available to the public
through the National Technical Information
Service, Springfield, Virginia 22161



U.S. Department of Transportation
Federal Aviation Administration

REPORT DOCUMENTATION PAGE

Form Approved
OMB No. 0704-0188

Public reporting burden for this collection of information is estimated to average 1 hour per response, including the time for reviewing instructions, searching existing data sources, gathering and maintaining the data needed, and completing and reviewing the collection of information. Send comments regarding this burden estimate or any other aspect of this collection of information, including suggestions for reducing this burden, to Washington Headquarters Services, Directorate for Information Operations and Reports, 1215 Jefferson Davis Highway, Suite 1204, Arlington, VA 22202-4302, and to the Office of Management and Budget, Paperwork Reduction Project (0704-0188), Washington, DC 20503.

1. AGENCY USE ONLY (Leave blank)

2. REPORT DATE

April 2000

3. REPORT TYPE AND DATES COVERED

Final Report
January 1983 - December 1986

Motion of Aircraft Wake Vortices in Ground Effect

5. FUNDING NUMBERS

FA027/A0433

6. AUTHOR(S)

David C. Burnham* and James N. Hallock

7. PERFORMING ORGANIZATION NAME(S) AND ADDRESS(ES)

U.S. Department of Transportation
Research and Special Programs Administration
John A. Volpe National Transportation Systems Center
55 Broadway
Cambridge, MA 02142-1093

8. PERFORMING ORGANIZATION
REPORT NUMBER

DOT-VNTSC-FAA-00-06

9. SPONSORING/MONITORING AGENCY NAME(S) AND ADDRESS(ES)

U.S. Department of Transportation
Federal Aviation Administration
Office of Aviation Research
800 Independence Ave., SW
Washington, DC 20591

10. SPONSORING/MONITORING
AGENCY REPORT NUMBER

DOT/FAA/AAR-00/16

11. SUPPLEMENTARY NOTES

*Scientific and Engineering Solutions, Inc.
Orleans, MA

12a. DISTRIBUTION/AVAILABILITY STATEMENT

This document is available to the public through the National Technical Information Service.

12b. DISTRIBUTION CODE

13. ABSTRACT (Maximum 200 words)

This report addresses the wake-turbulence separation standards for close-spaced parallel runways. Ground-wind anemometer data collected at Kennedy (landing) and O'Hare (takeoff) airports are analyzed to assess the lateral transport probability for wake vortices. A model is developed to predict the lateral transport probability and is used to analyze possible reductions in the wake-turbulence limits on parallel runways for reduced ranges of aircraft classes (e.g., only Small and Large aircraft). Unfortunately, adoption of the calculated reduced separation standards cannot be recommended because of uncertainties in the analysis.

14. SUBJECT TERMS

parallel runways, wake turbulence, wake vortices

15. NUMBER OF PAGES

102

16. PRICE CODE

17. SECURITY CLASSIFICATION
OF REPORT

Unclassified

18. SECURITY CLASSIFICATION
OF THIS PAGE

Unclassified

19. SECURITY CLASSIFICATION
OF ABSTRACT

Unclassified

20. LIMITATION OF ABSTRACT

PREFACE

In the United States wake turbulence data from landing and takeoff operations were collected at a variety of airports from 1973 through 1980. The Wake Turbulence Program hiatus from 1981 through 1983 was followed by a period of extensive data analysis and report writing which terminated in 1987 before any of the reports were published. The publication of these reports started in 1994 and is now completed with this report, which was actually the first of two dealing with parallel-runway operations. The report is based on the 1986 draft; comments will be added where appropriate to relate the results to the current understanding of wake turbulence and current operational issues.

Previous studies in the United States Wake Vortex Program have concentrated on the aircraft spacings required for safe operations on a single runway. Large amounts of data collected at airports, using three different sensing systems, were analyzed for the following purposes: a) to assess the safety of single-runway separation standards and b) to develop wake vortex avoidance systems (WVAS), where the single-runway separations are adjusted in real time in accordance with the current duration of the wake-vortex hazard.

This report is the first of two that will use existing wake-vortex data to evaluate separation standards, procedures, and WVAS systems for parallel runway configurations. This study presents data on the lateral motion of wake vortices in ground effect for both landing and takeoff and analyzes the separation required for the wake-turbulence-independent operation of two parallel runways.

The wake turbulence program at the Volpe Center was suspended between 1981 and 1983. During this period program personnel were assigned to other work and many of the bulky data printouts were discarded to make room for other projects. Consequently, some information which would have been useful in this analysis was not available, either because it had been forgotten or because it could not be easily regenerated.

This project was started before the hiatus in the wake vortex program. At that time computer programming was carried out by Karen Viglione and Scott Heald. Recent programming was carried out by Tonyo Poweigha of SDC and Michael Feldhusen of Dynatrend. Yolanda McCleave assisted in the data analysis.

Joe Yarmus of the Volpe Center was the first author of the original report draft. Since he is no longer available to take responsibility for the final draft, his contribution is acknowledged here rather than as an author.

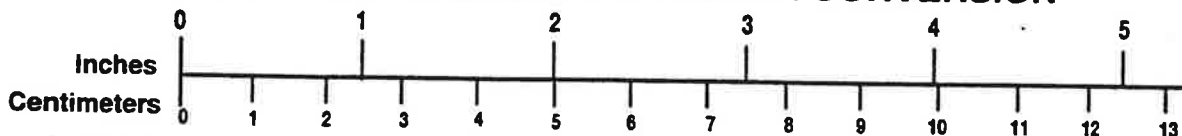
METRIC/ENGLISH CONVERSION FACTORS

ENGLISH TO METRIC

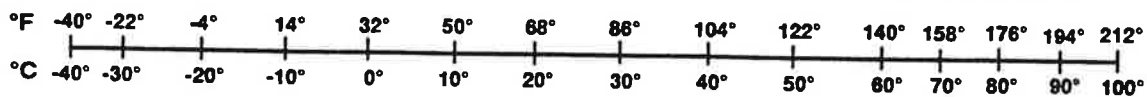
METRIC TO ENGLISH

<p>LENGTH (APPROXIMATE)</p> <p>1 inch (in) = 2.5 centimeters (cm) 1 foot (ft) = 30 centimeters (cm) 1 yard (yd) = 0.9 meter (m) 1 mile (mi) = 1.6 kilometers (km)</p>	<p>LENGTH (APPROXIMATE)</p> <p>1 millimeter (mm) = 0.04 inch (in) 1 centimeter (cm) = 0.4 inch (in) 1 meter (m) = 3.3 feet (ft) 1 meter (m) = 1.1 yards (yd) 1 kilometer (km) = 0.6 mile (mi)</p>
<p>AREA (APPROXIMATE)</p> <p>1 square inch (sq in, in²) = 6.5 square centimeters (cm²) 1 square foot (sq ft, ft²) = 0.09 square meter (m²) 1 square yard (sq yd, yd²) = 0.8 square meter (m²) 1 square mile (sq mi, mi²) = 2.6 square kilometers (km²) 1 acre = 0.4 hectare (he) = 4,000 square meters (m²)</p>	<p>AREA (APPROXIMATE)</p> <p>1 square centimeter (cm²) = 0.16 square inch (sq in, in²) 1 square meter (m²) = 1.2 square yards (sq yd, yd²) 1 square kilometer (km²) = 0.4 square mile (sq mi, mi²) 10,000 square meters (m²) = 1 hectare (ha) = 2.5 acres</p>
<p>MASS - WEIGHT (APPROXIMATE)</p> <p>1 ounce (oz) = 28 grams (gm) 1 pound (lb) = 0.45 kilogram (kg) 1 short ton = 2,000 pounds (lb) = 0.9 tonne (t)</p>	<p>MASS - WEIGHT (APPROXIMATE)</p> <p>1 gram (gm) = 0.036 ounce (oz) 1 kilogram (kg) = 2.2 pounds (lb) 1 tonne (t) = 1,000 kilograms (kg) = 1.1 short tons</p>
<p>VOLUME (APPROXIMATE)</p> <p>1 teaspoon (tsp) = 5 milliliters (ml) 1 tablespoon (tbsp) = 15 milliliters (ml) 1 fluid ounce (fl oz) = 30 milliliters (ml) 1 cup (c) = 0.24 liter (l) 1 pint (pt) = 0.47 liter (l) 1 quart (qt) = 0.96 liter (l) 1 gallon (gal) = 3.8 liters (l) 1 cubic foot (cu ft, ft³) = 0.03 cubic meter (m³) 1 cubic yard (cu yd, yd³) = 0.76 cubic meter (m³)</p>	<p>VOLUME (APPROXIMATE)</p> <p>1 milliliter (ml) = 0.03 fluid ounce (fl oz) 1 liter (l) = 2.1 pints (pt) 1 liter (l) = 1.06 quarts (qt) 1 liter (l) = 0.26 gallon (gal) 1 cubic meter (m³) = 36 cubic feet (cu ft, ft³) 1 cubic meter (m³) = 1.3 cubic yards (cu yd, yd³)</p>
<p>TEMPERATURE (EXACT)</p> <p>$[(x-32)(5/9)] \text{ } ^\circ\text{F} = y \text{ } ^\circ\text{C}$</p>	<p>TEMPERATURE (EXACT)</p> <p>$[(9/5)y + 32] \text{ } ^\circ\text{C} = x \text{ } ^\circ\text{F}$</p>

QUICK INCH - CENTIMETER LENGTH CONVERSION



QUICK FAHRENHEIT - CELSIUS TEMPERATURE CONVERSION



For more exact and or other conversion factors, see NIST Miscellaneous Publication 286, Units of Weights and Measures. Price \$2.50 SD Catalog No. C13 10286

Updated 8/17/98

TABLE OF CONTENTS

<u>Section</u>	<u>Page</u>
1. INTRODUCTION.....	1
1.1 BACKGROUND	1
1.2 PURPOSE OF STUDY	2
1.3 SCOPE OF REPORT	2
2. BACKGROUND.....	3
2.1 SINGLE-RUNWAY OPERATIONS	3
2.2 GROUND-WIND VORTEX SENSING SYSTEM.....	3
2.3 DATA COLLECTION	3
2.4 DATA REDUCTION.....	4
2.5 SCOPE OF STUDY	6
3. SAFETY METHODOLOGY	7
3.1 LANDING.....	8
3.2 TAKEOFF	8
4. DATA ANALYSIS.....	9
4.1 DATABASES	9
4.2 METEOROLOGY	10
4.3 LANDING.....	12
4.3.1 Vortex-Demise Positions	12
4.3.1.1 Vortex 1 vs. Vortex 2.....	16
4.3.1.2 Survival Probability	17
4.3.2 Residence Times	22
4.3.3 Vortex-Demise Times.....	25
4.3.4 Model Parameters	25
4.3.5 GWVSS Detection Threshold	30
4.4 TAKEOFF	33
5. SAFETY ANALYSIS SUMMARY.....	39
5.1 MODEL DESCRIPTION	39
5.1.1 Components.....	39
5.1.2 Safety Analysis.....	39
5.2 PARALLEL-RUNWAY SPACING ANALYSIS.....	40
6. CONCLUSIONS	41

TABLE OF CONTENTS (cont.)

<u>Section</u>	<u>Page</u>
6.1 PARALLEL-RUNWAY SEPARATION STANDARD	41
6.2 VORTEX MODELING	41
6.3 SAFETY METHODOLOGY	41
6.4 GWVSS DETECTION THRESHOLD	41
7. RECOMMENDATIONS	43
APPENDIX A - MODELS FOR VORTEX TRANSPORT AND PERSISTENCE IN GROUND EFFECT	A-1
A.1 GOAL AND PHILOPOPHY	A-1
A.2 MODEL DEFINITIONS	A-1
A.2.1 Ambient Wind Distribution	A-2
A.2.2 Vortex Persistence Probability	A-2
A.2.3 Vortex Lateral Transport Model: Landing	A-3
A.2.4 Single-Runway Residence Probability	A-3
A.2.5 Lateral Transport Probability	A-4
A.2.6 Parallel-Runway Residence Probability	A-5
A.2.7 Model Justification	A-7
A.2.8 Takeoff Modeling	A-8
A.2.8.1 Probability of a Vortex Reaching Ground Effect	A-9
A.2.8.2 Probability of a Vortex Being Detected at a Lateral Position	A-9
A.3 SPECIFIC MODELS	A-10
A.3.1 Wind Distribution	A-10
A.3.2 Vortex Decay	A-10
A.3.3 Calculations	A-11
APPENDIX B - LANDING DATA PLOTS	B-1
B.1 TRANSPORT DISTANCE PLOTS	B-1
B.2 RESIDENCE TIME PLOTS	B-1
B.3 VORTEX-DEMISE TIME PLOTS	B-1
B.4 STATISTICS OF PLOTS	B-2
APPENDIX C - TAKEOFF DATA PLOTS	C-1
REFERENCES	R-1

LIST OF FIGURES

<u>Figure</u>	<u>Page</u>
Figure 1. Kennedy Airport Landing Test Site.....	4
Figure 2. O'Hare Airport Takeoff Test Site Layout.....	5
Figure 3. Kennedy Headwind Distribution	9
Figure 4. Kennedy Crosswind Distribution	10
Figure 5. Kennedy Crosswind Distribution, Headwind < 15 knots	10
Figure 6. O'Hare Headwind Distribution	12
Figure 7. O'Hare Crosswind Distribution	12
Figure 8. Probability of Decay, B-747, Wind Magnitude less than 8 knots, 10-m Averaging Radius.....	13
Figure 9. B-707 Cumulative Vortex Survival Probability	18
Figure 10. B-747 Cumulative Vortex Survival Probability	19
Figure 11. Cumulative Vortex Survival Probability vs. Distance, All Crosswinds:	20
Figure 12. B-747 Cumulative Vortex Survival Probability vs. Distance by Crosswind:	21
Figure 13. Kennedy Crosswind Distribution for Vortices Transported at Least 900 Feet - All Baselines - All Aircraft Types	21
Figure 14. Cumulative Residence Probability vs. Time, All Kennedy Baselines, No Crosswind Selection: Left: B-707, Right: B-747	22
Figure 15. Cumulative Residence Probability vs. Time, Inner (I) and Outer (O) Heathrow Baselines: Left: B-707, Right: B-747	23
Figure 16. Kennedy Crosswind Distribution for Residence Time \geq 80 Seconds.....	24
Figure 17. Kennedy Cumulative Survival Probability vs. Time, All Crosswinds.....	26
Figure 18. Kennedy B-707 Cumulative Survival Probability vs. Time, Crosswind:	27
Figure 19. Kennedy B-747 Cumulative Survival Probability vs. Time, Crosswind:	28
Figure 20. Crosswind Dependence of B-747 Vortex Decay.....	29
Figure 21. Crosswind Dependence of B-707 Vortex Decay.....	29
Figure 22. B-707: Log of Cumulative Vortex Survival Probability vs. Time Squared	31
Figure 23. B-747: Log of Cumulative Vortex Survival Probability vs. Time Squared	32
Figure 24. O'Hare B-707 Cumulative Vortex Survival Probability vs. Distance.....	37
Figure 25. O'Hare B-747 Cumulative Vortex Survival Probability vs. Distance.....	38
Figure 26. Coordinate System	A-2
Figure 27. Plan View of Possible Vortex Locations after an Aircraft Has Landed on the Left Runway.....	A-8
Figure 28. Comparison of Calculated and Observed Cumulative Survival Probability vs. Distance for B-707	A-13
Figure 29. Comparison of Calculated and Observed Cumulative Survival Probability vs. Distance for B-747	A-14
Figure 30. Calculated Probability of a Wake Vortex Being Transported at Least 900 Feet vs. Crosswind, B-707 and B-747: Top: Positive Crosswinds, Bottom: Negative Crosswinds	A-15

Figure 31. Mean Inverse Crosswind vs. Distance for B-707	A-16
Figure 32. Mean Inverse Crosswind vs. Distance for B-747	A-16
Figure 33. Calculated and Observed Cumulative Residence Probability vs. Time for B-747	A-17
Figure 34. Kennedy B-727 Cumulative Vortex Survival Probability vs. Distance	B-3
Figure 35. Kennedy DC-8 Cumulative Vortex Survival Probability vs. Distance	B-4
Figure 36. Kennedy DC-9 Cumulative Vortex Survival Probability vs. Distance	B-5
Figure 37. Kennedy DC-10 Cumulative Vortex Survival Probability vs. Distance	B-6
Figure 38. Kennedy L-1011 Cumulative Vortex Survival Probability vs. Distance	B-7
Figure 39. Kennedy B-727 Cumulative Residence Probability vs. Time	B-8
Figure 40. Kennedy DC-8 Cumulative Residence Probability vs. Time	B-9
Figure 41. Kennedy DC-9 Cumulative Residence Probability vs. Time	B-10
Figure 42. Kennedy DC-10 Cumulative Residence Probability vs. Time	B-11
Figure 43. Kennedy L-1011 Cumulative Residence Probability vs. Time	B-12
Figure 44. Kennedy B-727 Cumulative Survival Probability vs. Time	B-13
Figure 45. Kennedy DC-8 Cumulative Survival Probability vs. Time	B-14
Figure 46. Kennedy DC-9 Cumulative Survival Probability vs. Time	B-15
Figure 47. Kennedy DC-10 Cumulative Survival Probability vs. Time	B-16
Figure 48. Kennedy L-1011 Cumulative Survival Probability vs. Time	B-17
Figure 49. O'Hare B-727 Cumulative Survival Probability vs. Time	C-2
Figure 50. O'Hare B-737 Cumulative Survival Probability vs. Time	C-3
Figure 51. O'Hare DC-9 Cumulative Survival Probability vs. Time	C-4
Figure 52. O'Hare DC-10 Cumulative Survival Probability vs. Time	C-5
Figure 53. O'Hare L-1011 Cumulative Survival Probability vs. Time	C-6

LIST OF TABLES

<u>Table</u>	<u>Page</u>
Table 1. Wake Vortex Class Limits Before 1996	3
Table 2. Approach Separation Standards (NM) before 1994	3
Table 3. GWSS Installations	4
Table 4. Landing Separation Times	8
Table 5. Database Statistics	9
Table 6. Kennedy Baseline #1 Vortex-Demise Positions for Port and Starboard Vortices by Aircraft Type	14
Table 7. Kennedy Baseline #2 Vortex-Demise Positions for Port and Starboard Vortices by Aircraft Type	15
Table 8. Kennedy Baseline #3 Vortex-Demise Positions for Port and Starboard Vortices by Aircraft Type	16
Table 9. Comparison of Upwind and Downwind Vortex Pair Transport (All Baselines, Verified Records Only) ..	17
Table 10. Transport Probability Estimated Lines	17
Table 11. Comparison of Safe Residence Time Probabilities for Various Wake Classes Using JFK and LHR Data	24
Table 12. Crosswind Dependence of Vortex Decay	25
Table 13. Vortex Decay Parameters	29
Table 14. Comparison of MAVSS and GWSS Decay Data	30
Table 15. O'Hare Baseline #1 Vortex-Demise Positions for Port and Starboard Vortices by Aircraft Type	34
Table 16. O'Hare Baseline #2 Vortex-Demise Positions for Port and Starboard Vortices by Aircraft Type	35
Table 17. O'Hare Baseline #3 Vortex-Demise Positions for Port and Starboard Vortices by Aircraft Type	36
Table 18. Parallel-Runway Safe Separation Analysis	40
Table 19. Estimated Separations for Wake-Turbulence-Independent Operation of Parallel Runways	41
Table 20. Coordinate System	A-2
Table 21. Lateral Motion of Wake Vortices in Ground Effect	A-3
Table 22. Crosswind Limits on Vortex Residence: Single Runway	A-4
Table 23. Crosswind Limits on Vortex Residence: Parallel Runway	A-6
Table 24. Motion of Wake Vortices Out of Ground Effect	A-8
Table 25. Decay Model Parameters	A-11
Table 26. Calculations for the Lateral Transport Probability for a B-707 with Positive Crosswinds	A-12

Page intentionally blank

EXECUTIVE SUMMARY

OVERVIEW

The goal of this study was to determine how far wake vortices can move in ground effect. This information has an immediate application to defining the minimum safe separation between parallel runways where operations are not affected by wake turbulence. Under IFR conditions, possible wake-turbulence encounters are the limiting factor in setting the required separation standard, which is currently set at 2500 feet (reduced from 3000 feet during 1984). Runways separated by less than this standard are treated as a single runway for IFR operations.

The analysis of this report will examine whether further reductions in the safe parallel runway separation are feasible. It will also consider what runway separations may be safe when the aircraft using the runways are restricted to various combinations of the Heavy, Large, and Small wake-vortex classes. The general safe separation requirement of 2500 feet is based on the most critical combination, namely Heavy aircraft on one runway with Small aircraft on the other.

The data used for the study were collected at two airports (Kennedy for landing and O'Hare for takeoff) using the ground-wind vortex sensing system (GWVSS). Both data collection sites were instrumented with three lines of ground-wind anemometers perpendicular to the aircraft flight path. Of particular interest to this study is that the lines extended out to at least 2000 feet perpendicular to the extended runway centerline (on one side). Thus, the maximum lateral motion could be determined for each vortex moving in that direction. Note that the GWVSS has a detection threshold that, for low winds, is generally below the hazard threshold. Because this study makes use of detection data to estimate the hazard probability, the relationship of the GWVSS detection threshold to the wake-turbulence hazard is critical. This study made the first quantitative estimate of the ratio of the hazard threshold to the detection threshold.

The simplest method of assigning a "safe" parallel runway separation is to determine the maximum lateral distance a vortex is observed to travel using a sensor with a detection threshold less than the hazard threshold. A safety factor can then be added to account for limited amounts of data, limited variations in meteorological conditions, and, in the case of the GWVSS system, the expected increase in detection threshold with increased crosswind. The maximum lateral motion distances detected with the GWVSS system were 1500 and 1800 feet for landing and takeoff, respectively. Unfortunately, using reasonable safety factors would increase these values to the point where no significant reduction below the current 2500-foot standard would be possible. A more precise understanding of the issues of wake-turbulence transport would be required to reduce the current standard. It should be noted that GWVSS data collected at the Frankfurt Airport in Germany found that wake vortices generated on landing travel at least 1700 feet under certain conditions of wind and atmospheric stability.

A second method developed for analyzing parallel runway separations offers the possibility of a more precise definition of the "safe" separation. This method is based on the observed safety of the 1975-1994 arrival separation standards for a single runway. No accidents occurred over almost two decades, except where the separations were not maintained, typically in visual approaches. A vortex transport and decay model was developed to compare the encounter probabilities for the single and parallel runway situations. This approach appears to be reasonable for landing aircraft, but is more difficult to justify for departing aircraft because of the greater amount of airspace involved (much of it out of

ground effect). In addition, there are insufficient wake-turbulence data over the runway surface where a takeoff encounter would most likely occur. The formulation of the model cannot be used for definitive results because it makes the erroneous assumption that the GWVSS detection threshold is independent of the crosswind. Furthermore, the old model does not account for the increase in the GWVSS threshold caused by the increase in vortex height which is often observed for the downwind vortex and sometimes observed for the upwind vortex. An improved GWVSS detection model, and perhaps an improved vortex decay model, would be needed to make the model accurate enough to justify reducing the separation standard below 2500 feet. Even in its present state the transport and decay model gave useful indications of how much the parallel runway separation standard might be reduced if the aircraft using the runways were restricted to particular wake-turbulence classes.

CONCLUSIONS

The following conclusions were drawn from the study:

1. The study encountered too many uncertainties in critical issues to allow a definite recommendation for changes in the parallel runway separation standard.
2. The modeling of vortex transport and decay gave useful information, but the calculated vortex transport and residence probabilities did not agree very well with the measured values.
3. The safety methodology developed for this study is a promising start toward a precise determination of the parallel runway separation standard. The table to the right shows the results of the analysis. NOTE: These separations are listed as an indication of what a complete study might produce and are NOT recommended for adoption.
4. In this study, the GWVSS detection threshold was estimated for the first time.

Estimated Separations for Wake-Turbulence-Independent Operation of Parallel Runways

Classes	Safe Separation (ft)
Heavy/Small	1900
Heavy/Large	1300
Heavy/Heavy	700
Large/Small	1100
Large/Large	600

RECOMMENDATIONS

The results of this study were not as useful as originally hoped because of the limited understanding of many critical issues. The following recommendations are addressed toward an increased knowledge of these issues.

1. Software should be recreated to access the original GWVSS data tapes. The GWVSS anemometers could perhaps give a better estimate of ambient crosswind. In addition, current processing algorithms can give an estimate of vortex height and circulation.
2. The available monostatic acoustic (MAVSS) data (which include vortex strength) should be examined with respect to the maximum transport distances. [The GWVSS and MAVSS transport probabilities were compared in Reference 1.]
3. The relationship between GWVSS signatures and the monostatic acoustic strength measurements should be studied using data collected concurrently on the same vortices.

4. The German data collection effort at Frankfurt should be monitored closely, because it is based on state-of-the-art sensors which are superior, in some respects, to those used in the earlier United States work. [Frankfurt data are currently being analyzed.]
5. Additional transport modeling efforts would be useful. Basing a model on MAVSS data rather than GWVSS data should improve its validity.

Page intentionally blank

1. INTRODUCTION

1.1 BACKGROUND

This report presents the first in a series of three studies^{1,2} based on wake vortex data collected at various airports from 1975 through 1980. The measurements from some of these data collection efforts are now incorporated into a set of databases which can be used to answer questions about wake vortex behavior. The ultimate goal of these studies was to improve airport capacity by adopting operational procedures that more accurately reflect wake vortex behavior.

Two wake-vortex sensors, the Ground-Wind Vortex Sensing System (GWVSS) and the Monostatic Acoustic Vortex Sensing System (MAVSS), were used to collect most of the available wake-vortex data. The GWVSS was used more extensively and has the capability of tracking stalled wake vortices, such as might pose a hazard to a following aircraft on the same runway. On the other hand, although the MAVSS cannot detect stalled vortices, it has the advantage of measuring vortex strength. Since it can readily detect moving vortices, it is useful for studying wake vortices that move from one runway to a parallel runway.

The analysis of wake vortices stalled near the runway centerline was the primary goal of wake-vortex studies^{3,4,5} before 1984. However, in 1984 the Volpe Center completed two draft studies of vortex lateral transport which pertain to the wake-turbulence hazard for closely-spaced parallel runways. Current separation standards require that parallel runways separated by less than 2500 feet must be considered a single runway for wake-vortex purposes.

The first 1984 study, presented in this report, used GWVSS data alone to analyze the probability of wake vortices reaching a parallel runway. A transport model was developed to relate the wake-vortex hazard probability for a parallel runway to that for a single runway. This relationship was then used to extend the single-runway separation standards, which are established as safe from 15 years experience, to parallel runways. The results of this study indicated that the parallel-runway separation standard might be substantially less than 2500 feet for some classes of aircraft. The major deficiency of this study was an invalid assumption about the GWVSS, namely that the wake-vortex detection threshold does not depend upon the crosswind.

The second 1984 study¹ analyzed the MAVSS collected concurrently with the GWVSS data during the O'Hare departure data collection effort. A comparison of MAVSS and GWVSS data showed that the GWVSS fails to detect many vortices which are indicated as hazardous by the MAVSS. The loss of GWVSS sensitivity for laterally moving vortices may be related to two effects, the masking of the vortex signals by the crosswind and/or the reduction in signal strength as the vortex height above the ground increases. In either case, the GWVSS data underestimate the wake-vortex lateral transport probability and hence are questionable for assessing wake-vortex safety with respect to vortex decay for parallel runways. Consequently, the MAVSS data should be used for parallel runway vortex decay studies.

Note that, under visual flight rules (VFR), aircraft typically use paired approaches to close-spaced parallel runways. Currently, efforts are underway to enable such approaches under some conditions requiring instrument flight rules (IFR). Since the wake-vortex safety of paired approaches depends

upon vortex transport over relatively short times (e.g., less than 50 seconds), the GWVSS may be adequate for assessing wake-vortex safety at low altitudes, since vortex decay is unimportant.

The third study² extended the analysis of the two earlier studies to examine how the crosswind affects lateral vortex transport. This analysis elucidated the differences between the GWVSS and MAVSS data and may assist in developing an improved lateral transport model that can validate parallel runway separation standards. In addition, the analysis provides additional information about algorithms for a parallel runway dynamic spacing system, such as has been under development⁶ in Germany since the mid 1980s. For example, simultaneous, dependent operations on close-spaced parallel runways may be permitted when the larger aircraft are assigned to the downwind runway. Basic questions for such a system are: (a) how much crosswind is needed to assure safety and (b) how well can the required crosswinds be predicted.

1.2 PURPOSE OF STUDY

This study was undertaken to analyze the movement of wake vortices in ground effect and to define the minimum safe separation distance between parallel runways for wake-turbulence-independent operations. This report will attempt to determine the feasibility of further reductions in the safe parallel runway separation standard, which during 1984 was reduced from 3000 to 2500 feet.

The data used for the study were collected at two airports (Kennedy⁷ for landing and O'Hare¹ for takeoff) using the ground-wind vortex sensing system⁸ (GWVSS). Both data collection sites were instrumented with three lines of ground-wind anemometers perpendicular to the aircraft flight path. Of particular interest to this study is that the lines extended out to at least 2000 feet on one side. Thus, the maximum lateral motion could be determined for each vortex moving in that direction. Note that the GWVSS has a detection threshold that, for low winds, is generally below the hazard threshold. Because this study makes use of detection data to estimate hazard probability, the relationship of the GWVSS detection threshold to the wake-turbulence hazard threshold is critical. This study made the first quantitative estimate of the ratio of the hazard threshold to the detection threshold.

The report is presented in the following sections: Section 2, Background; Section 3, Safety Methodology; Sections 4 and 5, Data and Separation Analyses; and Sections 6 and 7, Conclusions and Recommendations. Vortex Models and Landing and Takeoff Data are presented in Appendices A, B, and C, respectively.

1.3 SCOPE OF REPORT

This report is based on a 1986 draft and hence represents the wake-turbulence thinking of that era. No reanalysis of the data will be presented. However, some comments relating the study to current issues have been added.

2. BACKGROUND

2.1 SINGLE-RUNWAY OPERATIONS

Currently, aircraft are divided into three wake-vortex classes, Heavy, Large, and Small which are used to define separation standards⁹ for the prevention of hazardous wake-turbulence encounters. The assignment of aircraft to the classes is based on the maximum certificated gross takeoff weight (MCGTOW) limits shown in Table 1.

Table 1. Wake Vortex Class Limits Before 1996

Class	MCGTOW Limits (lbs)
Small	<12,500
Large	12,500 - 300,000
Heavy	>300,000

The single-runway approach separation standards (units of nautical miles, NM) for air traffic control are listed in Table 2. The pre-1994 form of these standards was reached in November 1975 when an additional nautical mile was added for the Small following aircraft. Since that time no accidents attributed to wake vortices have occurred except when these standards were not followed [typically for visual approaches and low (below glideslope) following aircraft]. Thus, these standards form a practical definition of safety from the wake-vortex point of view and can be used to define an equivalent level of safety for parallel runway operations.

Table 2. Approach Separation Standards (NM) before 1994

Aircraft Class	Follower		
	Heavy	Large	Small
Heavy	4	5	6
Large	3	3	4
Small	3	3	3

2.2 GROUND-WIND VORTEX SENSING SYSTEM

The ground-wind vortex sensing system (GWVSS) is described in detail in several^{4,8,10} earlier reports. It consists of a line of single-axis propeller anemometers laid out perpendicular to the aircraft flight path. The anemometers are oriented to measure the crosswind component of the wind (i.e., the component of the wind perpendicular to the runway direction) near the ground (usually 10 feet above the ground). After the aircraft wake vortices have descended into ground effect, each vortex induces a strong perpendicular wind near the ground. When the two vortices have separated, the strongest wind at the ground is located directly below the vortex. The vortices are tracked by noting the anemometer showing the greatest deviation from the ambient crosswind. Because the two vortices are rotating in opposite directions, the direction of the induced wind can be used to identify which vortex (port or starboard) is located above an anemometer.

The GWVSS is useful for detecting and tracking the lateral motion of wake vortices generated near the ground. For low winds, the vortex detection threshold appears to be below the vortex hazard threshold (discussed in Section 4.3.5), so that the disappearance of the GWVSS signal is a conservative indicator of the termination of the wake vortex hazard. In 1986, the GWVSS could not be used to sense vortex strength, although some promising strength algorithms had been examined. [Recent least-square-fit algorithms¹¹ can estimate circulation.]

2.3 DATA COLLECTION

Because of its low installation and maintenance costs, the GWVSS was the wake-turbulence sensing system most widely deployed¹² during the period (1973-1980) when the statistical databases on wake vortex behavior in ground effect were collected. Table 3 shows the airports instrumented, the type of

installation, and the number of aircraft operations measured. The data selected for this study were from the two installations where the GWVSS baselines extended for at least 2000 feet on one side of the runway, namely the Kennedy landing data and the O'Hare takeoff data. The sensor layout for these installations is shown in Figures 1 and 2.

2.4 DATA REDUCTION

The data reduction procedures used for GWVSS data were described in a number^{3,5,13} of reports. Briefly, the data are processed in two-second blocks. The vortex positions are identified as the anemometer locations showing the most negative and most positive signals in the two-second blocks, with a consistency parameter indicating what fraction of the data samples showed the same location. The assigned vortex

Table 3. GWVSS Installations

Airport	Dates	Number of Operations	Distance from Runway Threshold (m)
Kennedy Landing	3/76 - 1/77	4,503	#1 1160
			#2 731
			#3 335
Denver Landing	8/73 - 11/73	6,896	#1 474
			#2 135
Heathrow Landing	4/74 - 3/75	12,422	#1 450
			#2 732
Toronto Takeoff	8/76 - 10/77	5,633	#1 1770
			#2 2070
			#3 2530
O'Hare Landing	7/76 - 9/77	21,193	#1 472
			#2 472
			#3 381
O'Hare Takeoff	2/80 - 10/80	16,140	#A 1520
			#1 1800
			#2 2100
			#3 2620

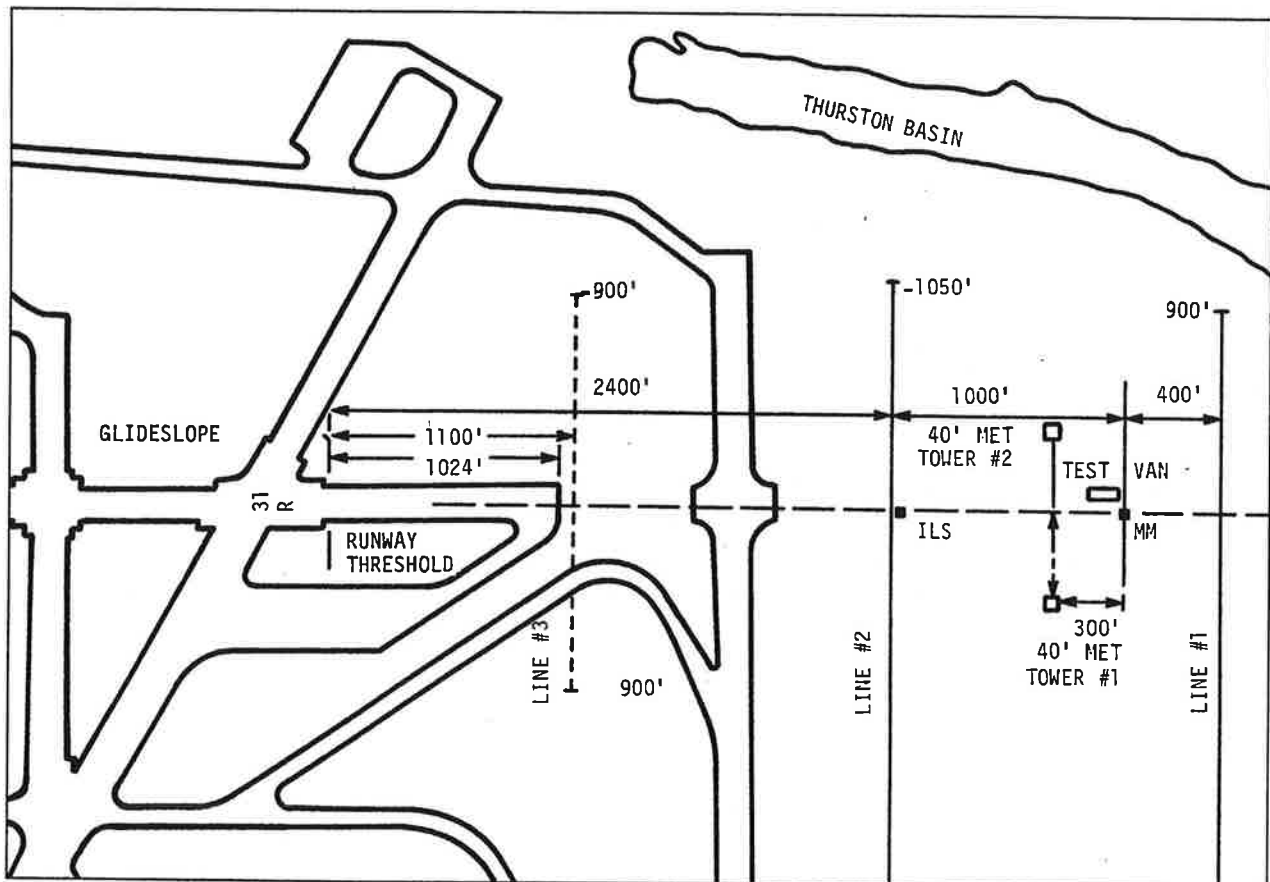


Figure 1. Kennedy Airport Landing Test Site

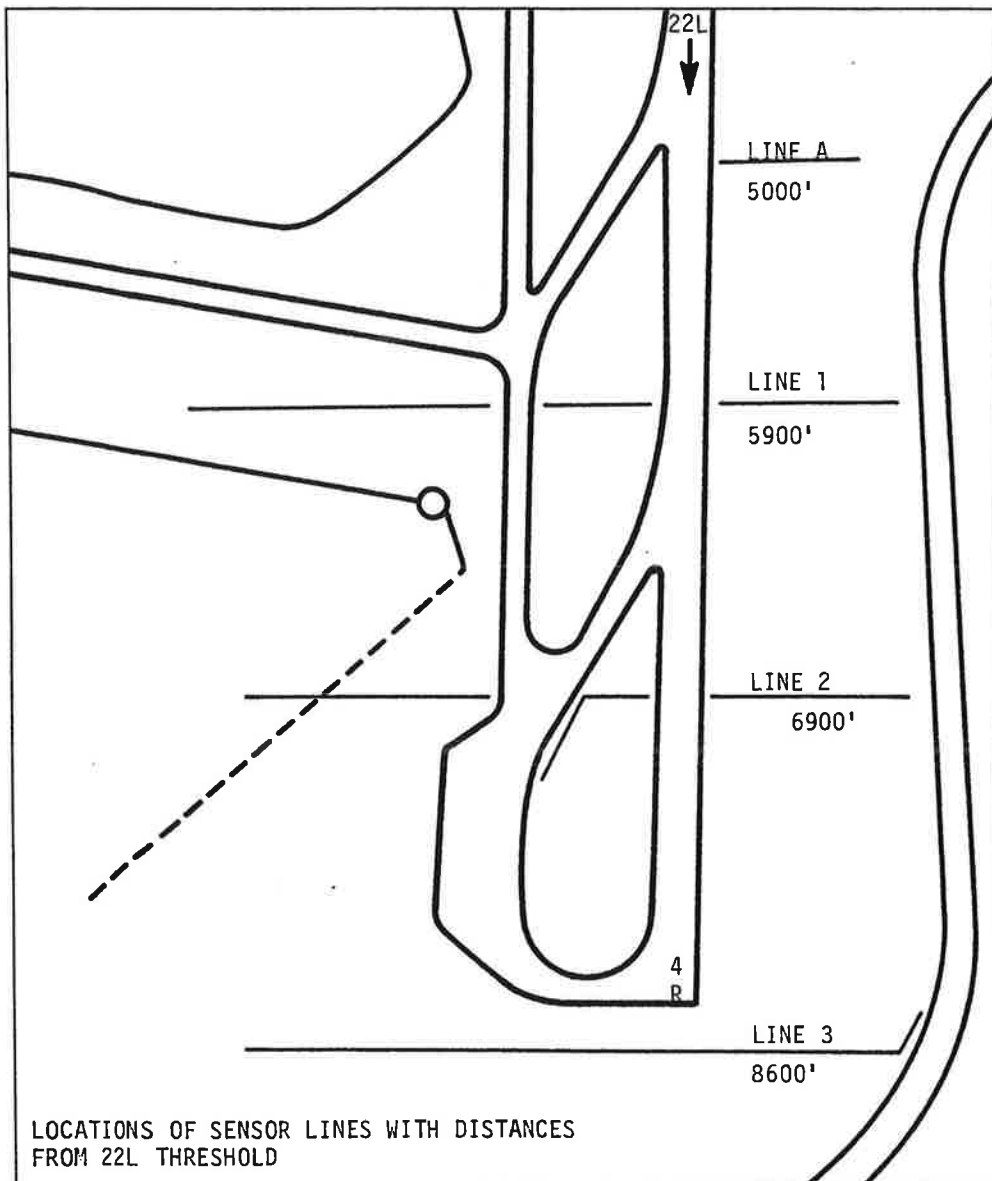


Figure 2. O'Hare Airport Takeoff Test Site Layout

locations were plotted on a lineprinter and each resulting vortex track was analyzed manually to determine seven parameters:

1. Lateral position at 30 seconds
2. Lateral position at 60 seconds
3. Lateral position at 90 seconds
4. Lateral position at 120 seconds
5. Residence time: time to exit or expire within a corridor 300 feet (400 feet for takeoff) wide centered on the extended runway centerline
6. Demise time: time a well-defined track no longer existed

7. Demise position: position where the vortex track terminated

Parameters 1 - 4 were determined automatically as the sensors showing highest/lowest readings. Parameters 5 - 7 were selected manually. Considerable judgment was required to define the vortex demise parameters. For many cases raw data stripcharts of the anemometer data were examined to make sure that the GWVSS measurements looked like the expected vortex signature. A number of atmospheric effects can give vortex-like tracks, especially when the crosswind is advecting turbulence directly down the GWVSS baseline (i.e., with little headwind).

2.5 SCOPE OF STUDY

This 1984 study made use of landing data from Kennedy International Airport and takeoff data from O'Hare International Airport. Neither of these data sets had been analyzed statistically before. Related statistical analyses were performed for other GWVSS data sets, the most complete being Heathrow³ and O'Hare⁵ for landing and Toronto¹³ for takeoff. Where possible, the results of the current study are compared with published analyses of similar data from other sites. No new analyses of data from other sites were possible because the databases were not accessible during the time of the study.

The major analytical advance in this report is an improved vortex decay model, originally developed^{14,15} for monostatic acoustic vortex sensing system (MAVSS) data. This study is the first GWVSS analysis since the model was developed. This model is characterized by a vortex persistence probability that decays exponentially with the square of the vortex age. A comparison of the MAVSS vortex strength decay with GWVSS vortex detection decay will allow a quantitative estimate of the GWVSS detection threshold.

Ideally this report should have been published immediately after the databases were originally generated. By 1984, much of the intermediate data needed to validate the results had been discarded and the software to reconstruct the intermediate data from the raw data tapes was no longer operational. Consequently, the databases used in this report contained considerable unvalidated data, which were not used, and also a few inconsistent data points that should have been checked against the original data.

3. SAFETY METHODOLOGY

The goal of the safety analysis is to determine the maximum lateral distance that a hazardous wake vortex can travel in ground effect. The straightforward method of answering this question is to collect data from a reasonable number of operations and determine the maximum distance traveled. This method was used to define the ambient wind ellipse giving safe three-mile single-runway separations^{3,13,16,17} in the development of the Vortex Advisory System (VAS). Unfortunately, this method fails to define how big a "reasonable number" must be to assure safety. To develop the VAS, data were collected for a large, but practical, number of operations, which was, however, far below the amount of data needed to define an acceptable hazardous encounter probability. The effective range of the data was extended by the fact that the GWVSS gives a conservative estimate of the vortex hazard, because the GWVSS vortex detection threshold is well below the vortex hazard threshold for low winds.

A more precise safety methodology was developed for this study along the lines¹⁷ of the VAS safety analysis. In the VAS safety analysis, an acceptable potential encounter probability was based on a safety of current separations. The analysis here makes use of the simplified model of vortex transport and persistence described in Appendix A. The following assumptions are used to define the safety analysis:

1. The current single-runway separation standards described in Section 2.1 are safe. Hence, the encounter probability at the current single-runway minimum separations is, by definition, an acceptable "safe" level.
2. The probability of a hazardous vortex encounter is proportional to the safety-corridor residence probability, i.e., the probability of a vortex being detected by the GWVSS within 150 feet of the extended runway centerline.
3. The constant of proportionality of assumption 2 is the same for corresponding single- and parallel-runway configurations.
4. The vortex transport and persistence model can be used to calculate the encounter probability on a parallel runway in terms of the probability of a vortex reaching the parallel runway.
5. The minimum safe parallel runway separation is reached when the parallel runway encounter probability drops to the "safe" single-runway encounter probability.
6. Assumption 3 is probably not valid since the GWVSS detection threshold depends upon the fluctuations in the crosswind and will be higher for the greater fluctuations associated with large crosswinds. The crosswinds leading to a vortex reaching a parallel runway are considerably larger than those leading to residence in the safety corridor (compare Figures 13 and 16). Because the crosswind fluctuations generally increase with the magnitude of the crosswind, the GWVSS detection threshold is likely to be larger for the parallel runway situation than for the single runway situation. This difference in thresholds is likely to be enhanced by the possible¹⁸ increase in the height of the downwind vortex in a crosswind, because the GWVSS signal is inversely proportional to the height of an isolated vortex. Perhaps the difference in thresholds can be addressed by incorporating a safety factor.

3.1 LANDING

The single-runway standards in Table 2 specify separations of 3, 4, 5, and 6 nautical miles for various pairs of wake-vortex generator and follower classes. For a typical landing ground speed of 135 knots, these distances translate into separation times of 80,

107, 134, and 160 seconds. These separation times are assumed to be safe, and are the basis of the calculation of safe residence probabilities. The minimum safe separation will be defined for the five pairs of classes listed in Table 4. Of course, the most restrictive combination Heavy/Small must be used to set the general parallel runway separation standard. However, in order to not be overly conservative (i.e., too low a safe residence probability), each generating class must be represented by the aircraft type(s) generating the most persistent wake vortices. The B-747 and B-707/DC-8 aircraft will be used to characterize the Heavy and Large classes, respectively. [Note that B-707 and DC-8 aircraft were common during the data collection periods.] The vortex decay for other smaller aircraft were checked to make sure that these two types actually generate the most persistent vortices (see Appendix B). Table 4 also shows the separation times which define the "safe" GWVSS residence probabilities for the five pairs of classes. The safe residence probabilities in the table were estimated using procedures discussed in Section 6.3.2.

Table 4. Landing Separation Times

Class Pair	Aircraft Data	Separation Time (s)	Safe Residence Probability
Heavy/Small	B-747	160	0.0010
Heavy/Large	B-747	134	0.010
Heavy/Heavy	B-747	107	0.06
Large/Small	B-707/DC-8	107	0.017
Large/Large	B-707/DC-8	80	0.10

3.2 TAKEOFF

The takeoff operation is not as easily analyzed as the landing operation. First, the vortex encounter hazard cannot be confined to ground effect because of the much greater variation in aircraft flight paths. Second, the GWVSS residence probability is more difficult to define because anemometers cannot be installed over the runway surface. Because of these difficulties, only the simple maximum transport distance methodology will be used for takeoff. These difficulties could perhaps be overcome by more complex modeling of the data.

4. DATA ANALYSIS

4.1 DATABASES

At the start of this project, the Kennedy and O'Hare GWVSS databases were located on Data General NOVA[®] minicomputers. These minicomputers had no general database management or statistical analysis software. During the course of the analysis, it became clear that much of the analysis could be done more efficiently using standardized software on a larger computer system. Consequently, the databases were moved to the National Institute of Health IBM-370 computer complex, and most of the analyses presented here were made using the Statistical Analysis System (SAS).

The sizes of the Kennedy (JFK) and O'Hare (ORD) databases are shown in Table 5. Each record includes residence time, demise time, and demise position, for port and starboard vortices on each of three baselines (a total of six vortices per record). Also included are meteorological data and verification status.

Data verification was required because of the potential for the software to mistake wind gusts for vortices and because of inconsistencies in the initial manual data reduction. Thus, to avoid having spurious vortex demise positions in the database, the raw anemometer strip charts were examined to determine whether the observed crosswind profiles resembled a true vortex signature. This procedure was carried out for approximately the first half of the JFK data records and all of the ORD records. Table 5 also illustrates several database features of critical importance to the analysis. First, there are a substantial number (more than half) of unverified records in the JFK data. Only the verified data were used in the analysis. Thus, over half of the records were excluded from consideration. Second, a substantial number of records in the JFK data had high headwinds (in excess of 15 knots, see Figure 3). High headwind data were also excluded from this analysis for reasons

Table 5. Database Statistics

Aircraft Type	Total Records	Verified Records	
		All Winds	Headwind < 15 knots
Kennedy Landing Data			
B-707	1,219	584	378
B-727	1,016	490	331
B-747	834	372	220
DC-8	465	203	137
DC-9	367	185	114
DC-10	213	85	59
L-1011	110	52	34
TOTAL	4,224	1,971	1,273
O'Hare Takeoff Data			
B-707	497	399	390
B-727	7,747	7,654	7,539
B-737	1,293	1,265	1,231
B-747	277	274	271
DC-8	22	21	20
DC-9	2,726	2,684	2,615
DC-10	1,390	1,378	1,368
L-1011	289	285	279
TOTAL	14,151	13,960	13,713

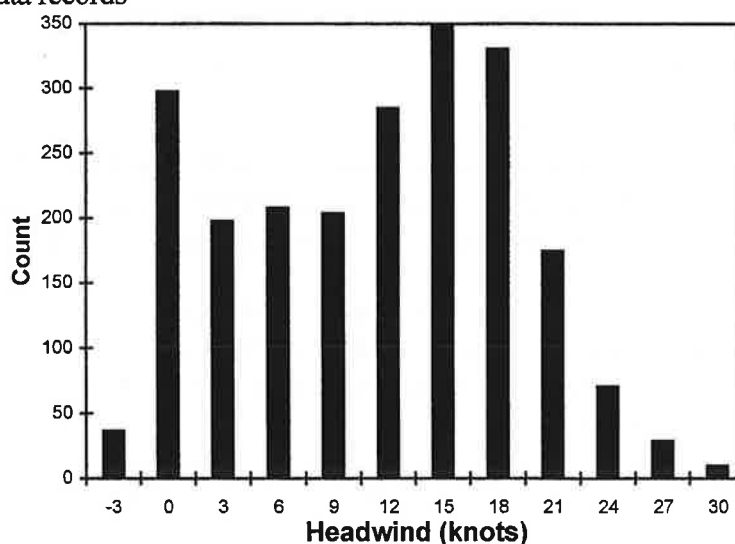


Figure 3. Kennedy Headwind Distribution

discussed below. Thus, over two thirds of the JFK records were excluded.

4.2 METEOROLOGY

The headwind and crosswind distributions for the Kennedy landing database are shown in Figures 3 to 5. The number of arrivals with high headwinds (Figure 3) is much larger than observed at other airports such as Heathrow³ and O'Hare.⁵ Consequently, the analysis of the Kennedy data will exclude data with headwinds larger than 15 knots, so that the results can be compared to earlier analyses and are

more representative of a typical airport, where any resulting separation standards will be used. The exclusion of high headwinds also eliminates the abnormally large fraction of Kennedy arrivals where the GWSS detected no vortices. The crosswind distributions before and after the high headwind exclusion are shown in Figures 4 and 5, respectively. With the headwind limitation, about 68 percent of the cases have a positive crosswind. Note that in these cases, unfortunately, the vortices are transported down the *short* end of the GWSS baselines (see Figure 1).

As shown in Figure 1, two meteorological towers with anemometers at 20- and 40-foot heights were installed at Kennedy. To minimize the influence of wake vortices on the wind measurements, the winds used in the analysis were taken from the 40-foot level on the upwind tower with respect to the crosswind.

The vortex transport model in Appendix A requires a distribution function for the ambient crosswind. The model considers that the probability of observing a vortex at a specified distance from the runway centerline varies with both the distance chosen and the ambient crosswind (see discussion, Appendix A). The model first calculates the transport probability as a function of distance and ambient crosswind and then applies the crosswind distribution to determine the total transport probability as a function solely of distance. The advantage of this approach is that the probability as a function of both distance and ambient crosswind can be modified for other airports with different crosswind conditions. Calculating the total transport probability as a function solely of distance merely requires

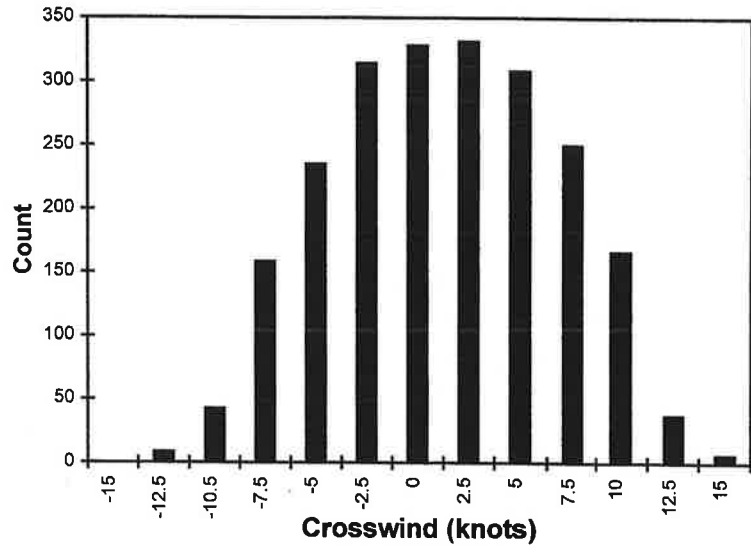


Figure 4. Kennedy Crosswind Distribution

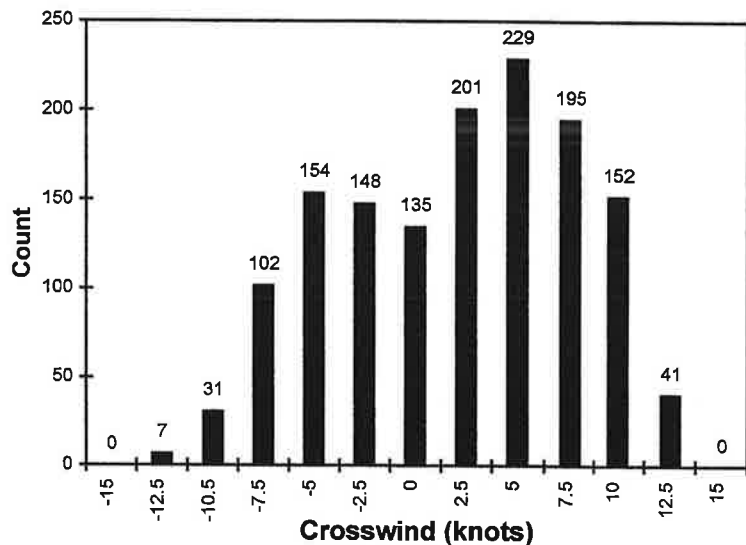


Figure 5. Kennedy Crosswind Distribution, Headwind < 15 knots

replacing the input crosswind distribution. It is therefore apparent that the choice of crosswind distribution for the purposes of making a preliminary assessment of the potential for reducing separation distances is somewhat arbitrary. Further assessments that consider airport-specific meteorological conditions may be necessary before such calculations are used to define separation standards.

For purposes of this analysis, a crosswind distribution was estimated from the observed crosswind distribution (Figure 5). For modeling simplicity, a Gaussian crosswind distribution was assumed with a mean of zero and a standard deviation derived from the data of Figure 5.

It can be noted (Figure 5) that the distribution of positive direction ambient crosswinds differs considerably from that of negative direction crosswinds at JFK airport. The distribution is biased toward positive crosswind. Separate wind distribution models were used for each direction. Each model used standard deviations to fit the crosswinds in that direction.

The standard deviation of the negative crosswinds was calculated from Figure 5 using the fact that for a Gaussian distribution approximately 68% of the values are less than one standard deviation from the mean. Thus, the procedure for estimating the standard deviation of the negative crosswinds was to calculate the crosswind value which was more negative than 68% of the observed negative crosswinds.

The method used to perform this calculation required two steps. First, calculate the total number of negative crosswinds from Figure 5. Note that the crosswinds listed in Figure 5 have been grouped and the listed crosswind is the group midpoint. In other words, the crosswinds labeled as -10 knots in Figure 5 in actuality range from -11.25 knots to -8.75 knots. The number of negative crosswinds consists of all crosswinds in negative crosswind groups, plus half of the crosswinds in the 0-crosswind group, i.e., the number of crosswinds with values ranging from 0 to -1.25 knots. Thus, the number of negative crosswinds is: $7 + 31 + 102 + 154 + 148 + 135 / 2 = 510$.

The second step is to calculate which crosswind is more negative than 68% of the negative crosswinds and estimate its crosswind value. This crosswind is the 163rd most negative crosswind: $(1 - 0.68) * 510 = 163$. That is, only 162 crosswinds out of 510 have higher (negative) crosswind values. Note in Figure 5 that $140 = 7 + 31 + 102$ crosswinds have more negative crosswind values than any crosswind in the -7.5-knot crosswind group. The least negative crosswind in this group is $-7.5 + 1.25 = -6.25$ knots. Thus, the crosswind under consideration is greater than -6.25 knots. It is the 23rd ($163 - 140 = 23$) most negative crosswind in the -5.0-knot crosswind group. To estimate the desired crosswind value it is then assumed that the 154 crosswinds in the 5.0-knot group are uniformly distributed and hence have values corresponding to their rank in the group. Therefore, noting that the group ranges from -6.25 to -4.75, the most negative is assumed to have a value of -6.25, the next a value of: $-6.25 + (1/154 * 2.5)$, the next a value of: $-6.25 + (2/154 * 2.5)$, etc. Thus, the desired value is: $-6.25 + (23/154 * 2.5) = -5.9$ knots. Thus, the standard deviation is 5.9 knots. Calculations for the standard deviation of the positive crosswinds are similar and yield a somewhat larger value of 7.6 knots.

The headwind and crosswind distributions for the O'Hare takeoff database are shown in Figures 6 and 7, respectively. Because the O'Hare headwind distribution exhibits fewer high headwinds, no headwind restrictions were applied to the O'Hare data. The crosswind distribution is asymmetric: 62 percent of the cases show positive crosswinds. Fortunately, positive crosswinds blow vortices toward

the long end of the GWVSS baselines (Figure 2). The two sides of the crosswind distribution were fitted to a Gaussian, using the same approach applied to the Kennedy data. For the O'Hare data (Figure 7), the crosswind standard deviations were found to be 4.0 and 6.3 knots for negative and positive crosswinds, respectively.

4.3 LANDING

The GWVSS survival and residence probabilities in earlier reports were plotted as a function of vortex age, usually using a logarithmic scale for the probability. The analysis of MAVSS data^{14,15} indicated that the probability decay plots became approximate straight lines when the logarithm of the probability was plotted against the square of the vortex age. Figure 8 shows a sample of such MAVSS data. The plots show how the probability of the vortex strength remaining above a strength threshold depends upon the vortex age. Each plot on a graph is for a different strength threshold, as is indicated on the graph. The x's at the bottom of the plot show the probability corresponding to one case, which is the lowest probability that can be plotted on a logarithmic scale. Since the total number of cases available for analysis decreases with age (because of the noise associated with the arrival of the next aircraft), the minimum probability rises with age.

The advantage of obtaining a straight line fit to a decay curve is that it can be extrapolated to lower probabilities than measured with an expectation of reasonable accuracy. In the present study considerable success was obtained in using a similar plotting format for GWVSS data, both for the age and distance dependence of the vortex survival probability.

4.3.1 Vortex-Demise Positions

Tables 6 through 8 contain all the verified demise positions (headwind less than 15 knots) for the Kennedy landing database. It is appropriate to mention here that the headwind restriction does not

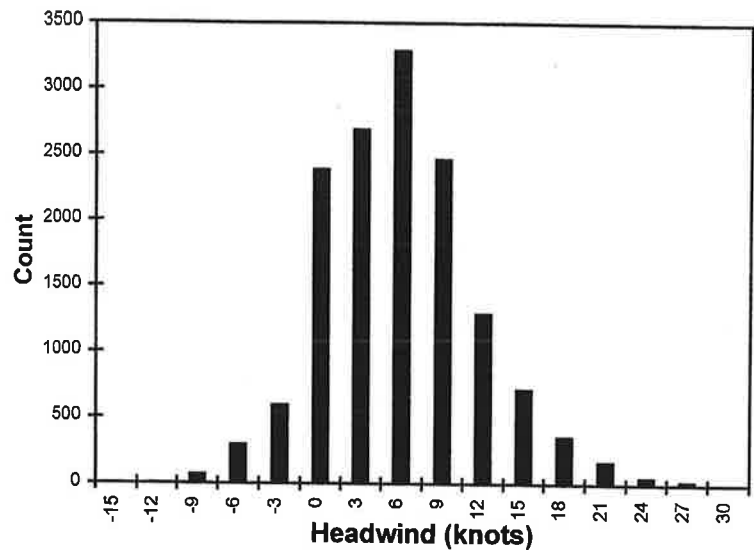


Figure 6. O'Hare Headwind Distribution

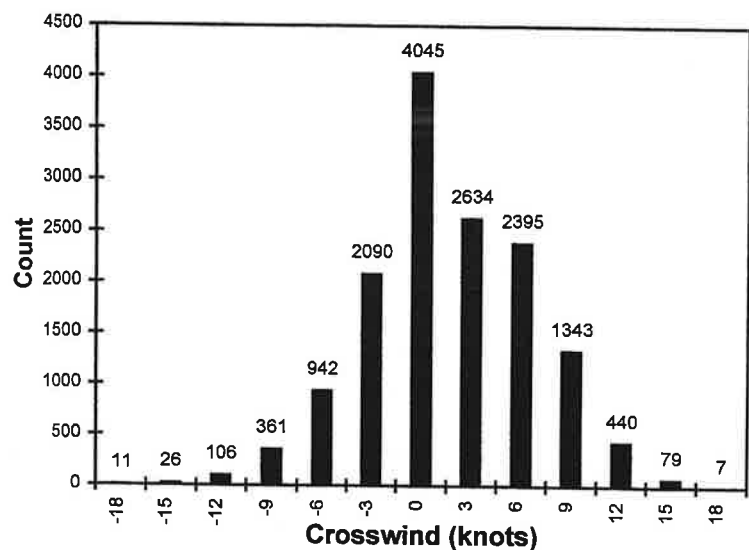


Figure 7. O'Hare Crosswind Distribution

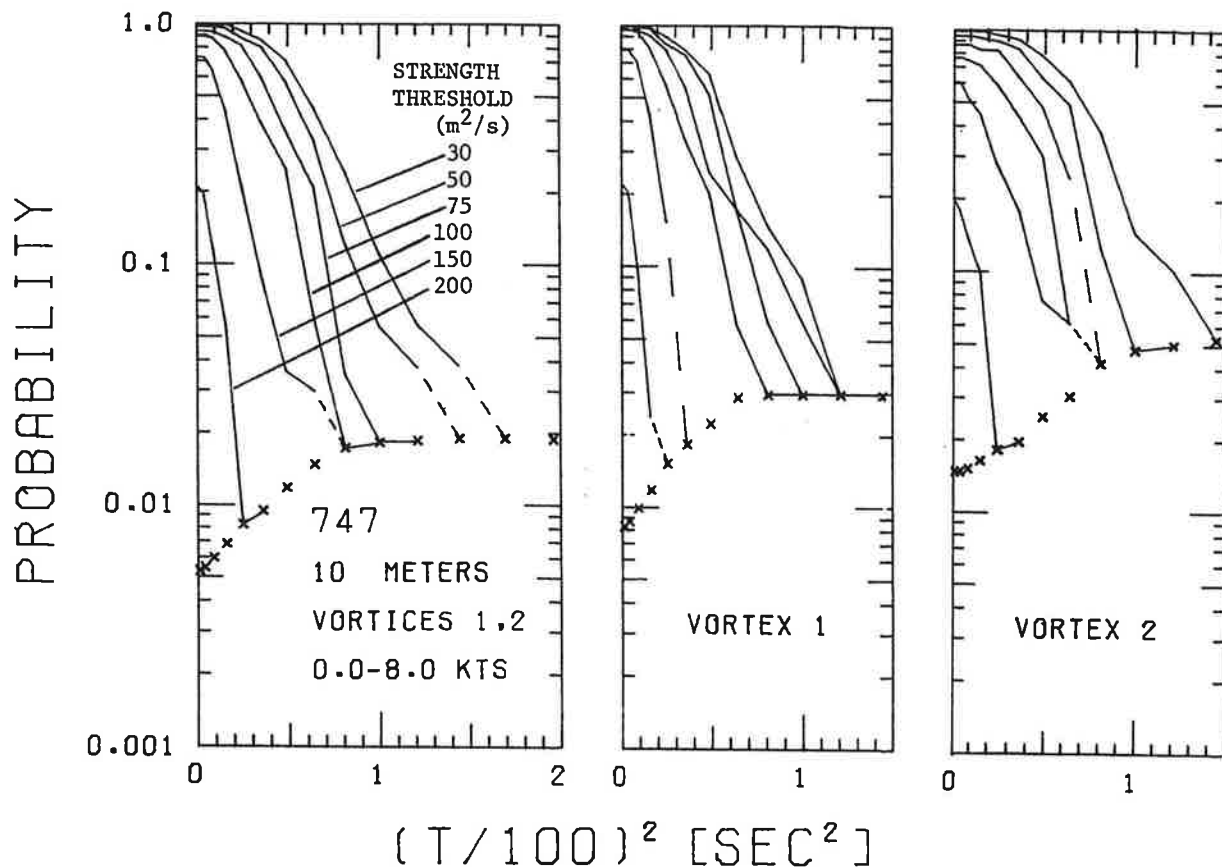


Figure 8. Probability of Decay, B-747, Wind Magnitude less than 8 knots, 10-m Averaging Radius

eliminate any long transport cases (in excess of 900 feet). Three tables are used to present port and starboard vortex demise positions for the three GWVSS baselines (see Figure 1). Each table lists the number of vortices which expired (became no longer detectable within the wind signal at the respective anemometer) at each anemometer location for each aircraft type. Undetected (next to last line in tables) vortices were either too weak with respect to the GWVSS detection threshold or were immediately dissipated by strong winds. The total number of valid cases (including arrivals where the vortex was not detected, and hence, no vortex-demise position was measured) is used to normalize the vortex transport probabilities.

Most of the undetected vortices are eliminated when the headwind is restricted to less than 15 knots, e.g., more than half of the B-707 cases with undetected vortices have headwinds in excess of 15 knots.

Several apparent anomalies of Tables 6 to 8 should be noted. First, there are no vortices listed as having expired beyond 900 feet in the positive direction. This is because the +900-foot anemometer was the last one in the line. Thus, when a vortex is assigned a vortex-demise position of +900 feet, one can only be certain that +900 feet is the last location where the vortex was detected. The actual vortex-demise position of that vortex may be considerably farther (and also the actual lifetime considerably longer) than indicated. The same limitations also apply to -900 feet on line 3, which was the last anemometer on that line. The second anomaly is the almost total lack of negative vortex-demise

positions for line 3. Probably, these anemometers were out of service for most of the test. A third anomaly in the tables is the large peak in vortex-demise positions at -900 or -1000 feet. This peak was caused by the very careful scrutiny given to all vortex-demise positions beyond those values. Many spurious vortex-demise positions were discovered by examining stripcharts of the raw anemometer data. Of 51 cases in the total JFK database in which a vortex-demise position was listed as beyond -900 feet, only 10 (20%) were from verified cases. (Recall that roughly half of the records were verified.) Unfortunately, the strong effect produced by this selective editing of the data means that the data for vortex-demise positions of less than 1000 feet in magnitude may be unreliable for determining the functional dependence of the transport probability upon lateral distance.

Table 6. Kennedy Baseline #1 Vortex-Demise Positions for Port and Starboard Vortices by Aircraft Type

Death Position (ft)	Aircraft Type														Tot		
	B-707		B-727		B-747		DC-8		DC-9		DC-10		L-1011				
	P	S	P	S	P	S	P	S	P	S	P	S	P	S			
-1500	1							1									2
-1000	1		1		2			0									4
-900	4		2		5			0						1			12
-800	8		3		6	4		3	1					0			25
-750	0		0		0	0		0	0					0	1		1
-700	17		6		11	1		5	0	1		1		1	0		43
-600	3	6	7	3	8	9		1	1	1		1		0	2		42
-500	17	5	14	1	15	3		9	1	2		3		4	1		75
-400	11	13	14	7	16	7		7	4	3		2	1	1	1		87
-350	3	5	5	6	4	6		1	1	2	2	0	1	0	1		37
-300	6	6	2	11	4	6		2	2	0	4	2	1	0	0		46
-250	2	9	3	10	0	10		1	7	3	3	0	1	0	1		50
-200	8	4	6	2	4	3		4	2	2	0	0	0	1	0		36
-150	1	3	4	2	0	4		1	2	0	1	1	0	0	1		20
-100	0	8	1	11	2	5		1	3	0	1	0	3	0	0		35
-50	4	4	6	1	5	3		4	3	1	0	0	0	2	0		33
0	6	2	2	3	4	2		2	0	0	1	0	0	1	1		24
50	6	4	6	2	4	1		0	3	0	0	0	0	1	0		27
100	5	0	3	4	3	3		3	3	1	0	0	1	0	1		27
150	4	3	3	8	2	3		2	3	1	2	1	1	0	0		33
200	7	4	9	4	1	1		2	0	2	0	1	1	1	0		33
250	5	8	5	5	4	3		4	2	1	1	0	0	1	0		39
300	9	12	5	8	3	5		0	2	2	1	0	0	0	3		50
350	8	8	12	6	0	6		1	3	1	0	0	2	0	1		48
400	7	13	7	23	6	8		6	11	0	8	1	2	1	4		97
500	11	7	12	14	13	8		4	10	0	1	1	1	1	1		84
600	19	23	8	16	16	24		8	11	2	2	8	7	2	2		148
700	6	22	4	22	13	36		3	13	1	2	2	7	0	5		136
800	10	19	15	11	20	25		10	11	1	1	4	5	2	1		138
900	11	6	8	3	23	9		6				7	2	4			79
UnDet	163	169	155	145	19	18		46	38	83	81	21	20	10	7		974
Total	378	378	331	331	220	220		137	137	114	114	59	59	34	34		2482

The vortex-demise position tables yield two simple observations about the maximum vortex-demise positions. First, the maximum transport distance was 1500 feet for first vortices and only 1200 feet for second vortices. (With respect to the ambient crosswind, the first vortex is the downwind vortex and the second vortex is the upwind vortex.) Second, the largest transport distances occur for Heavy wide-body aircraft and for the B-707 and DC-8 which straddle the Heavy/Large boundary.

Table 7. Kennedy Baseline #2 Vortex-Demise Positions for Port and Starboard Vortices by Aircraft Type

Death Position (ft)	Aircraft Type														Tot
	B-707		B-727		B-747		DC-8		DC-9		DC-10		L-1011		
	P	S	P	S	P	S	P	S	P	S	P	S	P	S	
-1500							1								1
-1200		1					0								1
-1000		0			1		1								2
-900		0	2	3	3		0	1							9
-800	6	5	7	1	13	3	2	0	3	1			2	2	45
-750	0	1	1	0	1	0	0	0	0	0			0	0	3
-700	17	1	7	0	10	2	4	0	1	0			2	0	44
-650	0	0	0	0	0	0	0	0	1	0			0	0	1
-600	27	1	7	0	20	2	7	2	3	0	3		1	0	73
-550	2	0	0	0	0	0	1	0	0	0	0		0	0	3
-500	12	3	10	1	6	1	1	1	4	0	2		3	0	42
-400	0	0	1	1	2	1	0	1	0	1	0		0	0	7
-350	12	25	12	18	9	13	5	7	2	5	5	1	0	3	117
-300	15	6	10	4	5	15	5	1	2	0	0	0	0	0	63
-250	14	11	11	12	6	3	3	4	3	0	0	0	4	0	71
-200	8	5	10	5	4	2	6	0	3	1	0	4	0	0	48
-150	1	4	5	2	4	0	2	1	4	0	1	0	0	1	25
-100	3	16	6	21	2	11	3	6	2	4	0	1	0	2	77
-50	4	11	5	10	7	6	3	7	1	3	0	0	2	1	60
0	16	7	10	7	10	3	4	1	3	1	2	2	2	0	68
50	4	5	8	4	2	6	3	1	2	2	1	0	0	0	38
100	3	1	3	4	1	1	1	1	3	0	1	0	0	0	19
150	12	6	10	13	4	6	4	6	3	1	3	3	2	1	74
200	4	1	2	0	1	2	1	1	0	0	1	0	0	0	13
250	7	4	11	1	4	2	2	1	3	0	1	1	3	0	40
300	6	15	3	11	3	3	2	8	2	7	0	2	0	1	63
350	11	6	20	5	4	5	6	2	5	1	1	1	0	0	67
400	20	29	27	34	12	9	13	8	5	12	0	7	0	4	150
500	13	20	11	26	6	15	4	10	2	6	3	5	3	4	128
600	11	33	10	25	9	21	5	17	1	5	4	4	0	2	147
700	29	10	16	6	16	7	12	7	3	3	6	4	5	3	127
800	15	20	15	19	22	23	9	9	1	3	6	1	4	1	148
900	25	40	13	23	29	49	7	16	3	2	13	17	1	4	242
UnDet	79	89	78	75	4	9	20	18	48	55	6	6	0	5	492
Total	378	378	331	331	220	220	137	137	114	114	59	59	34	34	2118

Table 8. Kennedy Baseline #3 Vortex-Disemise Positions for Port and Starboard Vortices by Aircraft Type

Death Position (ft)	Aircraft Type														Tot
	B-707		B-727		B-747		DC-8		DC-9		DC-10		L-1011		
	P	S	P	S	P	S	P	S	P	S	P	S	P	S	
-900							1						1		2
-600	2				1		0						0		3
0	2		1		1		0						0		4
50	8	6	6	7	4		2	3	1	1	3	1	2	1	45
100	7	18	8	9	2	6	1	5	1	1	0	0	1	1	60
150	23	14	21	9	17	5	12	1	8	4	2	0	1	1	118
200	5	17	3	10	3	2	5	4	3	4	0	4	0	0	60
250	6	4	6	7	4	6	4	4	3	3	0	2	2	2	51
300	15	8	14	7	9	4	8	4	4	1	2	1	0	0	77
350	11	27	15	18	8	8	5	14	5	7	1	7	2	1	129
400	39	40	32	40	22	23	6	19	10	9	8	11	2	3	264
500	24	20	24	16	15	19	8	9	1	3	9	4	3	3	158
600	18	29	5	19	9	21	4	9		6	3	4	0	3	130
700	7	18	3	14	6	27	3	5		4	4	3	3	3	100
800	5	13	1	1	6	8	4	4			4	3		1	50
900	2	13		9	5	13	1	2			2	4		2	53
UnDet	152	99	149	123	76	46	50	31	58	51	17	11	12	8	892
Total	378	378	331	331	220	220	137	137	144	114	59	59	34	34	2196

4.3.1.1 Vortex 1 vs. Vortex 2

The MAVSS data of Figure 8 were disaggregated into Vortex 1 and Vortex 2, which are the first and second vortices to arrive at a given MAVSS antenna. Vortex 2 is the one that may stall at the extended runway centerline and pose a potential hazard to a following aircraft on the same runway. On the other hand, Vortex 1 moves faster than Vortex 2 and would pose the greater hazard to a parallel runway if both types of vortices had the same decay rate. However, as shown in Figure 8, Vortex 2 generally persists longer than Vortex 1. Thus, the transport and decay have opposite relative effects on the parallel-runway hazard of vortices 1 and 2, and it is not obvious which would pose the greater hazard. Table 9 addresses the issue of which vortex (upwind or downwind) travels farthest. For each vortex pair, the vortex (upwind or downwind) which traveled the farthest and the distance it traveled were identified. The results were tabulated by distance group in Table 9.

As can be seen in Table 9, for extremely long transport distances the downwind vortices travel further. However, this is not the case for smaller distances. Note that there may be an asymmetry with respect to direction from the runway centerline. At a distance of 900 feet in the negative direction, the ratio of downwind to upwind vortices is 10:1, whereas at a distance of 900 feet in the positive direction the ratio is only 2:1. These last ratios may be somewhat overstated because in instances in which both the upwind and downwind vortices expired between the same anemometers, the downwind vortex was assumed to have traveled farther with respect to the runway centerline. In addition, note that when vortices travel beyond 900 feet in the positive direction, there are no data to indicate how far they have traveled. Thus, the downwind vortex may have actually traveled less than the upwind vortex with

respect to the runway centerline. Yet, as far as the algorithm used to develop Table 9 is concerned, the downwind vortex will be indicated as travelling farther with respect to the runway centerline.

4.3.1.2 Survival Probability

The vortex-demise position data in Tables 6 to 8 can be plotted in a useful form by calculating the probability of a vortex reaching a particular lateral position, which is the number of vortices expiring at or beyond that position divided by the total number of vortices. Figures 9 and 10 show such plots for all three baselines, for the B-707 and B-747, respectively. Plots for other aircraft are located in Appendix B. The figures plot the logarithm of the probability that a vortex will be transported a given distance (log of cumulative survival probability) against the square of the distance, with results that lie roughly on a straight line. The lines drawn on the figures are intended as a general indicator of the functional dependence and were not fitted mathematically. In each case the line passes through the point zero distance squared, and unity log cumulative survival probability. Thus, the line is a one parameter fit. The results presented in the figures are summarized in Table 10, which lists the slopes fitted to the plots. The figures show no dramatic dependence upon the distance of the GWVSS baseline from the runway threshold (see Figure 1 for the baseline locations).

Table 10. Transport Probability Estimated Lines

Figure	Aircraft	Slope	Crosswind (knots)	Direction of Motion
9	B-707	-0.042	All	Both
10	B-747	-0.030	All	Both
11L	B-707	-0.026	All	Positive
		-0.037	All	Negative
11R	B-747	-0.017	All	Positive
		-0.048	All	Negative
12L	B-747	-0.032	0-5	Both
12M	B-747	-0.015	6-10	Positive
		-0.038	6-10	Negative
12R	B-747	-0.010	10115	Both

Table 9. Comparison of Upwind and Downwind Vortex Pair Transport (All Baselines, Verified Records Only)

Farthest Distance (ft)	Upwind Farther than Downwind		Downwind Farther than Upwind	
	Number	%	Number	%
-1500	0	0	5	100
-1400	0	0	4	100
-1300	0	0	2	100
-1200	2	67	1	33
-1100	0	0	1	100
-1000	3	9	32	91
-900	4	9	43	91
-800	16	12	118	88
-750	0	0	2	100
-700	10	6	148	94
-600	24	11	193	89
-550	0	0	2	100
-500	17	7	223	93
-450	0	0	3	100
-400	15	9	158	91
-350	49	21	189	79
-300	34	14	209	86
-250	32	21	124	79
-200	64	27	175	73
-150	37	21	136	79
-100	36	45	44	55
-50	26	51	25	49
0	6	0	467	100
50	74	87	11	13
100	129	66	66	34
150	135	49	140	51
200	58	39	89	61
250	101	34	197	66
300	170	35	309	64
350	86	31	191	69
400	141	21	541	79
500	140	17	707	83
600	254	30	589	70
700	107	31	238	69
800	145	42	203	58
900	135	34	260	66
Total	2,050	17	10,048	83

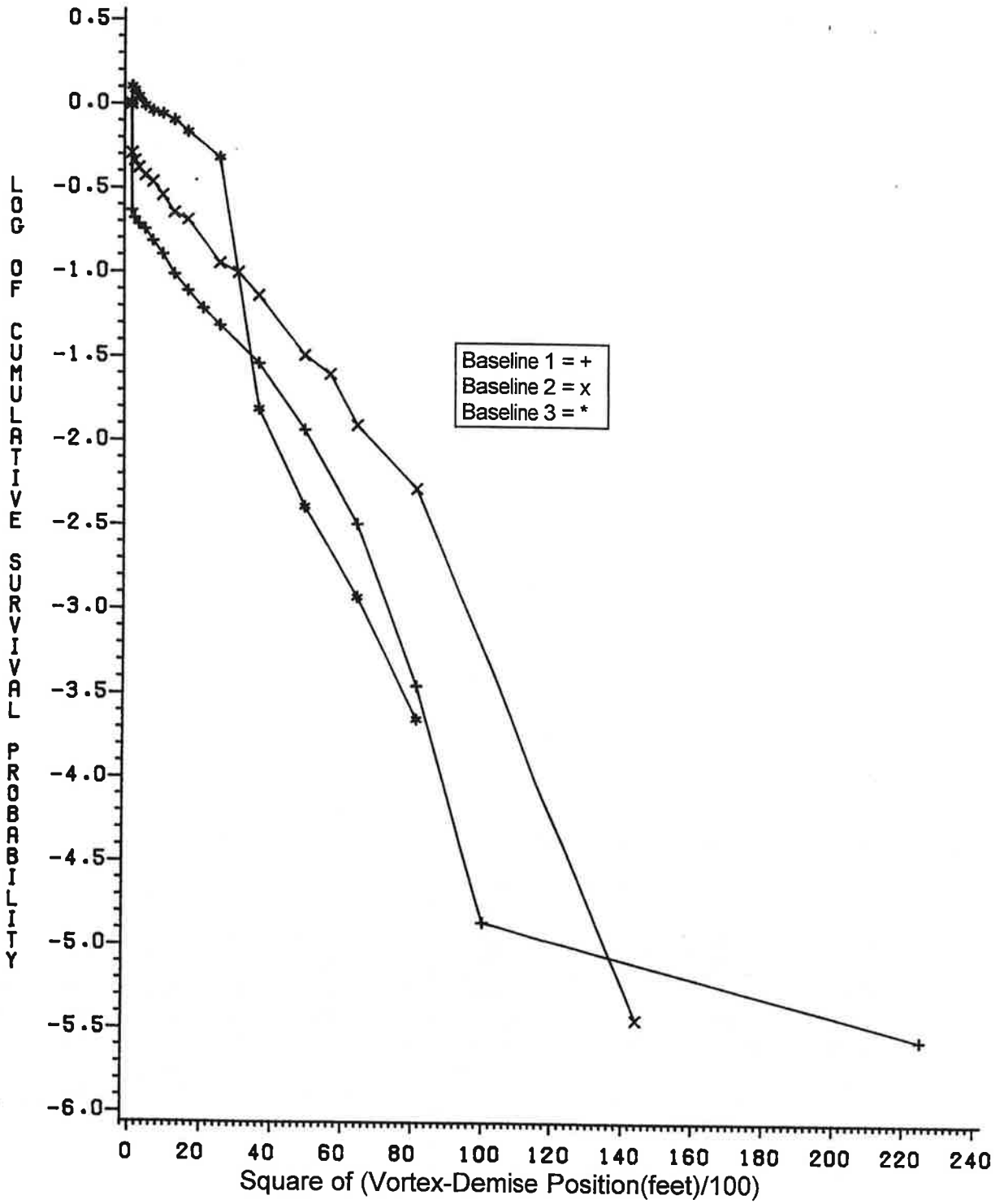


Figure 9. B-707 Cumulative Vortex Survival Probability

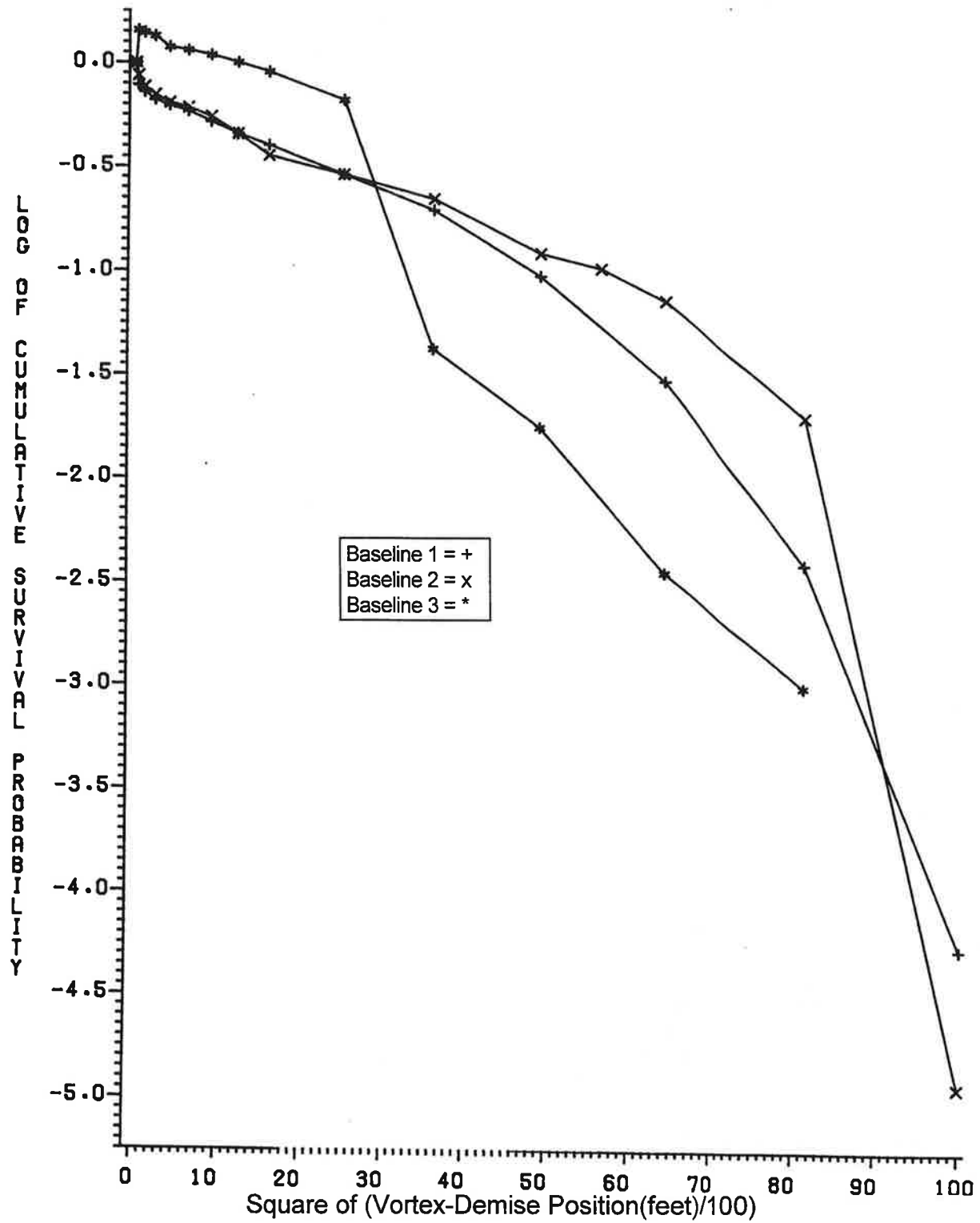


Figure 10. B-747 Cumulative Vortex Survival Probability

Figures 9 and 10 average port and starboard vortex data and combine vortex-demise positions on both sides of the runway. The relative normalization between the two sides of the runway was based on the number of vortices reaching 300 feet on either side. The existence of probabilities above 100 percent for small distances is caused by errors introduced by this normalization procedure.

Figure 11 shows how disaggregating by port and starboard vortex and side of the runway affect the results for Baseline 2. Transport distance probabilities are larger for positive directions than for negative directions. The starboard vortex moving in the negative direction (Vortex 2) shows the steepest drop.

The magnitude of the crosswind has a strong effect on the vortex transport probability. Figure 12 shows how the magnitude of the crosswind affects the transport of B-747 vortices for Baseline 2. For low crosswinds (left) the decay is rapid and similar for all cases. For intermediate winds (middle) the starboard vortices moving in the negative direction decay more rapidly than the other vortices; the low wind case (left) also shows a hint of this effect. Finally, for high crosswinds (right) both vortices decay

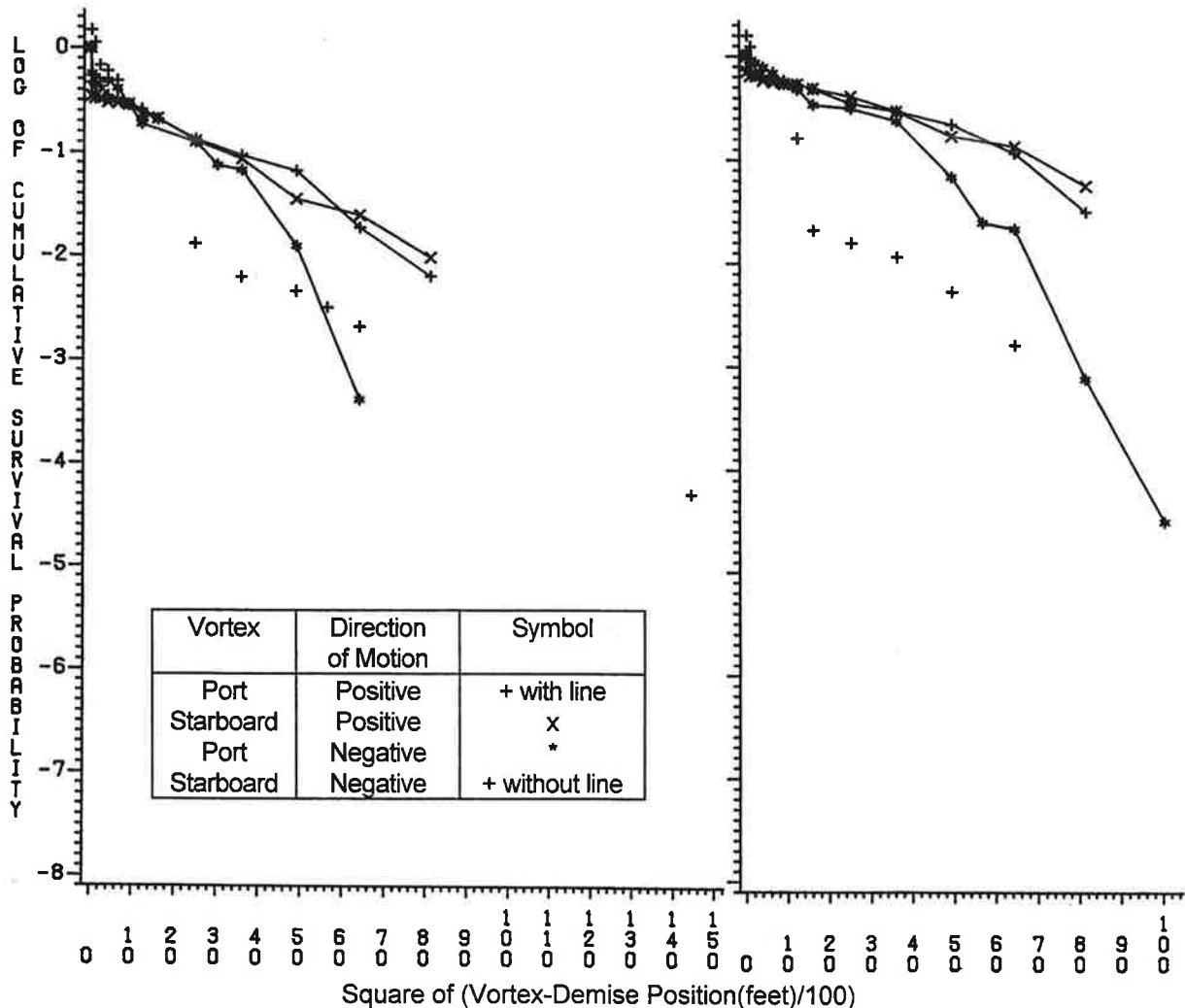


Figure 11. Cumulative Vortex Survival Probability vs. Distance, All Crosswinds:
Left: B-707; Right: B-747

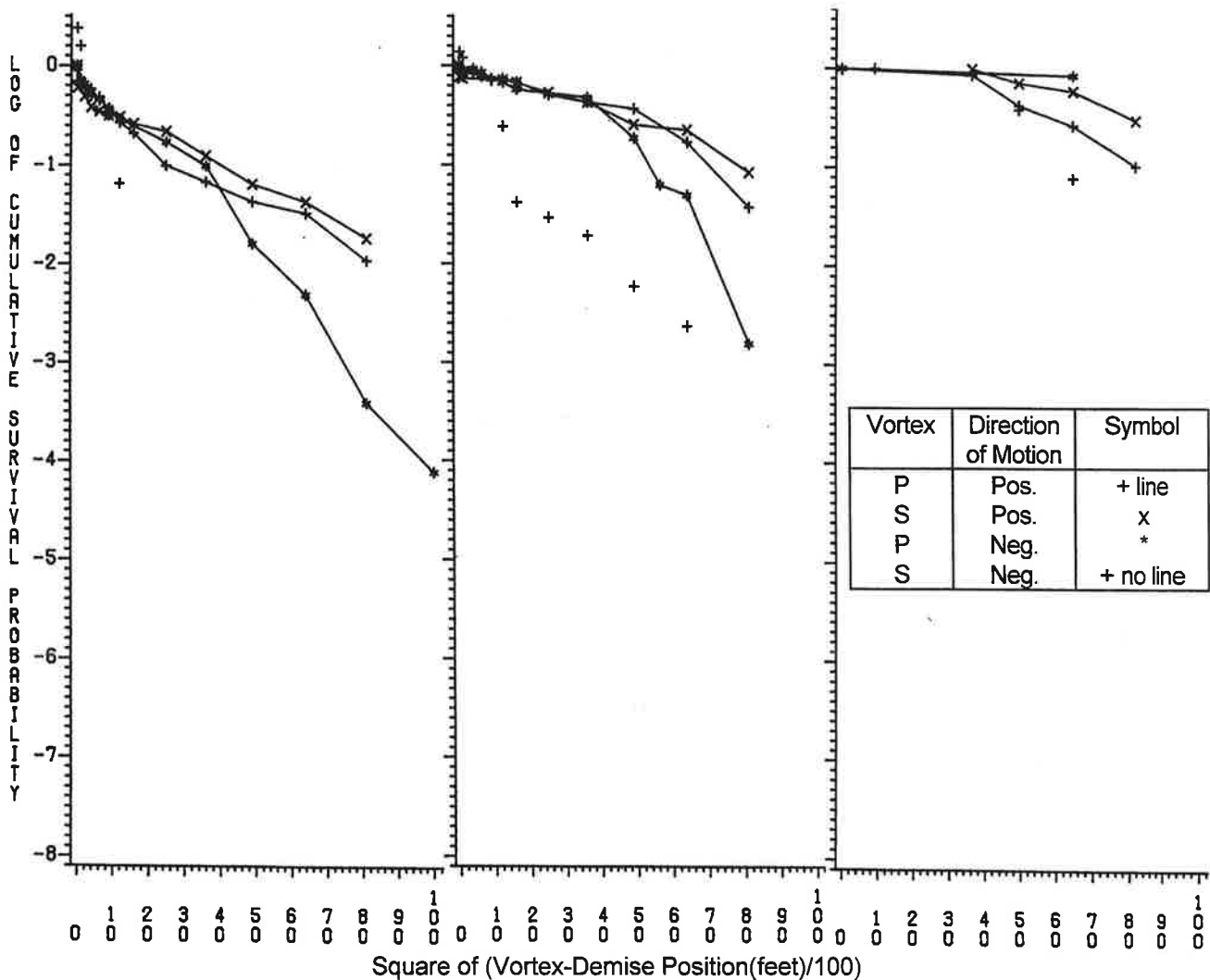


Figure 12. B-747 Cumulative Vortex Survival Probability vs. Distance by Crosswind:
 Left: 0-5 knots, Middle: 6-10 knots, Right: 11-15 knots

very slowly. Strong positive crosswinds appear to be very efficient in moving vortices past the +900 foot end of the baselines.

Figure 13 shows how different crosswinds contribute to the probability of a vortex moving a large distance. The crosswind distribution for all vortices reaching +900 feet is shown. The functional dependence of transport distance probability on crosswind is one of the major outputs from the vortex transport and decay model in Appendix A. Three effects shape the distribution; higher crosswinds:

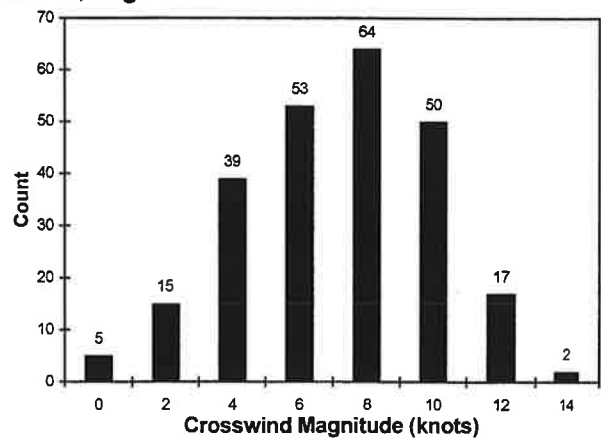


Figure 13. Kennedy Crosswind Distribution for Vortices Transported at Least 900 Feet - All Baselines - All Aircraft Types

1. Move the vortex faster so that it can travel farther before it decays, but
2. Also promote vortex decay, and
3. Are less likely to occur than lower crosswinds. (See Figures 4, 5, and 7.)

4.3.2 Residence Times

As far as the single-runway wake vortex hazard is concerned, the important residence time is that of the last vortex, port or starboard, to exit or expire within the safety corridor bounded by the lateral limits +150 and -150 feet. Normally, the last vortex remaining in the corridor is the upwind vortex. Figure 14 plots the residence probability (i.e., the probability that at least one vortex remains within the safety corridor) against the residence time for the B-707 and B-747, respectively, for all three baselines. No major difference between baselines is observed, although line 3 showed a somewhat lower probability for some distances. The plots in these two figures are against time rather than time squared. Yet, the results show many long residence time stragglers instead of the sharp downturn expected for linear time plots.

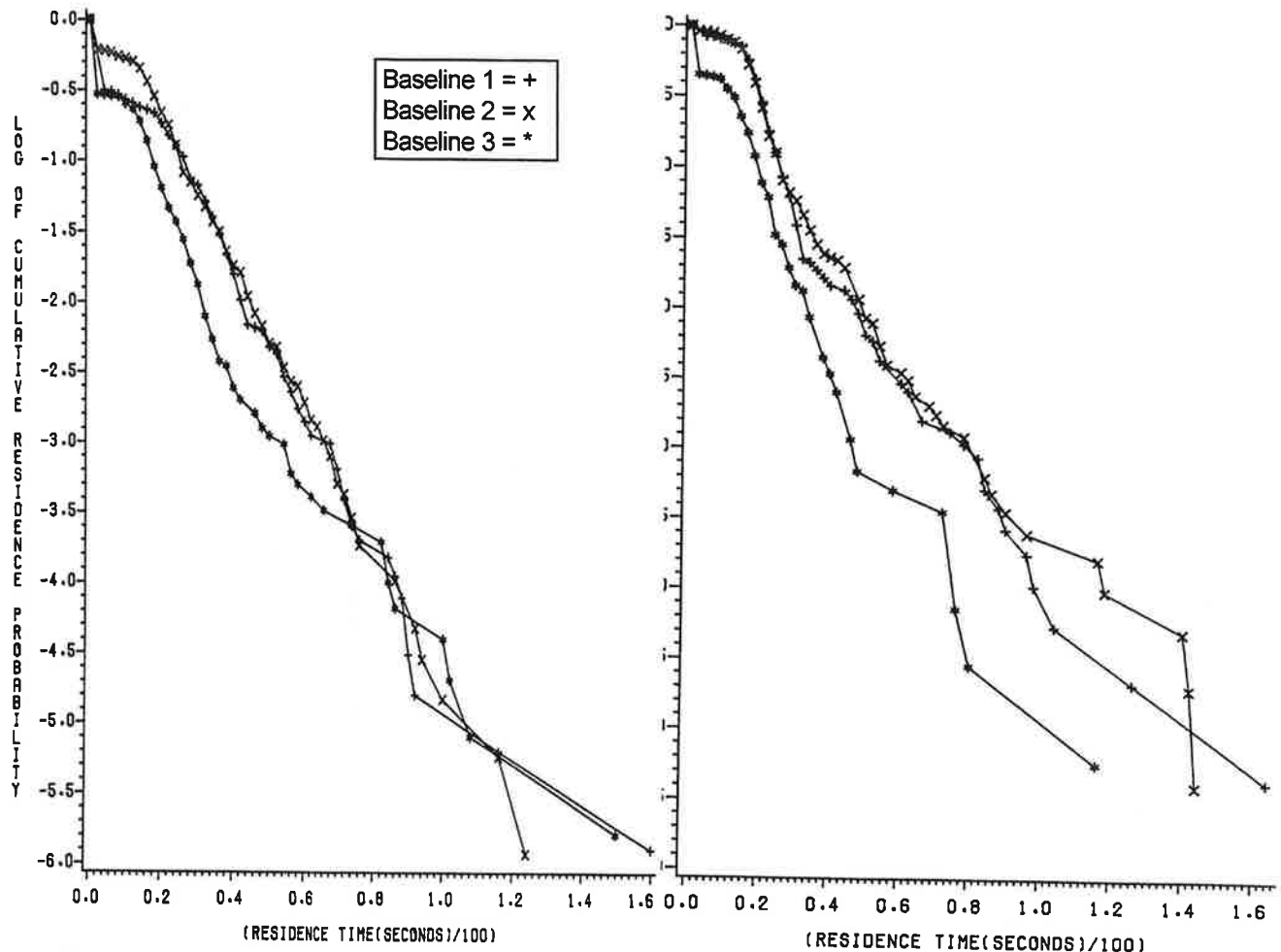


Figure 14. Cumulative Residence Probability vs. Time, All Kennedy Baselines, No Crosswind
 Selection: Left: B-707, Right: B-747

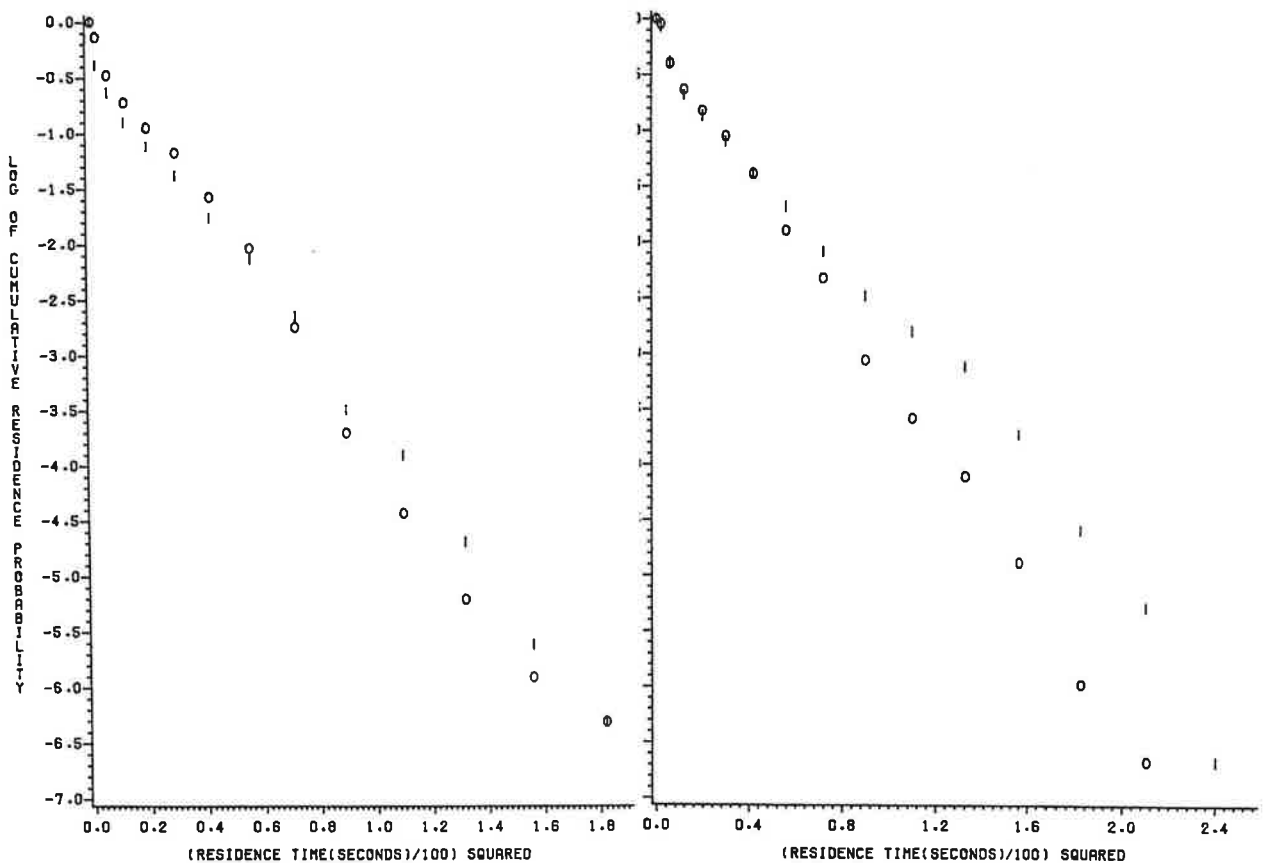


Figure 15. Cumulative Residence Probability vs. Time, Inner (I) and Outer (O) Heathrow Baselines: Left: B-707, Right: B-747

Figure 15 shows the Heathrow (LHR) residence probability data³ plotted against time squared. In contrast to the Kennedy data in Figure 14, a single line gives a reasonable fit to the data from each baseline. [Some difference is noted between the two baselines for the B-747 data. The lower persistence probability for the outer Heathrow baseline was attributed³ to hanger induced turbulence at that location.] The difference in functional dependence between the two airports may be due to the higher proportion of high headwinds at Kennedy (even with the exclusion of headwinds above 15 knots).

The safety analysis described in Section 3.1 uses the residence probability at times of 160, 134, 107, and 80 seconds, corresponding to the single runway separation times now required between pairs of wake-turbulence generator and follower classes. Table 11 compares the estimates of the probability of the residence times of 160, 134, 107, and 80 seconds using LHR inner baseline data and JFK data. The estimates in Table 11 were obtained as follows. First, a straight line with a y-axis intercept of 1.0 was drawn to the data, yielding a rough indication of the functional dependence of the probability of residence on the residence time. Then, estimates of the probability of residence corresponding to the critical residence times were selected from the fitted line. Note that this procedure is a one-parameter fit, i.e., the y-axis intercept was set a priori and only the linear slope may vary to best fit the data. Also note that this procedure relies on the judgment of the analyst, i.e., it is not a mathematical fitting procedure. A procedure of this type was deemed necessary here, and similar procedures are used throughout this report (e.g., to estimate the functional dependence of survival probabilities on time or

Table 11. Comparison of Safe Residence Time Probabilities for Various Wake Classes Using JFK and LHR Data

Class Pair	Safe Separation Time (sec)	Aircraft Type	Database	Total Cases	Cases Residence ≥ 80 sec	Cases Residence ≥ 100 sec	Safe Residence Probability
Heavy Small	160	B-747	JFK	601		9	0.005
			LHR	788		48	0.001
Heavy Large	134	B-747	JFK	601		9	0.010
			LHR	788		48	0.010
Heavy Heavy	107	B-747	JFK	601		9	0.02
			LHR	788		48	0.06
Large Small	107	B-707	JFK	1065	23		0.08
		DC-8	JFK	388	7		0.014
		B-707	LHR	2190	147		0.017
Large Large	80	B-707	JFK	1065	23		0.025
		DC-8	JFK	388	7		0.030
		B-707	LHR	2190	147		0.10

transport probabilities on distance). The procedure selected reflects the considerable amount of judgment required to (1) weight long-lived (or long-transport) over short-lived (or short-transport) vortices, (2) assess the validity of apparent outliers, and (3) weight the data from different baselines.

For the safety analysis (Tables 4 and 18), it was decided to use Heathrow inner baseline data because the Heathrow data had a greater number of observations with residence times in the critical long-lived region (100 seconds for Heavy wake generators, 80 seconds for Large wake generators). Note that the estimated safe residence probabilities from LHR data (Table 11) are greater than from JFK data for the Heavy/Heavy, Large/Small, and Large/Large wake generator/follower pairs. The reverse is true for the Heavy/Small generator/follower pairs. LHR and JFK data yield equal probabilities for the Heavy/Large generator/follower pairs. Thus, the effect of using JFK data estimates in the analysis (Section 5.1) would be to reduce the estimated safe parallel runway separation distance for the Heavy/Small aircraft class pair, and to increase the estimated safe parallel runway separation distance for Heavy/Heavy, Large/Small, and Large/Large aircraft class pairs. There would be no effect on the Heavy/Large class pair.

The effect of the crosswind on the residence time can be seen in Figure 16 which shows the crosswind distribution from all Kennedy residence times greater than 80 seconds. The distribution shows a dip at zero crosswind as might be expected since both vortices will exit the corridor in equal, relatively short times for zero crosswind. A longer residence time is expected when the crosswind cancels the normal induced motion of one of the two vortices. A negative (positive) crosswind

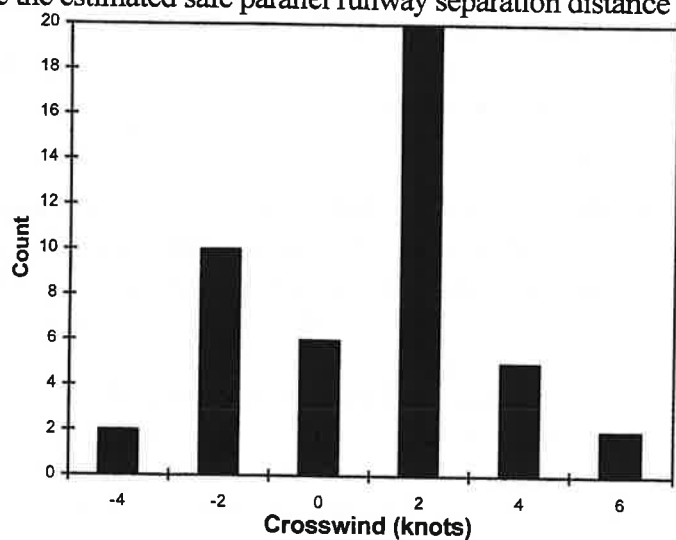


Figure 16. Kennedy Crosswind Distribution for Residence Time ≥ 80 Seconds
All Baselines - All Aircraft Types

corresponds to the starboard (port) vortex remaining in the corridor.

4.3.3 Vortex-Demise Times

The time of vortex demise is well defined except when it drifts off the end of the baseline. In that case the actual demise time may be longer than the measured demise time. Tables 6 to 8 show how many vortices appeared to expire at the +900-foot anemometer which was the end of the baseline. The data presented in this section will ignore this problem. Consequently, the vortex duration may be underestimated in some cases. Removing the +900-foot vortex-demise position cases from the analysis would make an even greater error in the estimated vortex duration since only long-lived vortices can travel 900 feet. One way of obtaining unbiased vortex-demise time plots would be to place limits on the crosswind so that no vortices reach +900 feet.

Figure 17 shows the probability of vortex survival (i.e., detection by the GWVSS) as a function of vortex age squared [$TSQ=(age/100)^2$] for all three baselines for B-707 and B-747 vortices. The data cannot be fitted by a single straight line. The decay is similar for all three baselines. The lower values for line 3 may be caused by half the line being inactive for most of the tests. Figures 18 and 19 show the vortex decay disaggregated by the magnitude of the crosswind. These plots can be fitted reasonably by single straight lines. The nonlinear dependence in Figure 19 thus appears to be a consequence of combining data for different crosswinds.

4.3.4 Model Parameters

In this section the fitted lines for Figures 20 and 21 will be used to determine how the slope of the decay curve is affected by the crosswind. This dependence is needed for the vortex decay model in Appendix A. Table 12 shows the observed decay slopes S for the four crosswind ranges along with the mean or mean square of the crosswind for each range. [The wind parameters listed in Table 12 are those used to fit the vortex decay; mean for B-747 and mean square for B-707.]

Table 12. Crosswind Dependence of Vortex Decay

Aircraft	Crosswind Range (ft/sec)	Mean Crosswind (ft/sec)	Mean Square Crosswind (ft/sec) ²	Slope
B-747	0-5	3		-1.0
	6-10	8		-1.7
	11-15	13		-2.5
	16-20	17		-3.2
B-707	0-5		8	-1.0
	6-10		52	-1.7
	11-15		149	-3.2
	16-20		250	-4.5

The estimated slopes in Table 12 were obtained from the fitted lines in Figures 18 and 19. The slope S is defined with respect to the following equation for the residence probability:

$$P_R(t) = \exp[S \cdot TSQ], \text{ or}$$

$$S = \ln[P_R(t)]/TSQ,$$

where $TSQ = (t/100)^2$. Note that the logarithms plotted in Figures 17 through 19 are natural logarithms (ln).

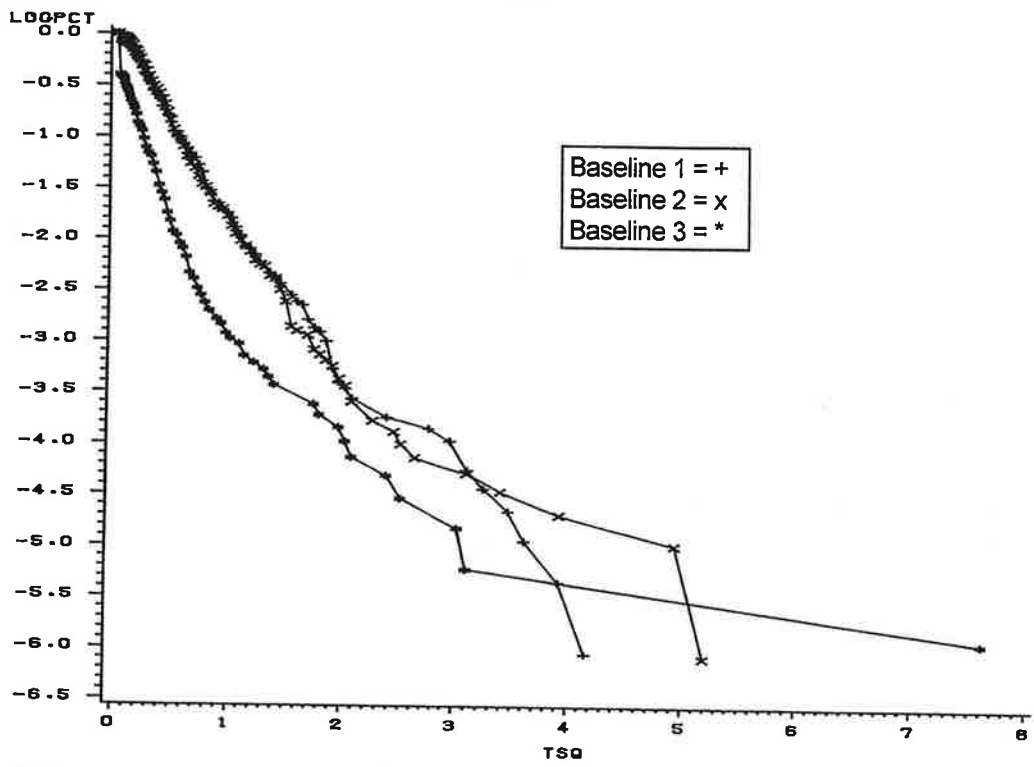
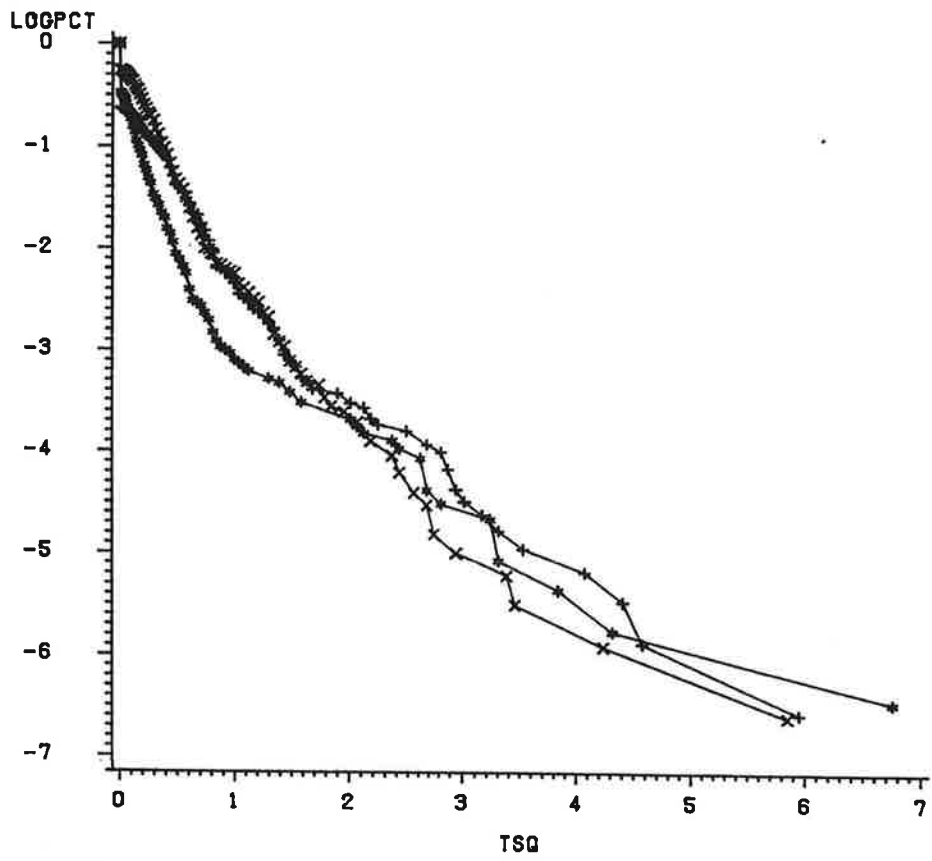


Figure 17. Kennedy Cumulative Survival Probability vs. Time, All Crosswinds
 Top: B-707, Bottom: B-747

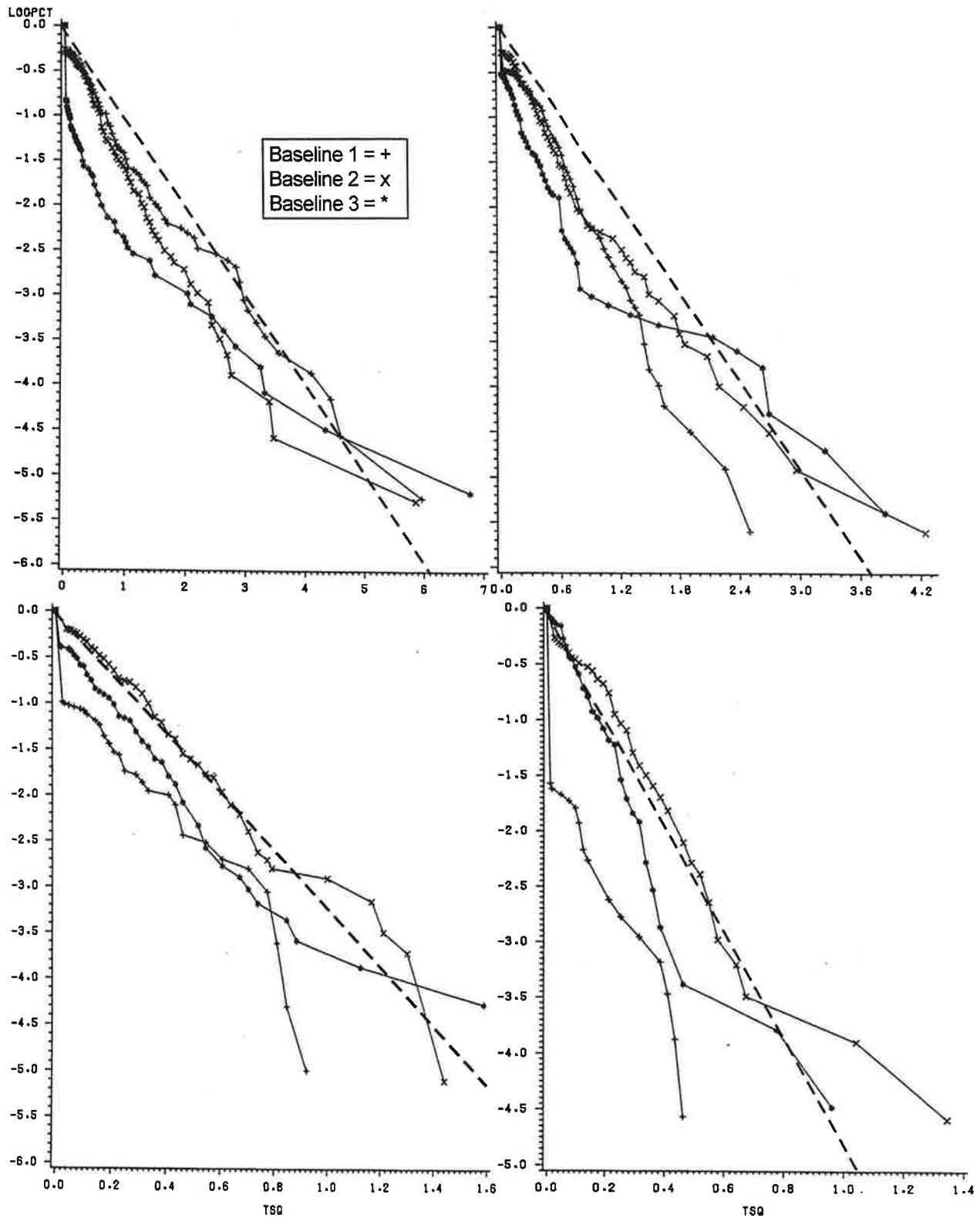


Figure 18. Kennedy B-707 Cumulative Survival Probability vs. Time, Crosswind:
 Top Left: 0-5 ft/sec, Top Right: 6-10 ft/sec, Bottom Left: 11-15 ft/sec, Bottom Right: 16-20 ft/sec

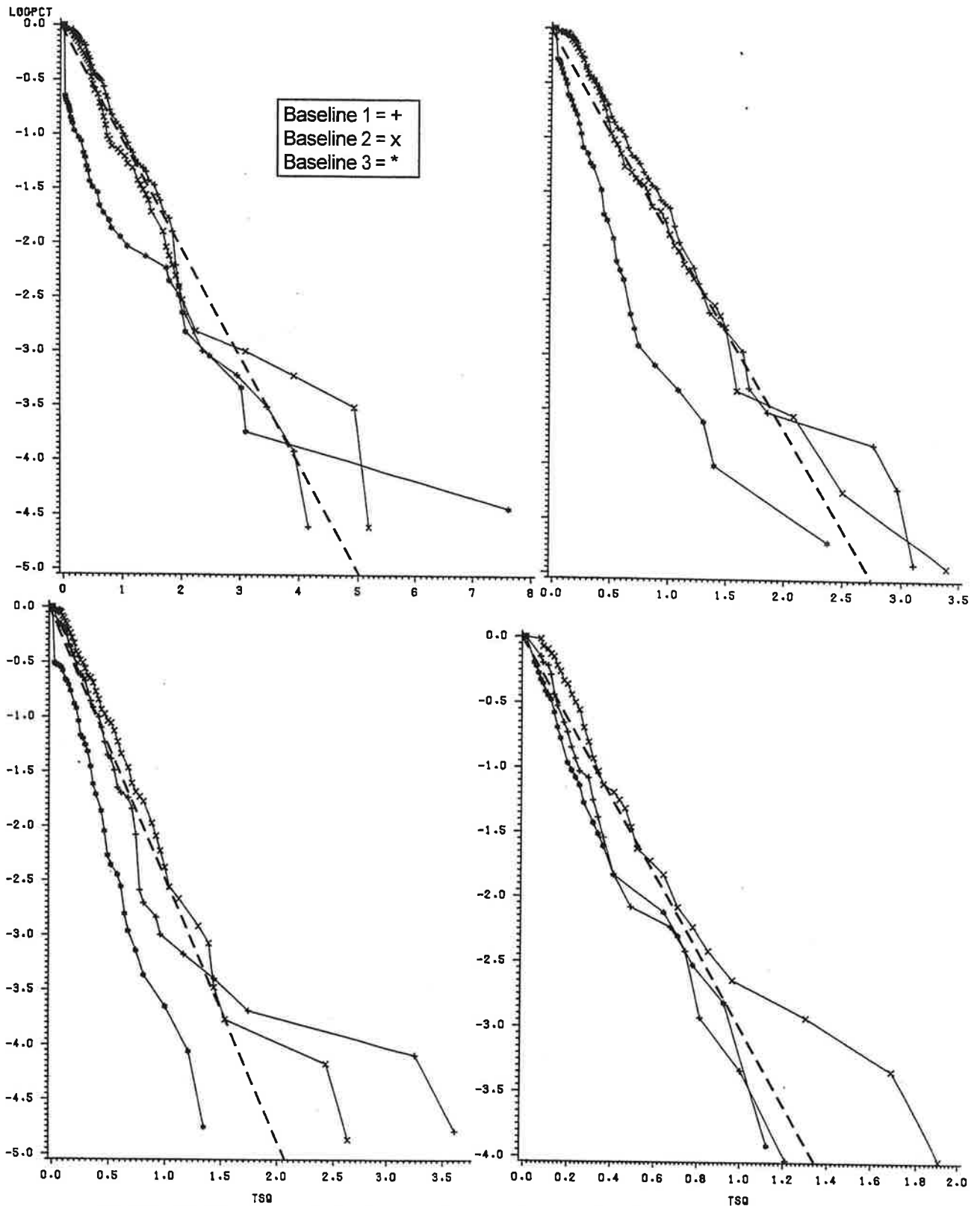


Figure 19. Kennedy B-747 Cumulative Survival Probability vs. Time, Crosswind:
 Top Left: 0-5 ft/sec, Top Right: 6-10 ft/sec, Bottom Left: 11-15 ft/sec, Bottom Right: 16-20 ft/sec

Table 12 suggests a different functional dependence for the two aircraft types. Although the low wind decay slopes are identical for the two aircraft, the B-707 decay is faster than that for the B-747 for higher crosswinds. The slope of the B-747 decay curve is approximately proportional to a constant plus a term proportional to the crosswind, whereas the B-707 decay curve is approximately proportional to a constant plus a term proportional to the square of the crosswind. These relationships are plotted in Figures 20 and 21, respectively.

Table 13 shows the values obtained by fitting straight lines to points in Figures 20 and 21, according to the following equation:

$$S = A(1 + (CW/B)^N).$$

The parameter B is the crosswind CW which doubles the decay rate and N is the power of the dependence.

Table 13. Vortex Decay Parameters

Aircraft	A	B (ft/sec)	N
B-707	-0.87	7.6	2
B-747	-0.55	3.7	1

It should be noted that the measured increase in the GWSS detection decay rate with increasing crosswind is not necessarily all due to vortex decay. The expected increase in the GWSS detection threshold with crosswind may account for some or much of the increase. The observed functional dependence for the B-707 is not what would be expected, however, on the basis of experience^{14,15} with the MAVSS decay data. Ignoring headwind effects, one would expect the GWSS detection threshold strength to increase proportionally to the crosswind. The MAVSS data suggest that the slope of the decay plots (logarithm of persistence probability versus time squared) is proportional to the strength threshold. Thus, one would expect a linear dependence of slope upon crosswind magnitude rather than the quadratic dependence observed for the B-707. Note that, this prediction involves the extrapolation of the MAVSS data to significantly lower vortex strengths.

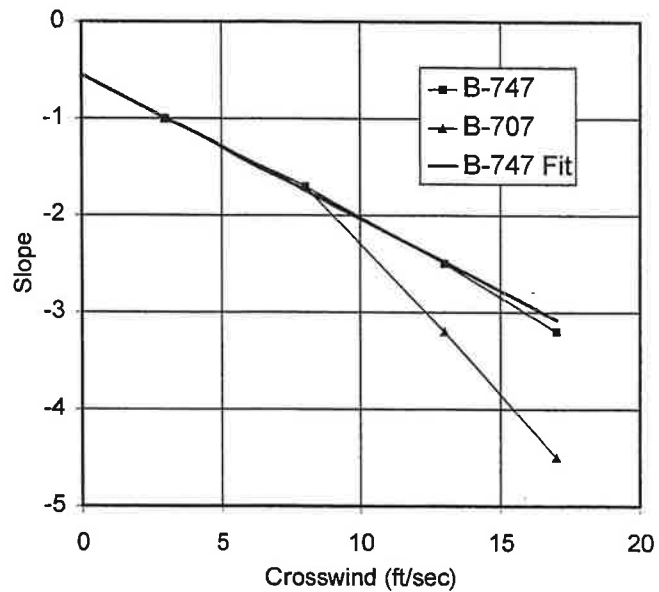


Figure 20. Crosswind Dependence of B-747 Vortex Decay

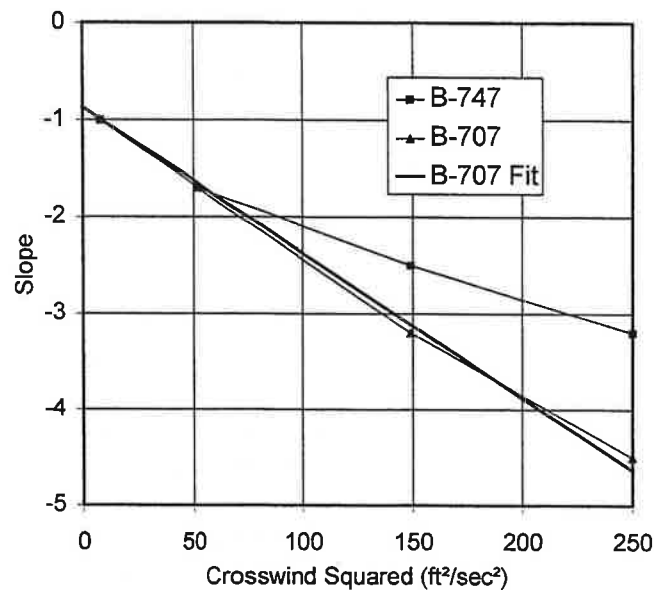


Figure 21. Crosswind Dependence of B-707 Vortex Decay

4.3.5 GWVSS Detection Threshold

An estimate of the GWVSS detection threshold relative to the vortex hazard threshold will be based on comparisons of the GWVSS and MAVSS vortex decay data under similar conditions. This comparison will be based on an extrapolation of the observed MAVSS decay to strengths well below the MAVSS detection threshold (mentioned in Section 4.3.4) and, hence, is subject to uncertainties. The MAVSS decay plots (e.g., Figure 8) to be used¹⁵ were subject to the wind restriction of magnitude less than 8.0 knots. In addition, the MAVSS does not measure successfully for crosswinds less than approximately 3 knots. Thus, the GWVSS plots (Figures 22 and 23) for comparison with MAVSS decay plots depict vortex decay for crosswinds stronger than 3 knots and total winds of less than 8.0 knots. The six plots show the vortex decay for B-707 and B-747 aircraft for the three GWVSS baselines, disaggregated by port/starboard and direction of the crosswind. The point of comparison selected was the value of $TSQ = (\text{time}/100)^2$ where the survival probability drops to 0.05. This value is generally reached with reasonable statistical confidence in all the plots. Table 14 compares the MAVSS and GWVSS values. The MAVSS strength threshold selected corresponds to the hazard model parameter¹⁷ $f = 0.5$ which is currently considered to be a reasonable estimate of the actual hazard threshold. Because the $f = 0.5$ strength is near the MAVSS detection threshold, the $(\text{time}/100)^2$ values used were extrapolated from $f = 1.0$ or $f = 0.75$ assuming that the decay rate is proportional to the strength threshold. The GWVSS values in Table 14 are based on the roughly fitted lines in Figures 22 and 23.

In addition to the $(\text{time}/100)^2$ values, Table 14 also contains a ratio of the average of all lines value of $(\text{time}/100)^2$ at probability of 0.05 to each line's value. For the GWVSS entries, this ratio represents the deviation from the average GWVSS value of $(\text{time}/100)^2$ where the probability of vortex survival is 0.05 for each baseline. For the MAVSS entries, this ratio represents the ratio of the GWVSS detection threshold to the hazard threshold, under the assumption that decay slope is proportional to the strength threshold. The MAVSS averaging radius (5, 10, and 15 meters) corresponds to half the wingspan of the encountering aircraft. Small general aviation aircraft are represented by the 5-meter value, while jet transports of the DC-9/B-737 size are represented by the 15-meter value. Although the B-747 MAVSS data show no consistent size dependence, the B-707 data show a consistently shorter hazard persistence for larger encountering aircraft. These results are based on a simplified analysis and have not considered some important¹⁵ measurement resolution factors.

Table 14. Comparison of MAVSS and GWVSS Decay Data

GWSS Line	B-707				B-747			
	Vortex 1 TSQ	Vortex 1 Ratio	Vortex 2 TSQ	Vortex 2 Ratio	Vortex 1 TSQ	Vortex 1 Ratio	Vortex 2 TSQ	Vortex 2 Ratio
1	1.0	1.30	1.8	1.33	1.5	1.00	4.5	0.89
2	1.5	0.87	2.6	0.92	1.5	1.00	3.5	-
3	1.3	1.00	2.9	0.83	0.9	-	1.5	-
AVG*	1.3	-	2.4	-	1.5	-	4.0	-
MAVSS Radius (m)								
5	0.88	1.5	1.12	2.1	1.26	1.2	1.34	3.0
10	0.62	2.1	0.86	2.8	1.32	1.1	1.32	3.0
15	0.57	2.3	0.74	3.2	0.96	1.6	1.36	2.9

*AVG for B-747 is an average of Lines 1 and 2 only.

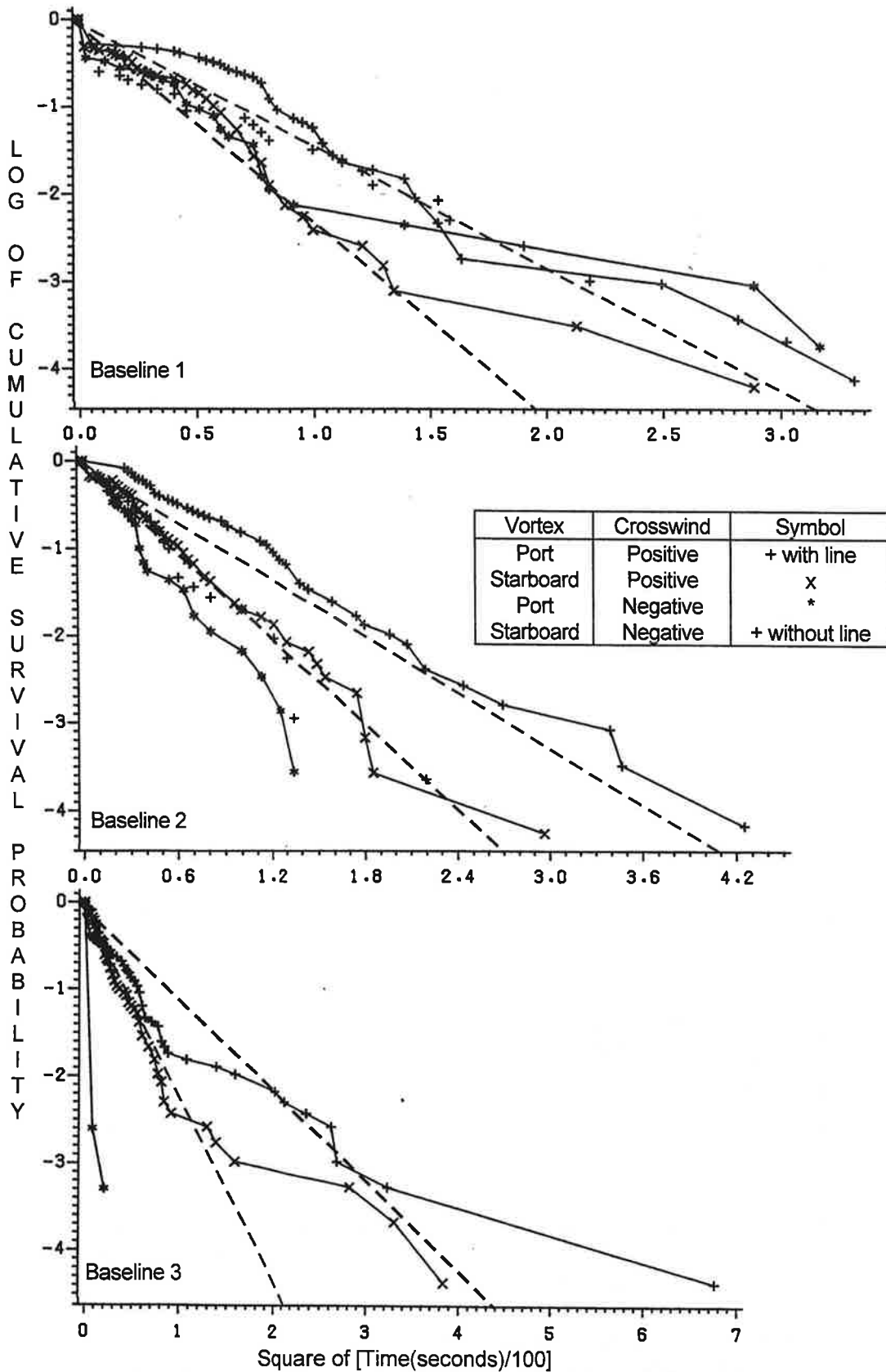


Figure 22. B-707: Log of Cumulative Vortex Survival Probability vs. Time Squared
 Crosswind Magnitude Less Than 3 Knots, Total Wind Magnitude Less Than 8 Knots

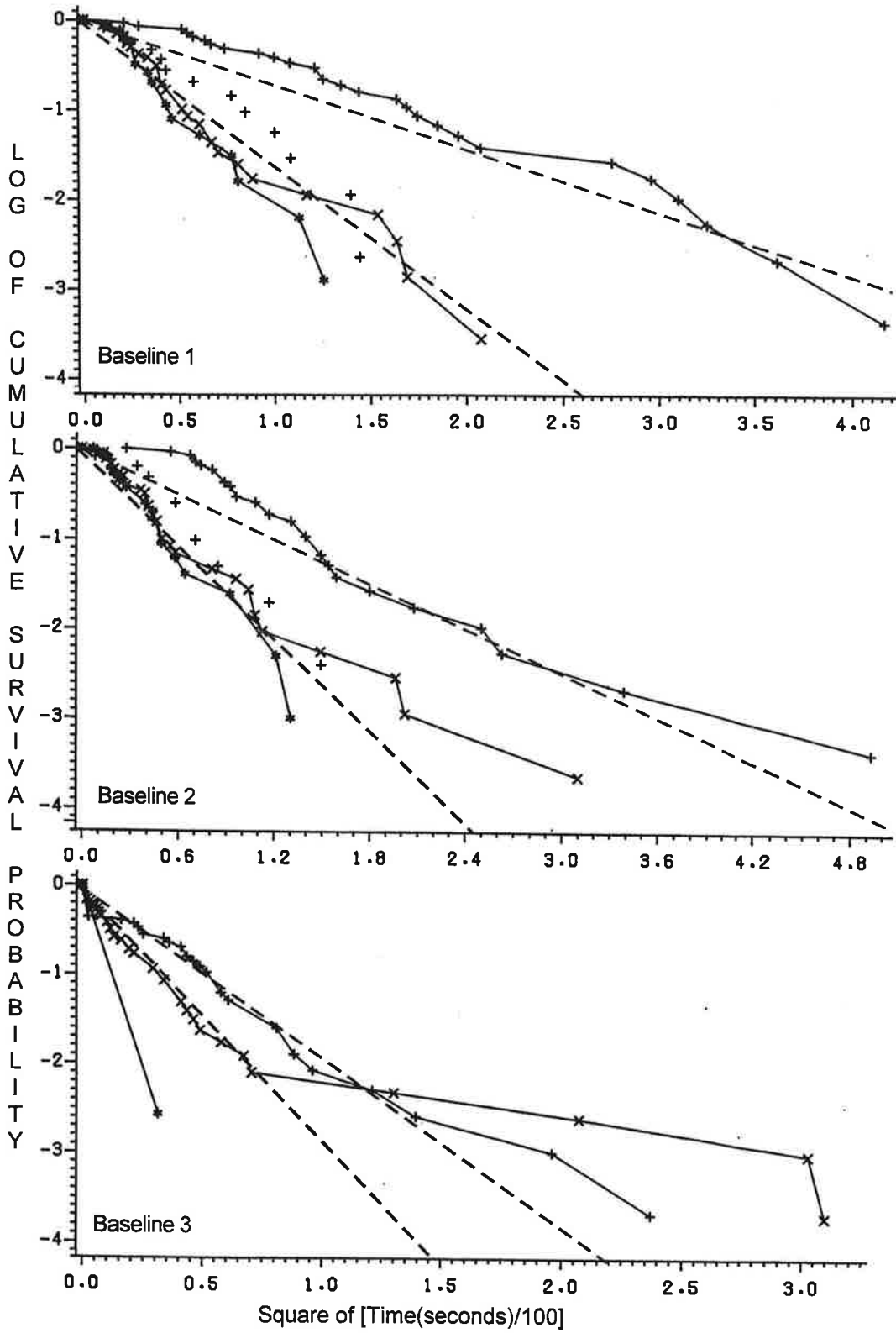


Figure 23. B-747: Log of Cumulative Vortex Survival Probability vs. Time Squared
 Crosswind Magnitude Less Than 3 Knots, Total Wind Magnitude Less Than 8 Knots

The results in Table 14 show that the ratio of the hazard threshold to the GWVSS detection threshold under low wind conditions (less than 8 knots) ranges from one to three with a trend of larger ratios for larger following aircraft and for second vortices. The B-707 and B-747 ratios are comparable. The ratios would be expected to decrease for higher winds.

4.4 TAKEOFF

Tables 15 to 17 show the vortex-demise positions observed in the O'Hare (ORD) takeoff tests. The maximum observed transport distance was 1800 feet. The ORD takeoff vortex-demise position tables are comparable to those for the JFK landing data (Tables 6 to 8). Lines 1 and 2 show a gap in the middle where no anemometers were installed on the runway surface. They also show unusual behavior on the positive side, where a number of anemometers were installed out of their nominal locations in order to avoid a taxiway (+480 to +730 feet).

Figures 24 and 25 show the lateral transport probability for all three baselines for B-707 and B-747 data, respectively. The data were restricted to aircraft that were off the ground but below 250 foot altitude at each baseline. (Aircraft altitude was determined from photographs.) These restrictions should assure that wake vortices should descend to the ground where the GWVSS can detect them. B-707 vortices appear to decay faster in the ORD (takeoff) than in the JFK (landing) data (compare Figures 9 and 24). However, the B-747 vortices appear to decay at roughly the same rate in the O'Hare and JFK data (Figures 10 and 25).

Residence time and vortex-demise time plots are not shown for the takeoff data because of the gaps in coverage in Lines 1 and 2. [A takeoff analysis dealing with the gaps in coverage is currently in process.]

Table 15. O'Hare Baseline #1 Vortex-Demise Positions for Port and Starboard Vortices by Aircraft Type

Death Position (ft)	Aircraft Type															
	B-707		B-727		B-737		B-747		DC-8		DC-9		DC-10		L-1011	
	P	S	P	S	P	S	P	S	P	S	P	S	P	S	P	S
-800	1	5	1	49	1	6		13	1	1	1	10	5	42		8
-700	2	16	3	203	2	8	1	16	0	0	1	31	7	82	1	20
-600	2	10	21	188	1	25	2	7	0	1	3	49	9	59	3	11
-500	5	15	75	282	12	28	3	8	1	2	12	82	21	77	2	12
-450	0	14	68	158	8	28	2	5	1	0	15	63	18	34	9	12
-400	3	9	52	299	7	47	1	8	0	2	15	59	15	68	2	14
-350	9	11	83	281	13	47	2	9	0	1	24	74	19	42	3	12
-300	76	12	80	388	17	40	4	4	1	1	25	96	19	61	1	13
-250	7	5	132	279	14	37	5	6	0	0	38	76	25	43	6	8
-200	2	8	82	207	11	38	3	8	0	1	31	54	20	48	2	16
-165	3	15	65	318	10	27	0	22	0	1	11	72	26	141	6	15
165	12	7	254	100	34	11	15	5	1	1	48	32	96	44	32	9
200	8	9	219	211	24	29	5	7	1		43	50	52	42	16	12
250	12	5	384	165	49	35	11	3	0		99	43	66	41	10	15
300	15	5	441	180	78	18	8	8	1		122	46	84	43	16	10
350	7	13	334	203	38	19	6	3	2		100	72	68	37	8	18
400	13	4	335	83	45	16	6	0	0		94	24	71	25	15	7
450	15	3	443	38	42	4	9	4	1		104	11	112	14	21	6
480	39	12	759	147	87	16	38	8			179	41	245	53	58	17
730	0	2	5	5	1		1	2			0	3	1	12	1	2
760	2		33	0	2		1	1			3		8	9	1	0
800	1		24	1	1		3				7		16	2	6	0
900	2		26	1	2		6				12		22	2	13	1
1000	1		15		0		3				2		14	1	6	
1100	2		6		0		3				2		10	1	5	
1200	1		4		0		1				1		6		1	
1300			2		1		0				0		4		3	
1400			1				1				1		3		1	
1500							0						0			
1600							0						1			
1700							1									
UnDet	236	227	3809	3957	792	813	136	130	12	11	1733	1738	326	366	41	51
Total	407		7745		1292		277		22		2726		1389		289	

Table 16. O'Hare Baseline #2 Vortex-Demise Positions for Port and Starboard Vortices by Aircraft Type

Death Position (ft)	Aircraft Type															
	B-707		B-727		B-737		B-747		DC-8		DC-9		DC-10		L-1011	
	P	S	P	S	P	S	P	S	P	S	P	S	P	S	P	S
-800		8	10	106		8	3	20			1	13	4	83	4	18
-700	2	4	15	109		13	1	7			2	17	4	48	0	18
-600	3	6	39	134	4	10	7	1		1	4	25	19	43	5	7
-500	5	9	86	275	10	20	4	8		1	12	44	20	59	5	7
-450	1	4	65	160	10	10	4	5	1	0	13	38	18	35	9	9
-400	2	7	55	235	4	33	0	8	0	1	9	66	14	62	0	23
-350	5	4	79	206	9	16	1	5	0	0	9	43	15	30	3	4
-300	5	8	88	268	13	27	0	5	0	1	20	53	19	44	3	11
-250	2	3	91	247	9	31	2	3	0	0	25	53	17	27	4	4
-200	2	8	73	166	6	16	0	8	1	1	14	34	15	55	4	10
-165	1	9	92	203	8	5	4	11	0	0	18	16	29	92	5	17
165	4	1	123	85	15	5	8	2	1	0	23	13	74	28	24	6
200	8	3	221	80	19	12	12	7	1	0	40	26	58	26	14	4
250	4	8	301	175	37	12	13	9	2	0	58	24	49	37	8	4
300	12	10	426	216	47	21	9	9	0	0	110	48	69	47	14	14
350	3	7	425	159	39	21	5	3	0	0	87	26	75	35	13	12
400	8	3	252	138	17	16	3	6	0	1	40	22	50	48	8	16
450	4	2	205	106	18	9	4	4	1		32	15	57	44	11	14
480	20	4	418	96	24	8	20	4			36	15	174	50	39	15
730	1	0	34	0	1	0	1	0			5	0	19	2	2	2
760	0	0	22	0	0	0	5	1			2	0	13	3	8	1
800	0	0	31	1	3	0	6	0			1	1	27	3	6	1
900	1	1	11	2	2	0	7	0			3		18	4	9	0
1000	1	1	15		1	1	4	0			2		20	7	6	0
1100	0		12				1	1			1		17	2	2	0
1200	2		11				4						21	1	5	1
1300			0				0						5	1	2	
1400			2				0						4		0	
1500			1				0						5		3	
1600							1									
UnDet	311	303	4543	4529	996	1001	148	150	15	16	2159	2134	460	473	73	71
Total	407		7746		1292		277		22		2726		1389		289	

Table 17. O'Hare Baseline #3 Vortex-Demise Positions for Port and Starboard Vortices by Aircraft Type

Death Position (ft)	Aircraft Type															
	B-707		B-727		B-737		B-747		DC-8		DC-9		DC-10		L-1011	
	P	S	P	S	P	S	P	S	P	S	P	S	P	S	P	S
-800		1	2	18			1	4				2	9	36	1	11
-700		2	1	25		1	0	6				0	6	29	1	2
-600		0	11	62	2	3	3	6			1	13	12	49	3	10
-500		0	15	92	0	4	2	3		1	3	17	12	38	5	12
-450		1	11	58	0	6	1	3		0	4	6	9	13	3	7
-400		2	16	42	1	2	3	0		0	1	9	17	11	2	3
-350	1	2	13	53	0	1	1	3		0	2	5	7	12	2	4
-300	0	1	21	44	1	3	1	0		0	2	7	11	16	1	2
-250	1	1	19	101	1	9	0	5		0	3	23	12	28	2	7
-200	0	0	22	70	1	5	2	2		0	4	14	13	15	0	0
-165	0	2	41	58	1	6	4	4		1	9	13	11	12	2	3
-100	1	1	31	40	3	1	1	2		1	3	6	11	11	1	1
-50	1	2	49	45	2	2	1	5			7	4	13	15	3	4
0	0	0	32	31	2	1	0	0			2	6	7	10	2	1
50	2	1	32	52	3	2	0	0			10	8	13	8	2	1
100	2	1	34	39	6	1	2	1			5	6	14	13	9	2
165	0	1	58	45	2	4	2	1	1		7	6	12	17	5	4
200	1	0	47	46	3	3	1	3	0		11	8	12	11	2	3
250	0	1	98	35	7	2	4	1	1		16	3	22	16	6	1
300	3	1	68	48	5	2	4	1			6	7	18	13	6	2
350	2	2	56	43	4	4	3	2			5	2	12	13	2	5
400	1	2	63	25	9	0	1	1			9	1	23	8	0	0
450	2	0	66	24	4	1	5	2			11	0	22	10	3	1
480	1	1	92	30	4	1	5	3			8	5	42	25	9	3
730	3	1	53	16	3	1	4	4			6	3	37	15	3	3
760	1		17	6			4	2			3		18	15	3	10
800	1		10	1			4	4			1		12	7	6	1
900			4	0			3	0			1		13	8	2	0
1000			3	0			2	1					9	4	3	0
1100			1	1			1	0					10	3	2	0
1200			1				2	2					8	6	1	0
1300			0				1	0					4	1		1
1400			2				1	0					1	0		
1500			1				1	1					2	0		
1600													0	0		
1700													1	0		
1800														1		
UnDet	376	373	6666	6506	1201	1200	204	201	19	18	2544	2510	923	890	193	181
Total																

OHARE DATA:

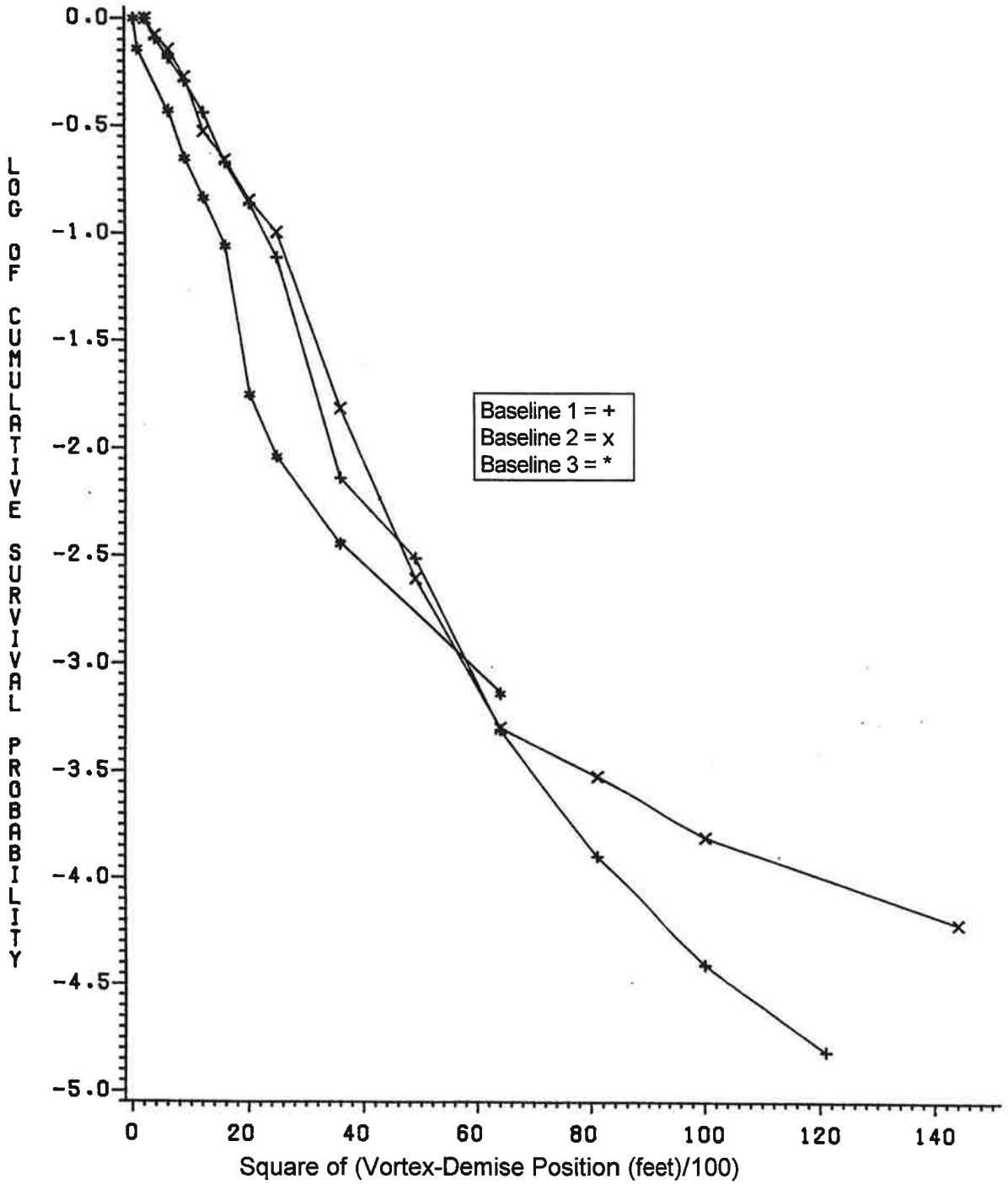


Figure 24. O'Hare B-707 Cumulative Vortex Survival Probability vs. Distance

O'HARE DATA:

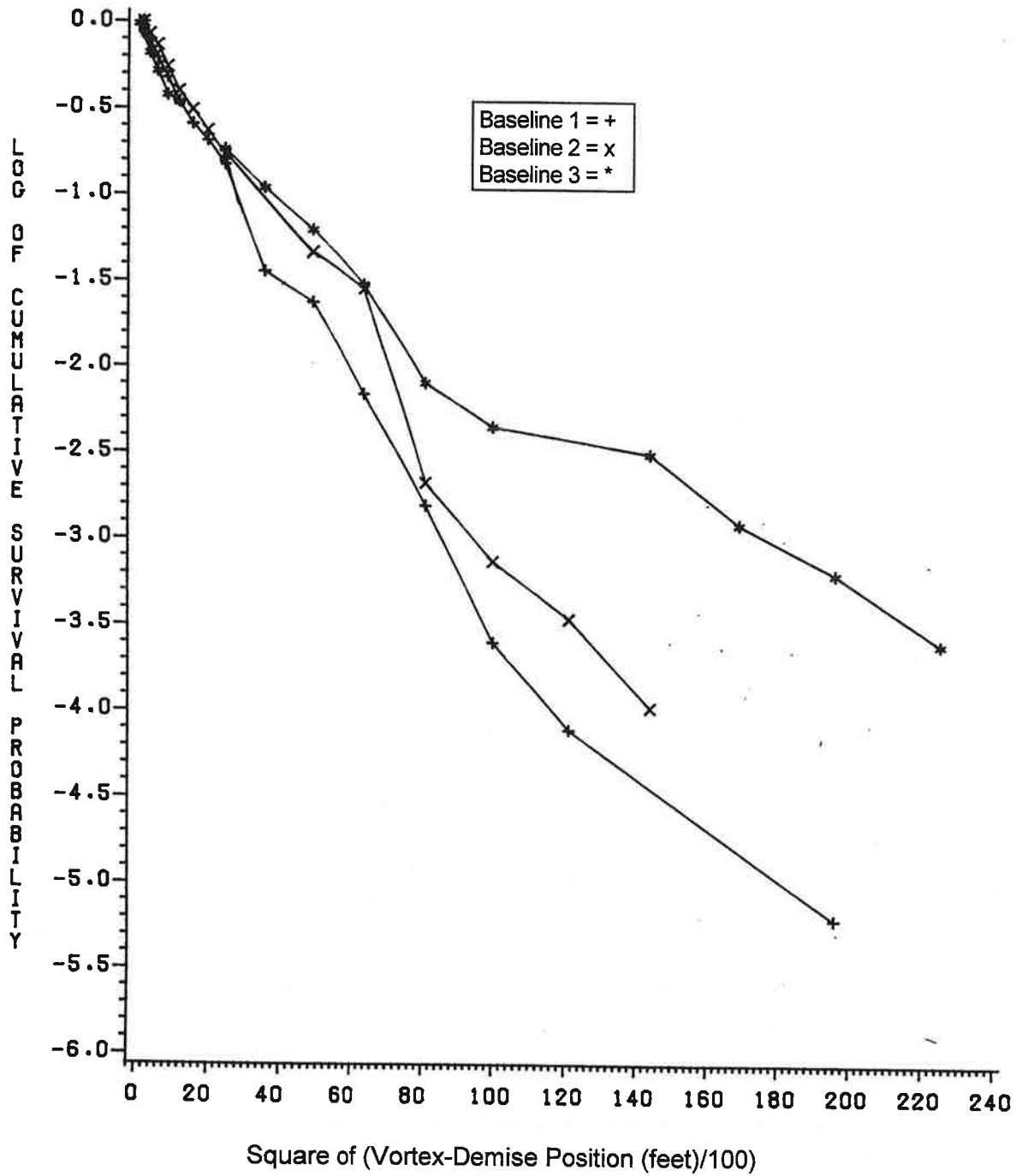


Figure 25. O'Hare B-747 Cumulative Vortex Survival Probability vs. Distance

5. SAFETY ANALYSIS SUMMARY

This chapter summarizes the safety analysis described in Appendix A. The spacing requirements for landing aircraft on parallel runways will be presented here.

5.1 MODEL DESCRIPTION

5.1.1 Components

The safety model consists of the following components:

1. Ambient wind distribution - The actual distribution is fitted to a normal distribution with the equivalent standard deviation.
2. Vortex decay model - The vortex lifetime is assumed to depend upon the ambient crosswind. The model was derived in Section 4.3.4 and resulted in different functional dependences for the B-707 than for the B-747.

5.1.2 Safety Analysis

The first step of the safety analysis is to calculate the encounter probability for single-runway arrivals. Since existing separation standards are assumed to be safe, the calculated encounter probability for the largest aircraft in the leader class at the single-runway spacing limits is assumed to be safe. The B-707 is taken to represent the Large leader class and the B-747 is taken to represent the Heavy leader class. The safe distance spacings (3, 4, 5, and 6 NM) in Table 2 can be converted to safe time spacings (80, 107, 133 and 160 seconds) by assuming a consistent landing speed (135 knots). Thus, the first three columns of Table 18 list (a) five class pairs from Table 2, (b) the representative aircraft type for the leader class (B-747 or B-707) and (c) the safe single-runway time spacing.

The encounter probability at a given plane perpendicular to the extended runway centerline is assumed to be proportional to the probability of a vortex residing within a safety corridor of width ± 150 feet from the extended runway centerline. [The residence probability versus time was calculated from the ambient wind distribution and the decay model. Figure 33 shows the results for the B-747.] Column four of Table 18 lists the assumed residence probabilities for the safe separation times. They were taken from Table 11 for LHR (more conservative than for JFK) and *not* from the model calculations.

The model then calculates the probability $P(D)$ that a vortex will be transported a lateral distance D . The results for the B-707 and B-747 are plotted in Figures 28 and 29, respectively. The midpoints between the two crosswind directions were used for the subsequent safety analysis.

Independent parallel runway approaches are assumed to be safe if the encounter probability $P_E(D)$ is no greater than the safe encounter probability calculated for single-runway approaches. The model calculates the relationship between the probability of a vortex transporting a distance D to the independent-arrival probability of encountering a vortex within a safety corridor of size $\pm d$ and obtains the simple ratio: $P_E(D)/P(D) = (2d/S)\langle 1/v \rangle$, where S is the time spacing of a stream of the "leading" aircraft and $\langle 1/v \rangle$ is the mean of the inverse crosswind leading to vortices reaching the parallel runway at spacing D .

Table 18. Parallel-Runway Safe Separation Analysis

Class Pair	Lead Aircraft	Safe Single-Runway Spacing (sec)	Safe Residence Probability	Leader Spacing S (sec)	P(D)	$(2d/S) < 1/v >$	Safe D (feet)
H/S	B-747	160	0.0010	107	0.0063	0.16	1900
H/L	B-747	133	0.010	107	0.053	0.19	1300
H/H	B-747	107	0.06	107	0.24	0.25	700
L/S	B-707	107	0.017	80	0.059	0.29	1100
L/L	B-707	80	0.10	80	0.26	0.38	600

The final step of the safety analysis is to find a value of D that gives $P_E(D)$ equal to the safe single-runway encounter probability. Independent parallel-runway operations should then be safe for that class pair for runway spacings equal to D or greater.

5.2 PARALLEL-RUNWAY SPACING ANALYSIS

Table 18 presents the results of the analysis described in the last section for $d = 150$ ft. The final four columns list the parameters of the analysis. The safe value of D was defined to only the nearest 100 feet, so that the analysis parameters do not precisely agree with the analysis equations.

The results show that there is a strong dependence of the safe separation upon the classes of aircraft involved. Because of the uncertainties in the assumptions of the model, the absolute values cannot be trusted. However, the results indicate that the wake-independent operation of parallel runways may be possible for restricted aircraft classes at separations much less than the current 2500-foot standard. Further investigation appears to be warranted.

Note that one assumption of the model, namely random, *independent* arrival times on the parallel runways is unrealistic and will have to be examined more closely since the actual operations permitted on close-spaced parallel runways must be *dependent* to prevent aircraft encounters.

6. CONCLUSIONS

The following conclusions were drawn from the four primary areas of the study.

6.1 PARALLEL-RUNWAY SEPARATION STANDARD

The study encountered too many uncertainties in critical issues to allow a definite recommendation for changes in the parallel runway separation standard. The following areas were significant problems:

1. The dependence of the GWVSS detection threshold on crosswind and vortex height.
2. Database quality, such as small numbers of critical cases, lack of intermediate data, and non uniform editing.
3. The lack of vortex strength data.

However, the analysis does indicate that more and better data could be used to set revised parallel runway separation standards. Such actions are currently underway.

6.2 VORTEX MODELING

The modeling of vortex transport and decay gave useful information, but the calculated vortex transport and residence probabilities did not agree very well with the measured values. The reasons for the disagreements were not identified, but some are related to the problems noted above. The model assumes that crosswind magnitude determines vortex decay; a more realistic model must consider turbulence, stratification and particularly the strong interaction of the wake with the ground, which appears to dominate wake decay near the ground.

6.3 SAFETY METHODOLOGY

The safety methodology developed for the study is a promising start toward a precise determination of the parallel runway separation standard. A refined transport and decay model is needed to complete this approach. Even in its present form, the safety methodology indicated how much the separation standard might be reduced when parallel runways are used only by certain classes of aircraft. Table 19 shows the results of the analysis.

Table 19. Estimated Separations for Wake-Turbulence-Independent Operation of Parallel Runways

Classes	Safe Separation (ft)
Heavy/Small	1900
Heavy/Large	1300
Heavy/Heavy	700
Large/Small	1100
Large/Large	600

NOTE: The separations in Table 19 are listed as an indication of what a complete study might produce and are NOT recommended for adoption.

6.4 GWVSS DETECTION THRESHOLD

In this study the GWVSS detection threshold was estimated for the first time. For winds less than eight knots the threshold was estimated to be one to three times lower than the vortex hazard threshold, with larger ratios for larger following aircraft. The detection threshold is expected to increase with increasing crosswind so that the assumption of constant threshold used in the current safety analysis is probably invalid. If the threshold is proportional to the crosswind, as might be

expected, the ratio could drop to significantly less than one for small aircraft in large crosswinds. In this case GWVSS detection is no longer a conservative indicator of the vortex hazard.

7. RECOMMENDATIONS

The results of this study were not as useful as originally hoped because of the limited understanding of many critical issues. The following recommendations are addressed toward an increased knowledge of these issues. Note that many of the recommendations have already been implemented, as indicated by the references.

1. New software should be written to access the original GWVSS data tapes. [The original software ran on minicomputers and disappeared long ago.] Of particular interest would be an examination of the few cases having either long lateral transport distances or long lifetimes. The goal of such an effort would be to determine the meteorological conditions leading to the most persistent vortex hazard. Reexamining the raw could help answer two other questions. Current processing software can derive vortex height and circulation values from GWVSS data. In addition, the GWVSS data could provide a more representative value for the ambient crosswind than was obtained from the distant wind towers.
2. The available monostatic acoustic (MAVSS) data should be examined¹ with respect to the maximum transport distances. Since this sensing system measures the vortex hazard directly, fewer questions of interpretation should arise than with the GWVSS data. The maximum transport distance instrumented was 1000 feet for landing and 1300 feet for takeoff.
3. The relationship between GWVSS signatures and the monostatic acoustic (MAVSS) strength measurements should be studied¹ using data collected concurrently on the same vortices. Such a study should yield a more realistic model for the GWVSS detection threshold.
4. The German data collection effort at Frankfurt should be monitored closely since they are using state-of-the-art sensors which are superior in some respects to those used in the earlier United States work. The Frankfurt site is ideal in many respects since the runways are often used during low turbulence conditions and one quarter of the aircraft are B-747's. [Many years of Frankfurt GWVSS data are currently being analyzed.]
5. Additional modeling efforts would be useful. Areas where modeling could help are the estimation of residence times on takeoff and corrections for the effects of a short baseline on vortex decay. A transport and decay model based on MAVSS data would be more convincing than the current one based on GWVSS data.

Page intentionally blank

APPENDIX A - MODELS FOR VORTEX TRANSPORT AND PERSISTENCE IN GROUND EFFECT

A.1 GOAL AND PHILOSOPHY

The goal of the modeling effort presented here is to define the minimum separation between parallel runways which will allow independent operations with respect to wake turbulence considerations. The definition of "safe" will be based on the observed safety of existing separations for aircraft landing or taking off. The modeling is required to transfer the single runway encounter probability, now accepted as safe, to the parallel runway situation. The same encounter probability should be considered safe for parallel runway operations. The unknown parameters in the models will be based on observed data. The consistency of the data for the single and parallel runway cases with the models will serve to justify the assumptions used in generating the models.

Since the models will be used to predict probabilities rather than detailed vortex trajectories, many approximations can be made to simplify the analysis without seriously affecting the final results which are integrals over the distribution of the ambient wind. More detailed models were presented¹⁹ in an earlier study.

Chapter 5 presents a summary of this appendix and the derived results for minimum parallel-runway spacing.

A.2 MODEL DEFINITIONS

The models to be defined here assume that the probabilities of vortex persistence at various lateral locations can be compared on a single line perpendicular to the aircraft flight path. This assumption is based on the expectation that the probability of an encounter at different positions along the flight path is comparable for each situation being considered. Not only does this assumption simplify the analysis, but it also makes the models compatible with existing ground-effect data which were collected by a sensor line perpendicular to the flight path. The justifications for this assumption will be presented in Section A.2.7 after the details of the various models have been discussed.

The assumption will be made initially that the vortex height can be ignored in so far as lateral transport and decay are concerned. This assumption is less valid for takeoff than for landing because of the greater variation in aircraft height over the region of space being considered. Section A.2.8 will address changes in the model which would make it more suitable for takeoff. In any case, the height dependence of the ambient wind and the detailed effects of height on the induced vortex motion will be ignored.

The models will be compared to data collected by the Ground-Wind Vortex Sensing System (GWVSS) which has a vortex detection threshold below the vortex hazard threshold, at least for low winds. The fact that the GWVSS detection threshold depends upon the turbulence level (and hence the wind strength) will be ignored in the analysis. Since current wake vortex theory holds that high turbulence levels promote vortex decay, the variation of the GWVSS detection threshold is assumed to be unimportant for determining separations standards which must be based on the most persistent vortices. Since the encounter geometry is identical for the single runway and parallel runway

situations, any errors in the hazard model should cancel out in probability comparisons between the two situations.

The coordinate system used in the analysis is defined in Table 20 and Figure 26.

Table 20. Coordinate System

Direction	Position	Wind
Along Runway	x + is out approach path from runway threshold	u + is headwind
Perpendicular to Runway	y + is to right from pilot's point of view zero is extended runway centerline	v + is to right from pilot's point of view
Vertical	z + is up	not used

A.2.1 Ambient Wind Distribution

The primary factor affecting the lateral transport of wake vortices is the ambient crosswind v . On the other hand, the decay of vortices will sometimes be assumed to depend upon the magnitude of the total wind $(u^2 + v^2)^{1/2}$, where u is defined as the headwind. Since the ambient wind will be the driving function for the models to be developed, it is necessary to define several wind distribution functions. $F(v)$ is the crosswind distribution and $G(u)$ is the headwind distribution. If the headwind and crosswind are *uncorrelated*, as will normally be assumed for simplicity, the total wind distribution $H(u, v)$ is given by the product $H(u, v) = G(u)F(v)$. These distributions satisfy the following integral relationships:

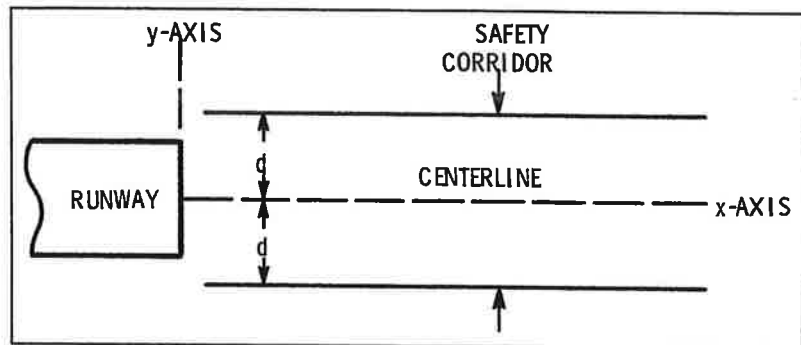


Figure 26. Coordinate System

$$\int_{-\infty}^{\infty} F(v)dv \equiv 1, \quad (1)$$

$$\int_{-\infty}^{\infty} G(u)du \equiv 1. \quad (2)$$

The following relationships are true even when the u and v distributions are correlated:

$$\int_{-\infty}^{\infty} H(u, v)du \equiv F(v), \quad (3)$$

$$\int_{-\infty}^{\infty} \int_{-\infty}^{\infty} H(u, v)dudv \equiv 1. \quad (4)$$

A.2.2 Vortex Persistence Probability

The basic vortex decay process is defined by the probability $Q(t, u, v)$ that the vortex lasts at least t seconds under ambient wind conditions u, v . As mentioned above, a useful new function for the dependence of decay upon u and v may be $Q^*(t, (u^2 + v^2)^{1/2})$ where the actual u, v dependence is only upon the wind magnitude. However, some data seem to show that a crosswind of a given magnitude is more effective in promoting vortex decay than a headwind of the same magnitude. For many purposes the dependence of Q upon the headwind u will be integrated out to leave the probability $P(t, v)$ that the vortex lasts at least t seconds with a crosswind v :

$$\int_{-\infty}^{\infty} G(u)Q(t, u, v)du \equiv P(t, v), \quad (5)$$

This equation assumes that the u and v distributions are uncorrelated, which may not always be true, if, for example, a well defined prevailing strong wind direction exists. One additional dependence of the vortex decay will be introduced on occasion. The vortex upwind with respect to the ambient crosswind is observed to decay more rapidly than the downwind vortex. Subscripts u (upwind) and d (downwind) will be used on the probabilities Q and P (e. g., P_u and P_d) when the decay of these two vortices is being distinguished.

A.2.3 Vortex Lateral Transport Model: Landing

The two wake vortices are assumed to be generated in ground effect at time $t = 0$ at y positions of $-b$ (port vortex) and $+b$ (starboard vortex). Their subsequent motion is influenced by the ambient crosswind v and their induced lateral velocities of $+i$ (starboard vortex) and $-i$ (port vortex). The resulting velocities and positions are listed in the Table 21.

Table 21. Lateral Motion of Wake Vortices in Ground Effect

Parameter	Port Vortex	Starboard Vortex
Initial Lateral Position	$-b$	$+b$
Transport Velocity	$v - i$	$v + i$
Lateral Position $y(t)$	$-b + (v - i)t$	$b + (v + i)t$
Average Crosswind to Reach Position Y at Time t	$i + (y + b)/t$	$-i + (Y - b)/t$

The last entry in the table shows what crosswind is needed for a vortex to arrive at position Y at time t . The parameters v and i were assumed to be constant in the derivation of the equations in Table 21. As far as transport is concerned, this assumption is unimportant as long as v and i are defined as the average values over the time t . This procedure causes problems only when the values change enough to cause the vortex to pass through the same position more than once. Further discussion of this issue will be presented in Section A.2.7. In the subsequent model development, the average crosswind velocity to reach a position Y will be used as a limit in an integration over the crosswind distribution $F(v)$. The distinction between velocity and average velocity will become unimportant since both will have very similar distributions.

A.2.4 Single-Runway Residence Probability

The standard analysis of single-runway safety assumes a safety corridor of ± 150 feet for landing and ± 200 feet for takeoff. Figure 26 shows the corridor geometry. Vortices residing inside the corridor

pose a potential hazard to following aircraft while those outside cannot affect the following aircraft. Define the limits of the safety corridor as $\pm d$ with respect to the runway centerline. Table 22 defines the crosswind limits for the two vortices which result in a vortex residing inside the corridor for at least a time t , using the last row of Table 21 to determine the average crosswind needed to reach the edges of the corridor.

Table 22. Crosswind Limits on Vortex Residence: Single Runway

Corridor Edges	Port Vortex	Starboard Vortex
$Y = -d$	$v_- = i + (b - d)/t$	$v_- = -i - (b + d)/t$
$Y = +d$	$v_+ = i + (b + d)/t$	$v_+ = -i - (b - d)/t$
Average Crosswind = $(v_- + v_+)/2$	$i + b/t$	$-i - b/t$
Width of Crosswind Band = $ v_+ - v_- $	$2d/t$	$2d/t$

One vortex will remain in the corridor for two bands of crosswind with mean values $i + b/t$ and $-i - b/t$ and width $2d/t$. As the time t increases, the width becomes narrower inversely with the time. The probability $P_T(t)$ of at least one vortex not transporting out of the corridor becomes an integral over the crosswind distribution $F(v)$ between the limits given in Table 22. For large times where the velocity width ($2d/t$) becomes very narrow, this probability can be approximated by:

$$P_T(t) = [F(i+b/t) + F(-i-b/t)] (2d/t) \quad (6)$$

This approximation is valid for width $2d/t \ll i+b/t$ or times $t \gg (2d-b)/i$. For long times the probability of a vortex not moving out of the corridor decays inversely with time.

Vortices can be lost from the corridor by decay as well as by transport. The proper way to calculate the probability $P_{RES}(t)$ of a vortex residing in the corridor is to integrate the product $F(v)P(t,v)$ over the limits in Table 22. The probability of residence for an increment in v is equal to the product of the probability $F(v)$ of crosswind v times the probability $P(t,v)$ that a vortex will last for time t with crosswind v . When the velocity bands are narrow, the following approximate result is obtained:

$$P_{RES}(t) = P(t, i+b/t)[F(i+b/t)+F(-i-b/t)](2d/t) \quad (7)$$

where the assumption has been made that $P(t,v)$ does not depend upon the sign of v . If a vortex remains in the safety corridor when the following aircraft arrives at time S after the arrival of the generating aircraft, then a wake vortex encounter may result. The probability of a potential vortex encounter is thus the residence probability at time $t = S$:

$$P_{ENCT}(S) = (2d/S)P(S, i+b/S)[F(i+b/S)+F(-i-b/S)] \quad (8)$$

A.2.5 Lateral Transport Probability

This section will evaluate the probability $P_D(Y)$ that a vortex will move past a point located a distance Y laterally from the runway where it was generated (i.e., from the extended runway centerline). Again, this probability is given by an integral over the crosswind distribution $F(v)$ times the persistence probability $P(T,v)$ where T is the time it takes the vortex to reach position Y with crosswind v . The relationship between Y and v was given for the two vortices in the last line of Table 21. For the moment, ignore the differences between the two vortices, considered as port and starboard or upwind

and downwind [$i=0, b=0, P_u(t, v) = P_d(t, v)$] so that the form of the lateral transport probability can be more easily recognized. The relationship between $T, Y,$ and v becomes: $T = Y/v$ and the lateral transport probability becomes:

$$P_D(Y) = \int_0^{\infty} F(v)P(Y/v, v)dv, \quad (9)$$

The integral extends over only one sign of the crosswind since the vortex can never reach point Y if it is moving in the opposite direction. Mathematically, this limitation is equivalent to insisting that T remain positive. Now, include the complications involved with distinguishing the two vortices. Assume that Y is positive so that the starboard vortex is the downwind vortex and the port vortex is the upwind vortex. The relationship between $T, Y,$ and v becomes:

$$\text{Upwind Vortex:} \quad T = (Y+b)/(v-i)$$

$$\text{Downwind Vortex:} \quad T = (Y-b)/(v+i)$$

The integrals for the two lateral motion probabilities become:

$$P_{Du}(Y) = \int_i^{\infty} F(v)P_u((Y+b)/(v-i), v)dv, \quad (10)$$

$$P_{Dd}(Y) = \int_{-i}^{\infty} F(v)P_d((Y-b)/(v+i), v)dv, \quad (11)$$

The structure of these integrals can be simplified by substitutions which subtract or add i :

$$P_{Du}(Y) = \int_0^{\infty} F(v+i)P_u((Y+b)/v, v+i)dv, \quad (12)$$

$$P_{Dd}(Y) = \int_0^{\infty} F(v-i)P_d((Y-b)/v, v-i)dv, \quad (13)$$

It is not clear, a priori, which vortex will have the larger probability $P_D(Y)$. The downwind vortex starts closer and moves faster but it also decays more rapidly. The total probability $P_D(Y)$ of a vortex moving a distance Y is given by the sum of $P_{Du}(Y)$ and $P_{Dd}(Y)$. This summing has a problem with normalization when the probabilities are large since the total probability could be as large as two. However, for very small probabilities the duration of the two vortices is not particularly correlated and the total probability of a vortex reaching a distance D from one generating aircraft is well represented by the sum.

A.2.6 Parallel-Runway Residence Probability

The first part of the parallel runway residence analysis is very similar to that for a single runway described in Section A.2.4. The difference is that the limits are set at $Y = D \pm d$ where D is the spacing between the two runways. The geometry is shown in Figure 27. The crosswind analysis for the parallel-runway case leads to Table 23 which is analogous to Table 22 for the single-runway case.

Table 23. Crosswind Limits on Vortex Residence: Parallel Runway

Corridor Edges	Port Vortex	Starboard Vortex
$Y = D - d$	$v_- = i + (b - d + D)/t$	$v_- = -i + (D - d - b)/t$
$Y = D + d$	$v_+ = i + (b + d + D)/t$	$v_+ = -i + (D + d - b)/t$
Average Crosswind = $(v_- + v_+)/2$	$i + (D + b)/t$	$-i + (D - b)/t$
Width of Crosswind Band = $ v_+ - v_- $	$2d/t$	$2d/t$

The parallel runway case has the same spread in crosswind as the single runway case, but the average crosswind in the velocity band leading to residence is larger. If the separation distance is large enough, the velocity band will be small enough to ignore the variation in either the crosswind distribution function $F(v)$ or the persistence probability $P(t, v)$. The condition for the validity of this approximation is that $D \gg 2d \pm b \pm it$, where the (+) is for the downwind (starboard) vortex and the (-) is for the upwind (port) vortex. As in the last section, D is assumed to be positive. The residence probability $P_{DRES}(t)$ for a vortex at time t becomes:

$$P_{DRES}(t) = (2d/t) \{ P_u[t, i+(D+b)/t] F[i+(D+b)/t] + P_d[t, -i+(D-b)/t] F[-i+(D-b)/t] \} \quad (14)$$

The following analysis will consider a particular longitudinal analysis location $x = X$ on the first runway. Now adopt a model for how aircraft are using the parallel runways. Assume that the generating aircraft are uniformly spaced by time S on the first runway. In *independent** operations, the aircraft using the second runway a distance D away can pass position X at any time relative to the operations on the first runway. [Ignore headwind effects that transport the wake in the x direction.] The residence probability $P_{DRES}(t)$ must therefore be integrated in time to obtain the encounter probability. Define time with respect to arrivals at location X on the first runway:

<u>Time</u>	<u>Aircraft Number</u>
S	n+1
0	n
-S	n-1
-2S	n-2
-3S	n-3
.	.
.	.

If the random arrival time of an aircraft at the analysis point on the second runway is in the range 0 to S , it may interact with the wake vortices from any of the preceding aircraft (n, n-1, n-2, n-3, etc.). Since the encounter probability is periodic with period S , there is no need to average the probability over more than one period. Thus, the encounter probability is given by the average over the range 0 to S :

$$P_{ENCT} = (1/S) \int_0^S [P_{DRES}(t) + P_{DRES}(t+S) + P_{DRES}(t+2S) + \dots] dt$$

* Note that, operations on close-spaced parallel runways are actually likely to be *dependent* to prevent aircraft encounters.

$$P_{ENCT} = (1/S) \int_0^{\infty} P_{DRES}(t) dt, \quad (15)$$

This integral can be simplified by changing to the crosswind as the integration variable. The following expression is obtained for the encounter probability:

$$P_{ENCT}(D) = (2d/S) \int_0^{\infty} (dv/v) \{P_u[(D+b)/v, v+i]F(v+i) + P_d[(D-b)/v, v-i]F(v-i)\} \quad (16)$$

The parallel runway encounter probability is thus very closely related to the probability for a vortex traveling at least a distance D. The difference is the factor 1/v inside the integral. This factor results from the fact that slowly moving vortices remain in the corridor for a longer time and therefore make a larger contribution to the encounter probability. The following relationship thus relates the encounter probability on a parallel runway separated by distance D to the probability that a vortex moves laterally at least a distance D:

$$P_{ENCT}(D)/P_D(D) = (2d/S) \langle 1/v \rangle \quad (17)$$

A.2.7 Model Justification

The safety model is based on an analysis of vortex transport and decay in a single plane perpendicular to the aircraft flight path. Variations in vortex behavior along the flight path are ignored under the premise that the variation along the flight path is essentially similar for the two situations being compared, namely the single runway encounter and the parallel runway encounter.

The variations in vortex motion and decay along the flight path can become very complex because of variations in crosswind and random turbulence. Figure 27 shows some possible variations for the vortex position. A complete analysis of the vortex encounter probability must take these variations into account. The net effect of such an analysis would be to define an effective distance along the flight path where the vortex behavior becomes uncorrelated so that encounter probability becomes independent. The total encounter probability then becomes the sum of the encounter probability at each independent location.

The difference between the single-runway and parallel-runway encounter situations is primarily in the magnitude of the crosswind. A single-runway encounter occurs with crosswinds comparable to the natural induced vortex motion, i.e., 5-9 ft/sec. The parallel runway encounters occur over a broad range of significantly larger velocities (see Section A.3.3). The shape of the vortex position at a given time, as shown in Figure 27, depends upon the variation of the crosswind and is independent of the mean wind. Since the higher crosswind is likely to be associated with larger crosswind variations, the vortex is likely to have more and bigger wiggles for the parallel runway situation. However, such wiggles promote vortex decay as well as increase the probability of a vortex encounter by reducing the correlation distance. Moreover, the hazard of a vortex encounter is reduced if the aircraft path intersects the vortex for only a very short time. Because of these canceling effects, the net difference between the single-runway and parallel-runway total encounter probability is likely to be small, certainly less than a factor of two in encounter probability.

The model assumes that the height of the vortex is unimportant to the analysis. In one case this assumption may not be completely true. The downwind vortex is frequently observed to rise after it has descended into ground effect, apparently because of wind shear effects. This rise would tend to make it more difficult to detect with the GWVSS system. However, because the downwind vortex is isolated from the upwind vortex when it rises, the induced wind at the ground decreases slowly (inversely with height) so that the detection threshold is unlikely to change by more than a factor of two or three. This variation in GWVSS detection threshold is likely to be less than that due to variations in crosswind turbulence. Measurements with the monostatic acoustic vortex sensing system (MAVSS) could be used to assess the magnitude of this effect.

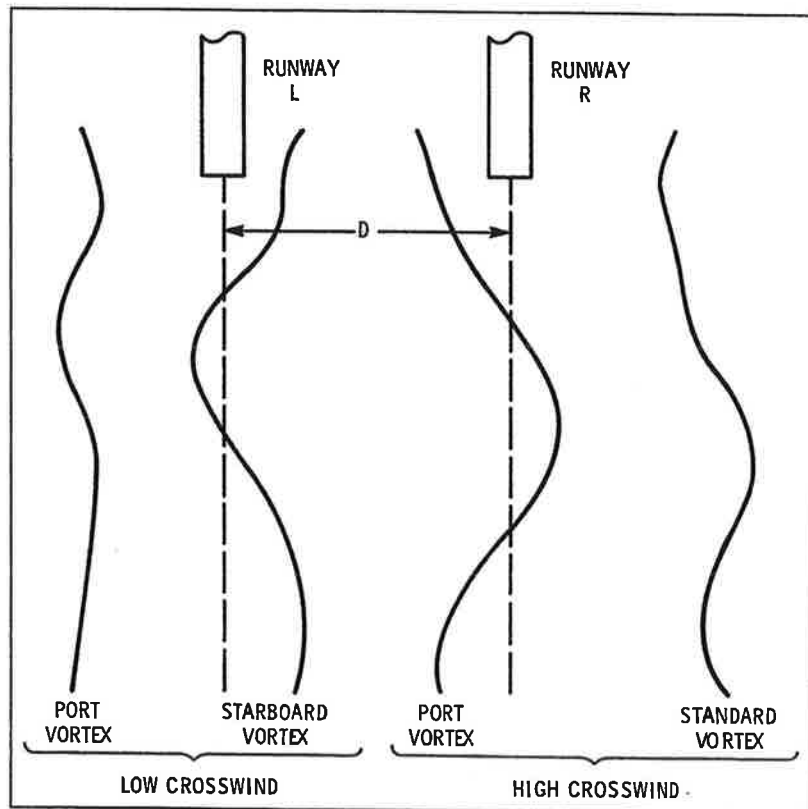


Figure 27. Plan View of Possible Vortex Locations after an Aircraft Has Landed on the Left Runway

A.2.8 Takeoff Modeling

The height h of vortex generation cannot be ignored on takeoff where the aircraft is climbing rapidly within the region where a potential wake vortex encounter could occur. The generation of wake vortices out of ground effect has three consequences for vortex transport and decay:

1. The vortex pair descends with velocity $-w$ until it reaches ground effect. If the vortices do not reach ground effect after a certain amount of time, w will eventually decrease anyway because of vortex decay.

Table 24. Motion of Wake Vortices Out of Ground Effect

Parameter	Port Vortex	Starboard Vortex
Initial Position:		
Lateral (y)	$-b$	$+b$
Vertical (z)	h	h
Out of Ground Effect	Time for Decay = Kt	
Lateral Velocity	v	v
Vertical Velocity	$-w$	$-w$
Lateral Position $y(t)$	$-b + vt$	$b + vt$
Crosswind to Reach	$(Y + b)/t$	$(Y - b)/t$
Position Y at Time t		
In Ground Effect	Time for Decay = $t - T(1-K)$	
at time $T = (h-b)/w$		
Lateral Velocity	$v - i$	$v + i$
Vertical Velocity	0	0
Lateral Position $y(t)$	$-b + vt - i(t - T)$	$b + vt + i(t - T)$
Crosswind to Reach	$i + (Y + b - iT)/t$	$-i + (Y - b + iT)/t$
Position Y at time t		

Assume that w remains constant for the times of interest in the model.

2. The vortex pair does not separate laterally until it reaches ground effect, after which it separates at the induced velocities $\pm i$.
3. The wake vortices may decay more slowly out of ground effect. This reduced decay is represented in the model by a time reduction factor K ($K < 1$) through which the time in the vortex decay probability $P(t, v)$ is reduced [to $P(Kt, v)$] out of ground effect. This method of representing the slower decay out of ground effect allows for a simple transition to the ground effect decay when the vortices reach the ground.
4. Define h as the height of vortex creation. Descending at rate $-w$, the vortices will reach ground effect at approximately time $T = (h-b)/w$, where the ground effect height b is assumed. The model assumes that the accelerated decay and induced lateral motion in ground effect starts when the wake would reach height b at a constant descent rate; this value is likely too high, but will be assumed since the same assumption will be made in the next section for the GWVSS detection height, where height b is perhaps too low. [Since the model will not be applied, the added complexity of defining two different ground effect heights is not warranted.] In the ideal vortex model, the asymptotic ground effect height is half the separation between the two vortices on generation and the descent velocity w is the same as the induced lateral motion velocity i in ground effect. Table 24 illustrates the assumed vortex trajectories. The crosswind v is assumed to be independent of height in this analysis.

A.2.8.1 Probability of a Vortex Reaching Ground Effect

The analysis of ground-wind vortex sensing data requires that the vortex reach ground effect (again, assume height b , but the actual detection height might be higher) before the vortex can be detected. This probability is given by $P_{GE}(v) = P(KT, v)$ where $T = (h-b)/w$ is the time required for the vortex to descend into ground effect. The probability decreases as the height increases.

A.2.8.2 Probability of a Vortex Being Detected at a Lateral Position

The analysis of Section A.2.5 must be modified when a vortex is generated out of ground effect. The detection requirement means that there is a minimum time $T = (h-b)/w$ which must elapse before the vortex can be detected. Since a vortex will not be detected at position Y if it passes the position before reaching ground effect, detection at position Y imposes an upper limit on crosswind given by

$$(Y \pm b)/v_{max} = T' = (h-b)/w$$

$$v_{max} = w(Y \pm b)/(h-b).$$

Table 24 lists the crosswind to reach position Y (assumed to be positive) for the two vortices (port is upwind, starboard is downwind) and the time factor for the decay. The detection probability becomes:

$$P_{Du}(Y) = \int_0^{-i+w(Y-b)/(h-b)} F(v+i)P_u((Y+b-iT)/v, v+i)dv, \quad (18)$$

$$P_{Da}(Y) = \int_0^{i+w(Y-b)/(h-b)} F(v-i) P_d((Y-b+iT)/v, v-i) dv, \quad (19)$$

The probability of being detected at or beyond position Y is given by these expressions plus the probability that the vortex will be detected at a greater distance which must be obtained as an integral over detections at greater distances. This additional integral can be expressed as a crosswind integral which starts at the upper limit of these integrals and uses the probability that the vortex will last a time T .

$$P_{Du}(Y) = \int_{w(Y+b)/(h-b)}^{\infty} F(v) P_u((h-b)/w, v) dv, \quad (20)$$

$$P_{Dd}(Y) = \int_{w(Y-b)/(h-b)}^{\infty} F(v) P_d((h-b)/w, v) dv, \quad (21)$$

A.3. SPECIFIC MODELS

A.3.1 Wind Distribution

In evaluating experimental data it is always possible to use the measured wind distribution for analyzing the data. For many purposes, however, an analytical expression for the wind distribution is more useful. For example, an integral can be evaluated analytically rather than numerically.

The bivariate gaussian distribution is a convenient and reasonably representative description of how $H(u, v)$ depends upon the headwind u and crosswind v . $H(u, v)$ is given by the product $G(u)F(v)$ where $G(u)$ and $F(v)$ are given by the expressions:

$$\begin{aligned} G(u) &= 2 [(2\pi)^{1/2} \sigma_u]^{-1} \exp(-u^2/2\sigma_u^2) & u > 0 \\ &= 0 & u < 0 \end{aligned} \quad (22)$$

$$F(v) = [(2\pi)^{1/2} \sigma_v]^{-1} \exp(-v^2/2\sigma_v^2) \quad (23)$$

The headwind distribution is truncated for tailwinds since runways are normally selected to avoid tailwinds.

A.3.2 Vortex Decay

The decay of wake vortices has been found to obey the following expression:

$$\begin{aligned} P(t, u, v) &= \exp[-Q - \alpha(u, v)t^2], & t^2 > Q/\alpha \\ &= 1, & t^2 < Q/\alpha \end{aligned} \quad (24)$$

The dependence of the decay parameter α upon u and v can be modeled by the following expression:

$$\alpha(u, v) = \alpha_0 + \alpha_2(u^2 + v^2) \quad (25)$$

which indicates more rapid decay at higher wind speeds. The product of $P(t, u, v)G(u)$ can be integrated over the headwind to yield the following result for the crosswind decay probability:

$$P(t, v) = (1 + 2\alpha_2 t^2 \sigma_u^2)^{-1/2} \exp[Q - \alpha(v)t^2] \quad (26)$$

$$\alpha(v) = \alpha_0 + \alpha_2 v^2 \quad (27)$$

The effect of the headwind distribution is to produce a normalization factor that decreases as $1/t$ for long times, i.e., where $2\alpha_2 \sigma_u^2 t^2 \gg 1$. The dominant factor remains the exponential. The limit $t^2 > Q/\alpha$ was ignored in the headwind integral, so that the results are valid only for times where $\alpha_0 t^2 > Q$.

It was found in Section 4.3.4 that an exponential fit without any headwind consideration could be used to fit the data. The form of the slope α can be written as:

$$\alpha(v) = \alpha_0 + \alpha_2 v^2 = \alpha_0 [1 + (v/\beta)^N] \quad (28)$$

where the power, N , of the crosswind is allowed to vary and a new parameter β is defined as the crosswind that doubles the decay slope. Table 25 shows the values of the parameters derived from the data. [Note that the numbers differ slightly from those in Table 13, which were rederived independently from the data in the process of generating Figures 20 and 21.]

Table 25. Decay Model Parameters

Aircraft	N	α	β
B-707	2	0.8	7.1 ft/sec
B-747	1	0.6	4.0 ft/sec

A.3.3 Calculations

In addition to the constants listed in Table 25, the effective standard deviations for the wind distribution are needed to make the model calculations. The values 9.9 and 12.8 ft/sec (5.9 and 7.6 knots for Kennedy from Section 4.2) are used for negative and positive crosswinds, respectively.

Table 26 shows the calculations for the lateral transport probability for a B-707 with positive crosswinds. The velocity integral of the PF product is displayed explicitly along with the results of integrating up to a maximum crosswind of 25.5 ft/sec, which is about the maximum allowed crosswind (15 knots) for landing. Also shown in the table is the velocity giving the largest integrand and the inverse of the mean value of the inverse crosswind. These two values are generally very close together. The velocity distribution in the calculations is normalized for only a single sign so that the results can be compared to the measurements which were normalized to the number of cases with motion in a given direction. Without this change in normalization, the maximum transport probability to a given lateral position is one half since half the winds blow the other way and the ground-induced velocity is ignored here.

Figures 28 and 29 show the calculated transport probability (upward turning lines) for B-707 and B-747 vortices, respectively. For comparison the measured data for Line 1 are plotted (downward turning lines). The agreement is best for distances below 1000 feet, where most of the data points lie. The calculated probabilities are larger than measured and hence would form a conservative selection for the analysis of the "safe" separation. The contributions to the crosswind integral at 900 feet are shown in Figure 30. Figures 31 and 32 show the inverse mean value of inverse crosswind which is

Table 26. Calculations for the Lateral Transport Probability for a B-707 with Positive Crosswinds

CASE: B-707.P05

CALCULATION OF THE PROBABILITY OF A VORTEX MOVING Laterally BY MORE THAN A DISTANCE (FEET) D =

(D/1000)**2 =	0.	600.	900.	1300.	1700.	2000.	2300.	2500.
	.000	.360	.810	1.690	2.890	4.000	5.290	6.250

SINGLE-SIDED GAUSSIAN CROSSWIND DISTRIBUTION: SIGV = 12.8 (FT/SEC)

DECAY MODEL PARAMETERS: n = 2 Q = 0 A0 = .80 (100/SEC)**2 BETA = 7.1 FT/SEC

CROSSWIND (FT/SEC)	INTEGRAND:							
1.5	.061908	.000000	.000000	.000000	.000000	.000000	.000000	.000000
3.0	.060646	.001396	.000013	.000000	.000000	.000000	.000000	.000000
4.5	.058599	.007981	.000660	.000005	.000000	.000000	.000000	.000000
6.0	.055849	.014172	.002552	.000089	.000001	.000000	.000000	.000000
7.5	.052502	.017769	.004587	.000325	.000009	.000000	.000000	.000000
9.0	.048683	.019267	.006048	.000627	.000029	.000002	.000000	.000000
10.5	.044526	.019365	.006840	.000894	.000056	.000004	.000000	.000000
12.0	.040168	.018573	.007082	.001075	.000082	.000008	.000000	.000000
13.5	.035742	.017235	.006926	.001164	.000102	.000011	.000001	.000000
15.0	.031371	.015588	.006503	.001177	.000114	.000013	.000001	.000000
16.5	.027158	.013798	.005919	.001131	.000118	.000015	.000001	.000000
18.0	.023191	.011983	.005250	.001045	.000116	.000015	.000001	.000000
19.5	.019533	.010227	.004555	.000936	.000108	.000015	.000001	.000000
21.0	.016227	.008585	.003874	.000817	.000098	.000014	.000001	.000000
22.5	.013297	.007095	.003235	.000697	.000086	.000012	.000001	.000000
24.0	.010748	.005774	.002656	.000581	.000073	.000011	.000001	.000000
25.5	.008569	.004690	.002145	.000476	.000061	.000009	.000001	.000000
INTEGRAL	.940207	.287971	.102248	.016334	.001351	.000188	.000017	.000003
VPEAK:	.0	9.9	12.1	14.5	16.6	18.0	19.3	20.1
1/(1/V):	4.1	10.7	12.6	14.5	16.1	17.1	18.0	18.5

needed for the safety analysis. The values do not depend upon the decay parameter β which is the only difference between the B-707 and the B-747.

Figure 33 compares the calculated and measured residence probability for the B-747. As in the transport probability, the measured points are lower and agree better at the ends of the measurements. The calculated curves are valid only for probabilities much less than one and therefore no points are plotted with probability above 0.3.

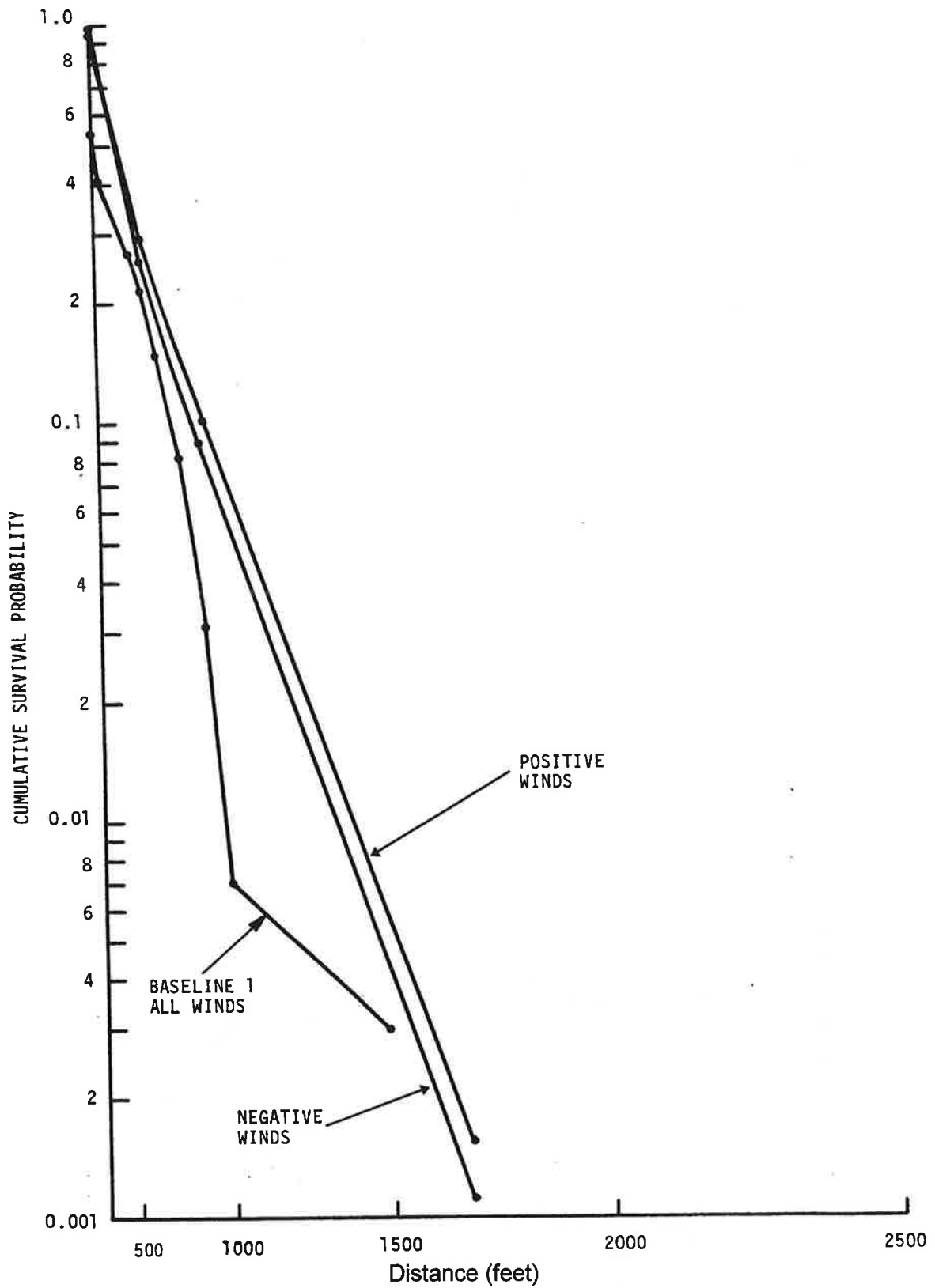


Figure 28. Comparison of Calculated and Observed Cumulative Survival Probability vs. Distance for B-707

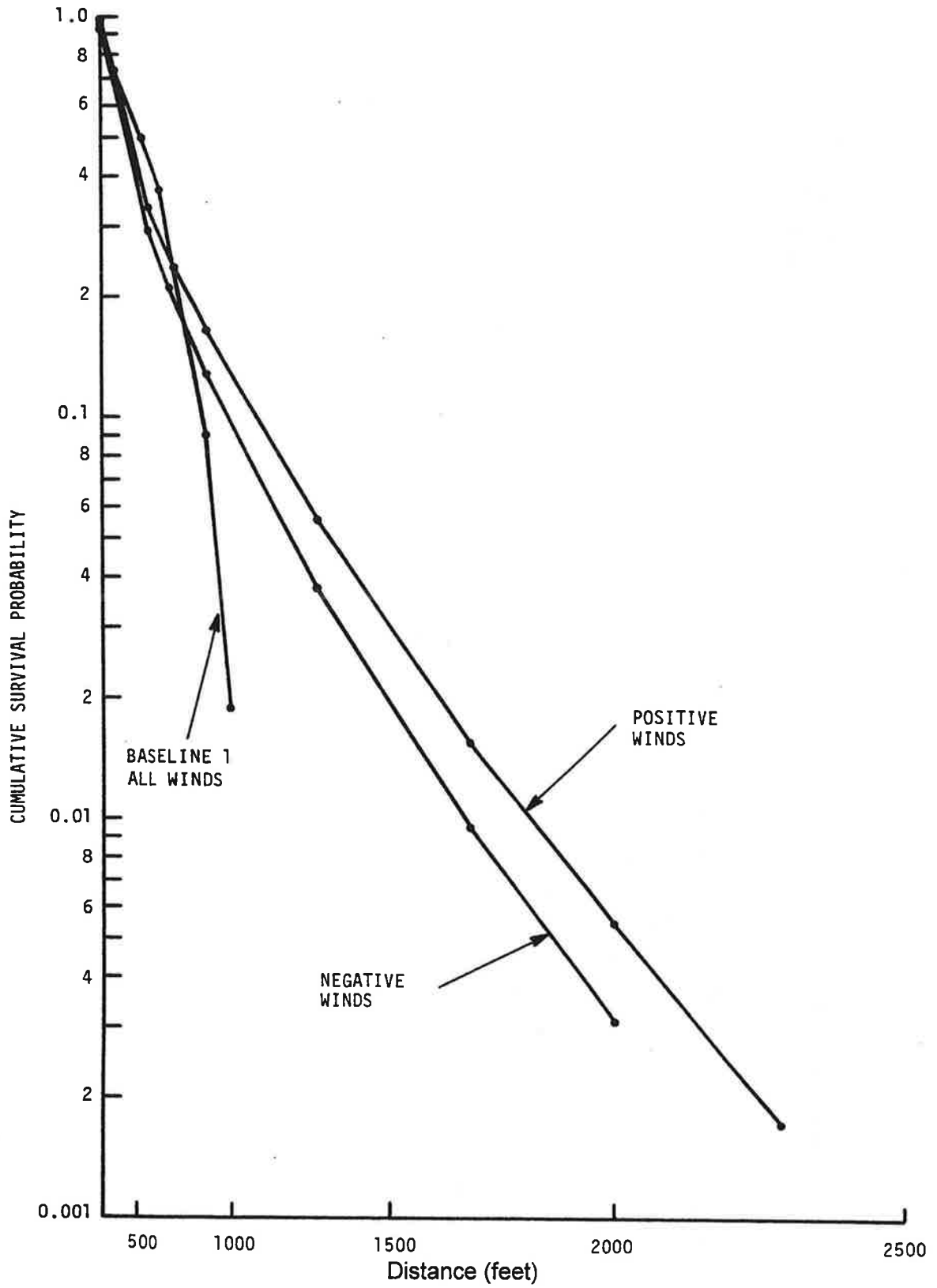


Figure 29. Comparison of Calculated and Observed Cumulative Survival Probability vs. Distance for B-747

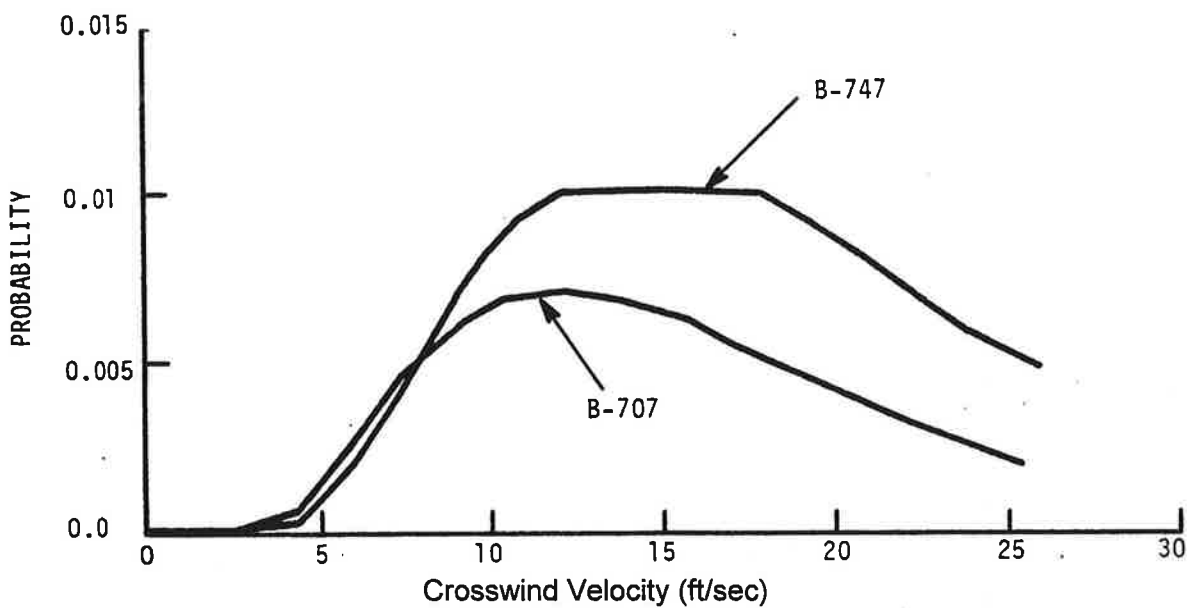
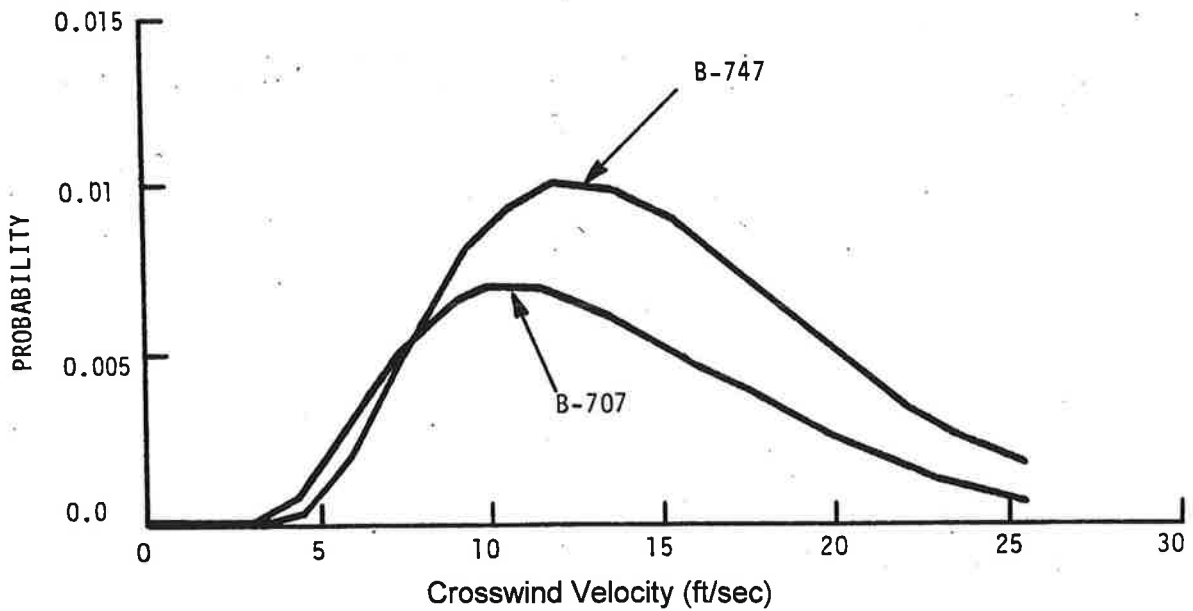


Figure 30. Calculated Probability of a Wake Vortex Being Transported at Least 900 Feet vs. Crosswind, B-707 and B-747: Top: Positive Crosswinds, Bottom: Negative Crosswinds

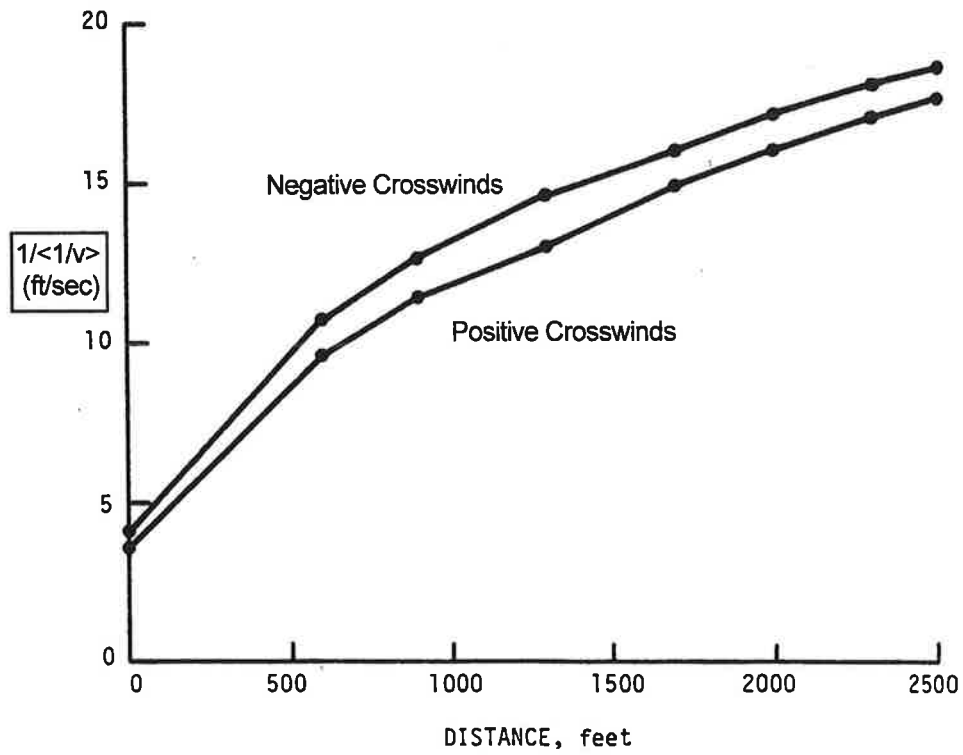


Figure 31. Mean Inverse Crosswind vs. Distance for B-707

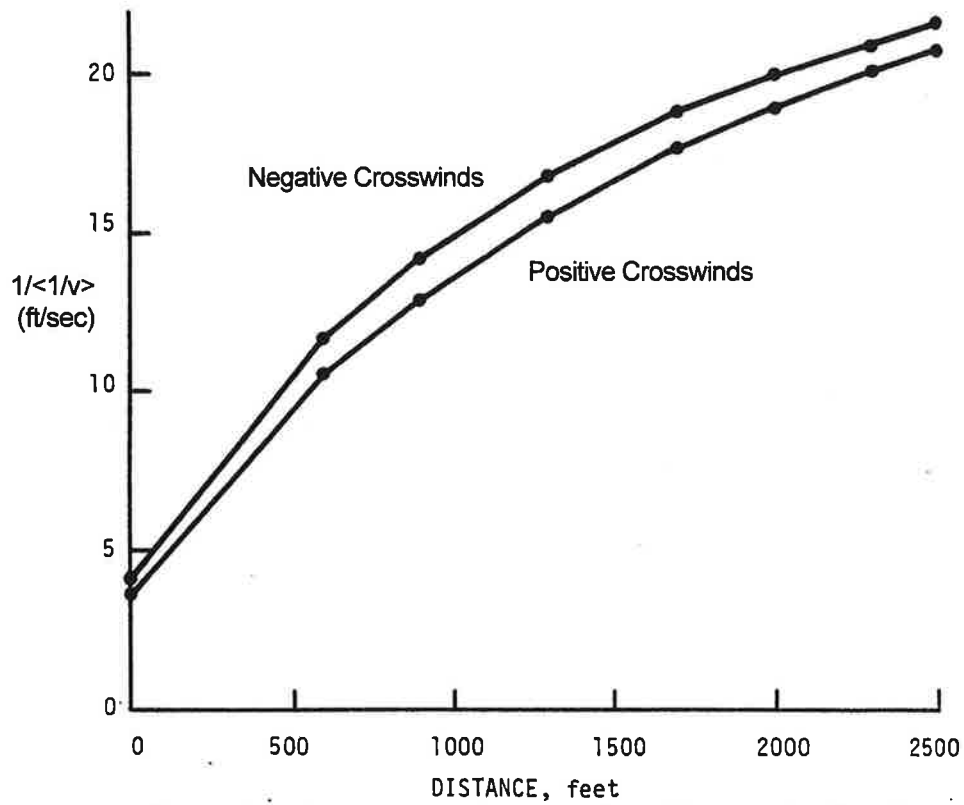


Figure 32. Mean Inverse Crosswind vs. Distance for B-747

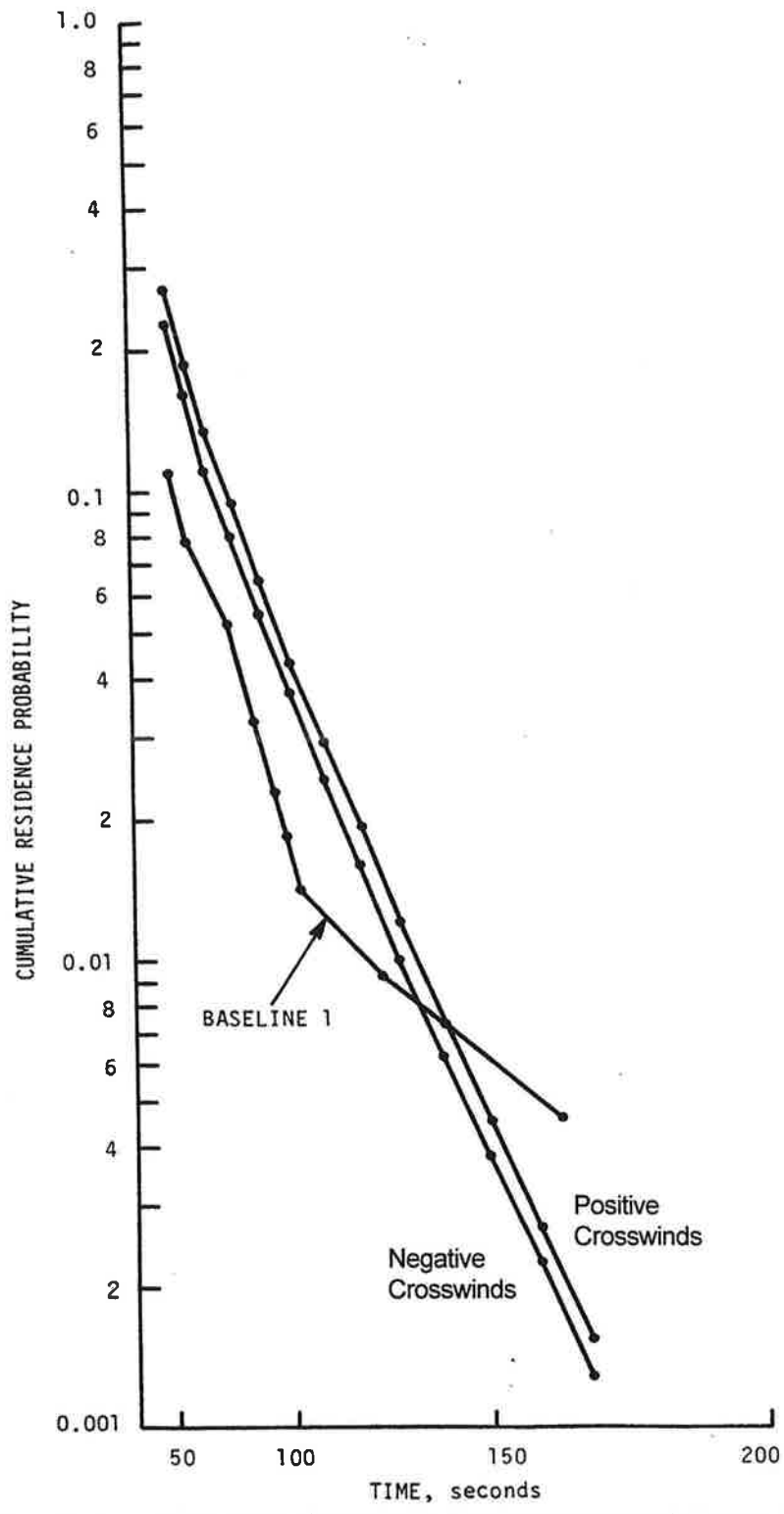


Figure 33. Calculated and Observed Cumulative Residence Probability vs. Time for B-747

Page intentionally blank

APPENDIX B - LANDING DATA PLOTS

This appendix contains transport distance, residence time, and vortex-demise time plots comparable to the plots in the main text. However, the plots contained in this appendix are for aircraft other than the B-707 and B-747. Data used to develop the plots in this appendix were restricted to verified data and headwinds of less than 15 knots (see Sections 4.1, 4.2).

In the body of the report, the B-707 was chosen to represent the Large wake class and the B-747 was chosen to represent the Heavy wake class. Of the aircraft included in this section, the DC-8 is comparable to the B-707. The B-727 and DC-9 are classified as Large and are lighter than the B-707. The L-1011 and DC-10 are somewhat lighter than the B-747, though in the same Heavy class. Thus, as an initial approach assuming vortex persistence increases with aircraft weight, the B-707 and B-747 would have the most persistent, and longest transport vortices, and thus were chosen to represent their respective classes.

B.1 TRANSPORT DISTANCE PLOTS

Comparing Figures 34, 35 and 36 with Figure 9, it appears that the transport distances for vortices produced by the B-727, DC-8, and DC-9 are roughly equal to transport distances for vortices produced by the B-707. Comparing Figures 10, 37 and 38, it appears that the transport distance for vortices produced by the B-747 and L-1011 are roughly equal, and somewhat less than for vortices produced by the DC-10.

Thus, it would appear that the B-707 and B-747 were satisfactory choices to represent their respective classes.

B.2 RESIDENCE TIME PLOTS

Figures 39 to 43 refer to residence time within the safety corridor (see Section 4.3.2). Comparing Figures 39, 40 and 41 with Figure 14 (left), it is seen that the residence time for wake vortices produced by the B-727, DC-8, and DC-9 are roughly equal to the residence time for vortices produced by the B-707.

Comparing Figures 14 (right), 42, and 43, it is seen that the residence time for vortices produced by the B-747 and L-1011 are roughly equal, but somewhat longer than vortices produced by the DC-10.

B.3 VORTEX-DEMISE TIME PLOTS

Comparing Figures 17 (top), 44, 45 and 46, it is seen that vortices produced by the B-707, B-727, and DC-8 have roughly equal demise times which are somewhat longer than the demise times for vortices produced by the DC-9.

Comparing Figures 17 (bottom), 47 and 48, it is seen that the B-747, DC-10, and L-1011 have roughly equal vortex-demise times.

B.4 STATISTICS OF PLOTS

The lowest probability that can be plotted is one case divided by the total number of cases. Since the total number of cases varied with aircraft type, the range of the plots varies considerably for different aircraft types. The large statistical variations for small number of cases means that the lower portions of the plots are statistically uncertain and are strongly affected by outliers. Consequently, the bottoms of the plots frequently exhibit statistical anomalies (for example, see Figures 35 (Baselines 1 and 2), Figure 45 (Baseline 1) and Figure 48 (Baseline 1)).

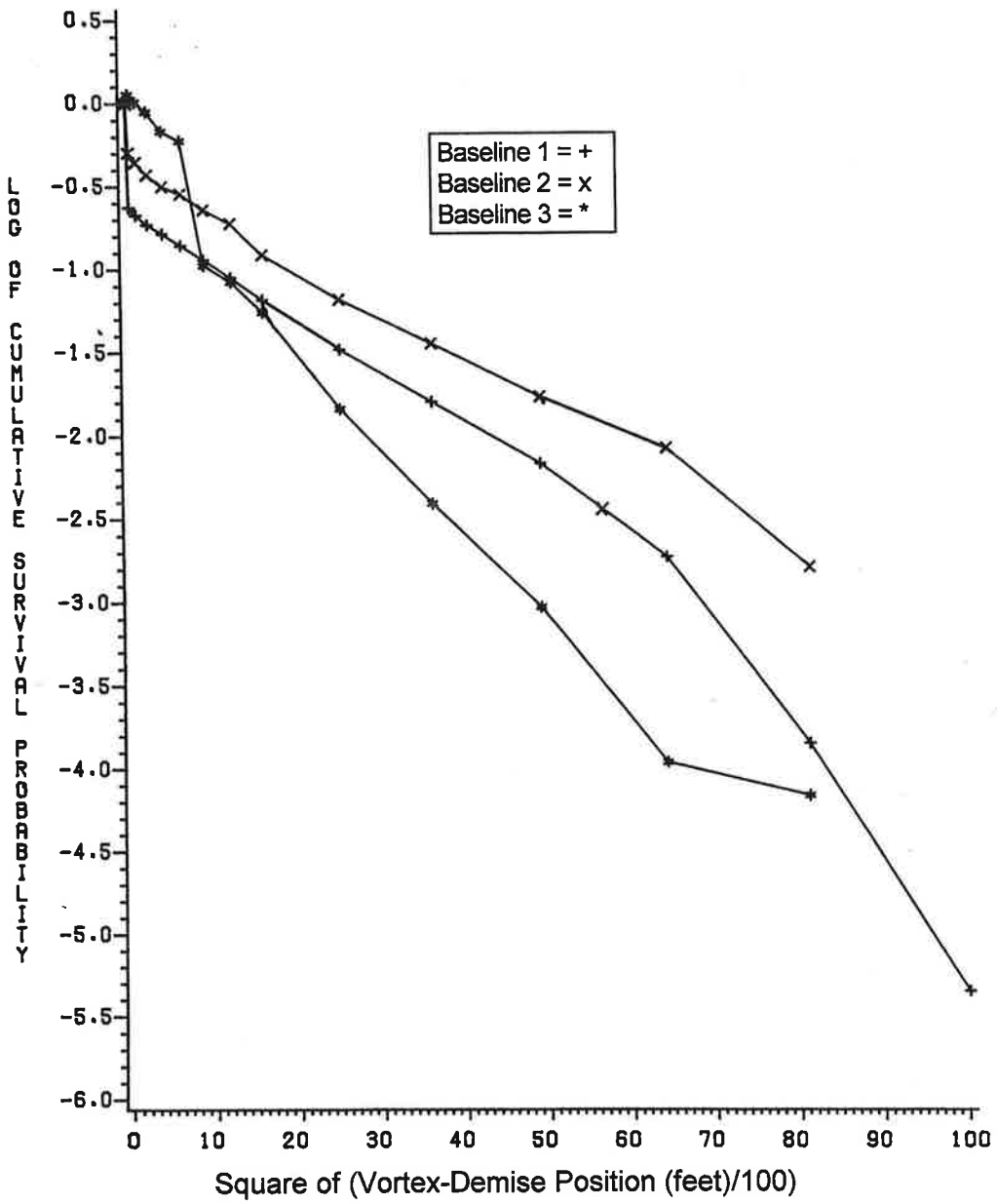


Figure 34. Kennedy B-727 Cumulative Vortex Survival Probability vs. Distance

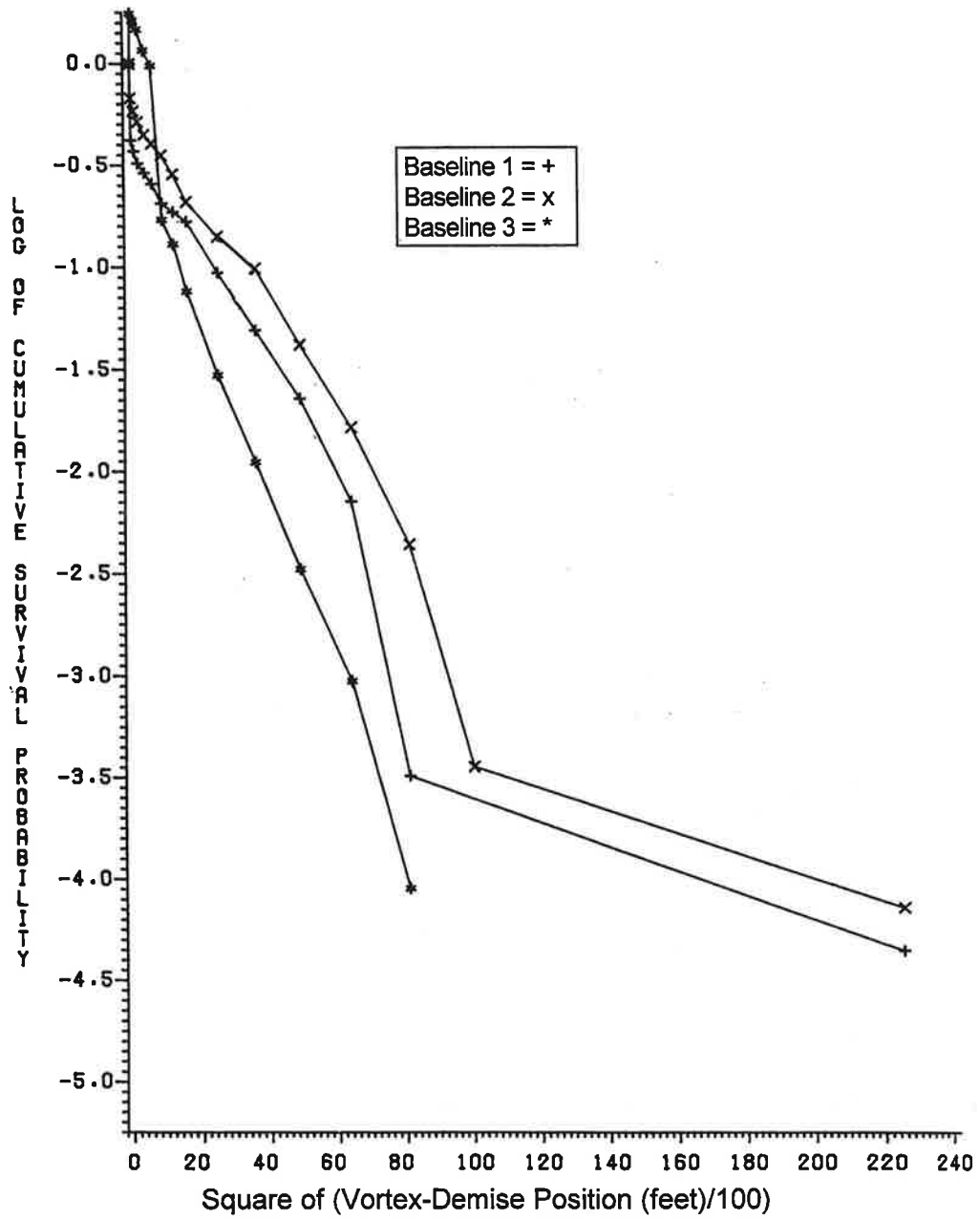


Figure 35. Kennedy DC-8 Cumulative Vortex Survival Probability vs. Distance

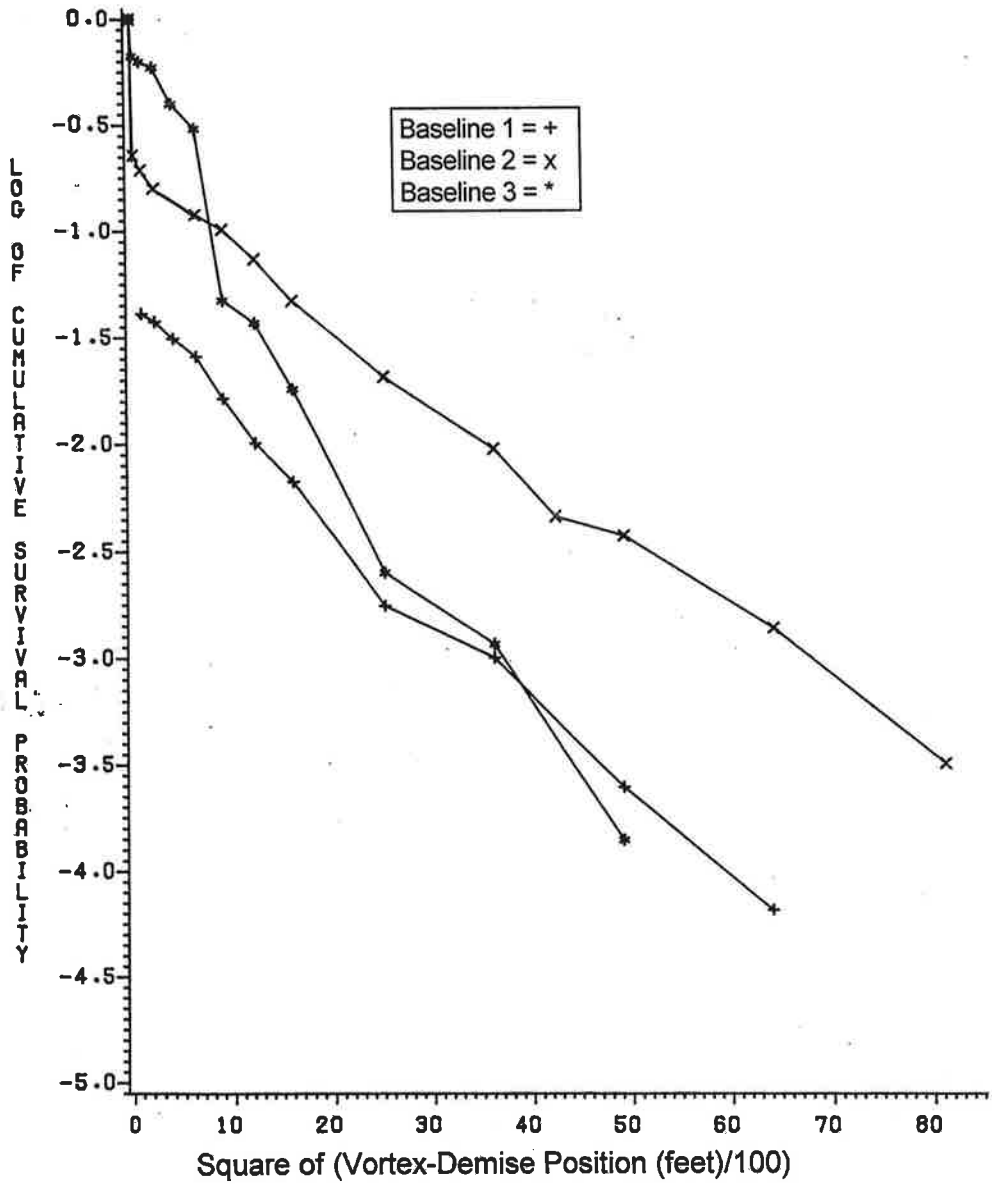


Figure 36. Kennedy DC-9 Cumulative Vortex Survival Probability vs. Distance

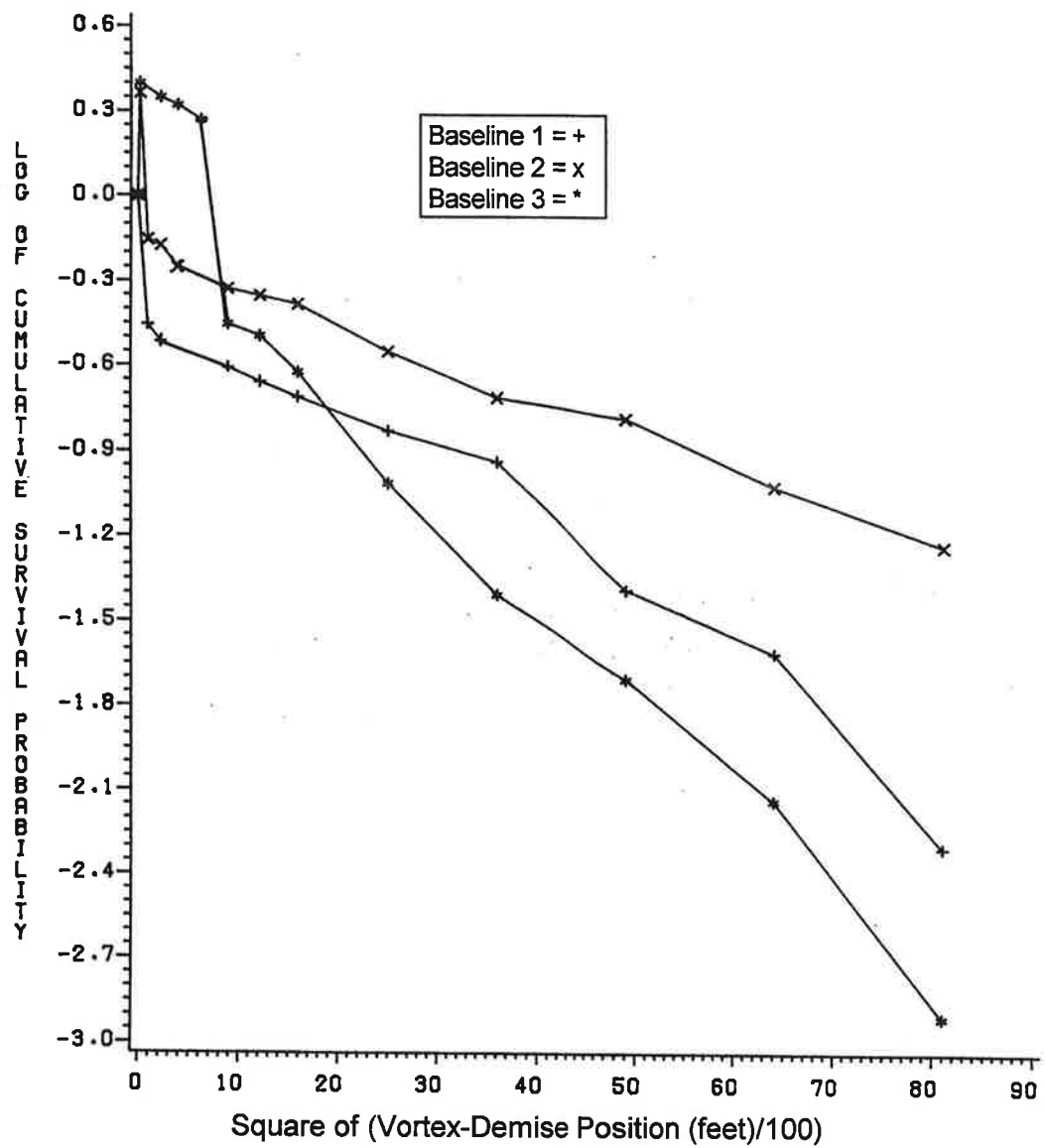


Figure 37. Kennedy DC-10 Cumulative Vortex Survival Probability vs. Distance

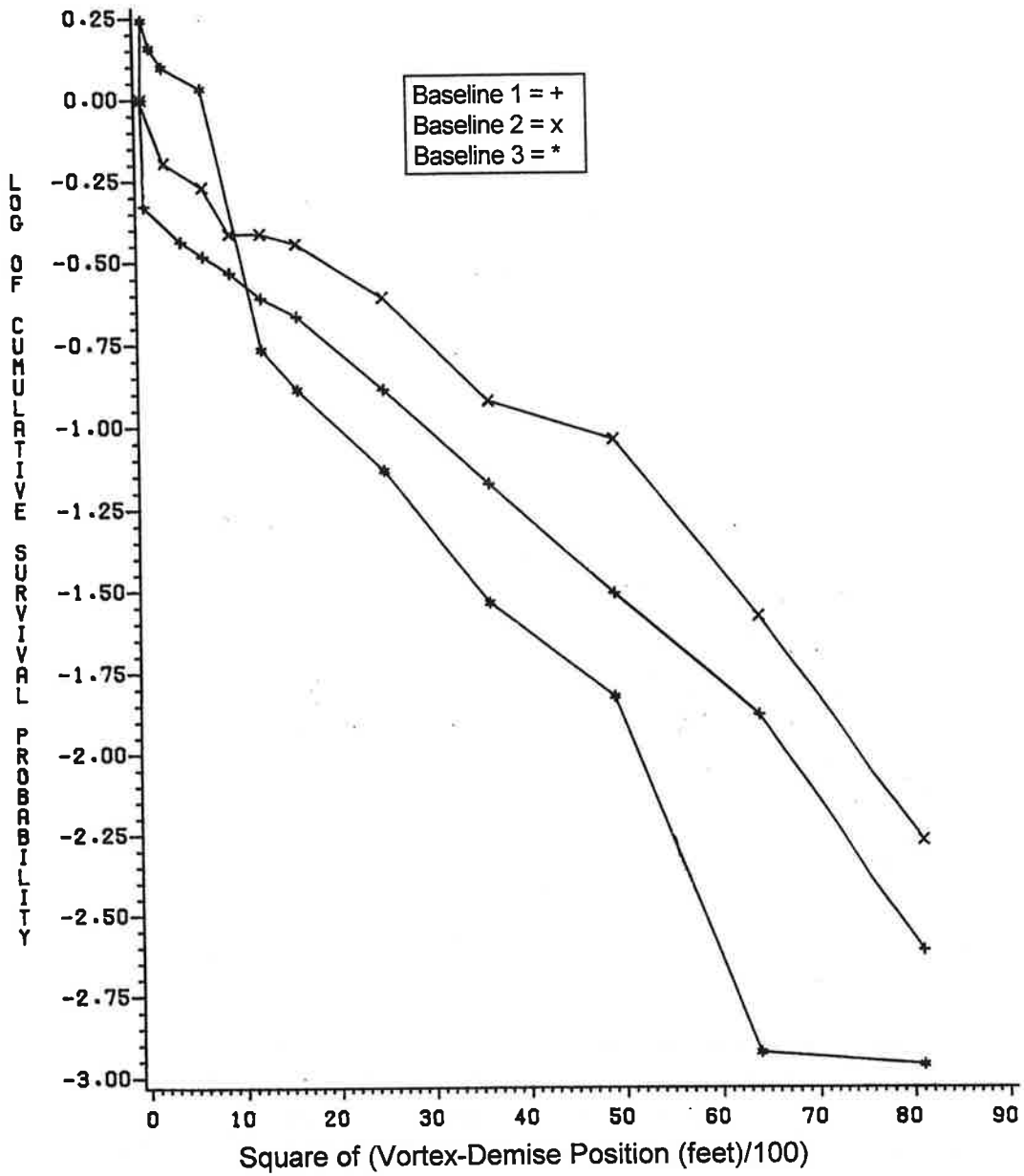


Figure 38. Kennedy L-1011 Cumulative Vortex Survival Probability vs. Distance

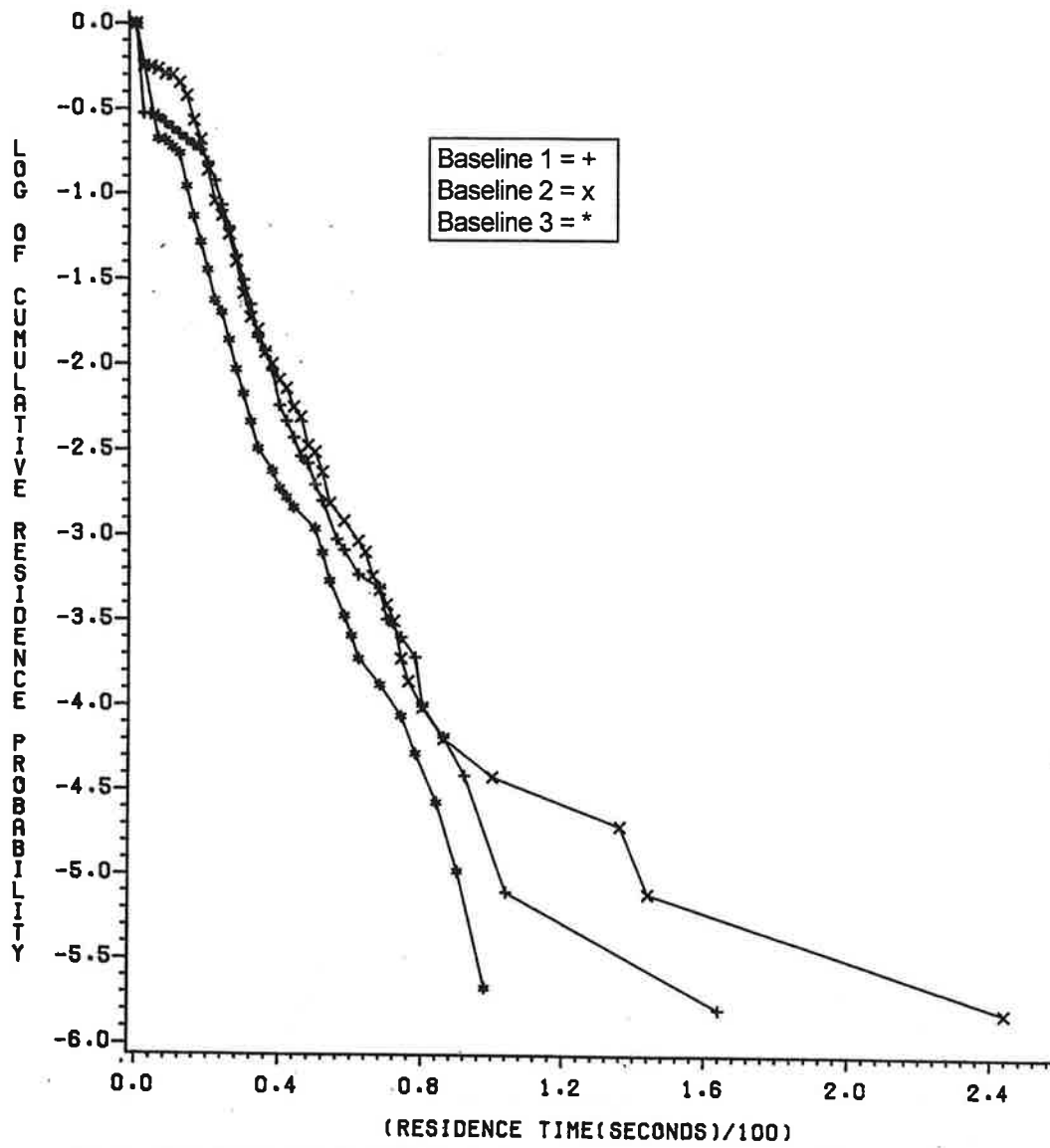


Figure 39. Kennedy B-727 Cumulative Residence Probability vs. Time

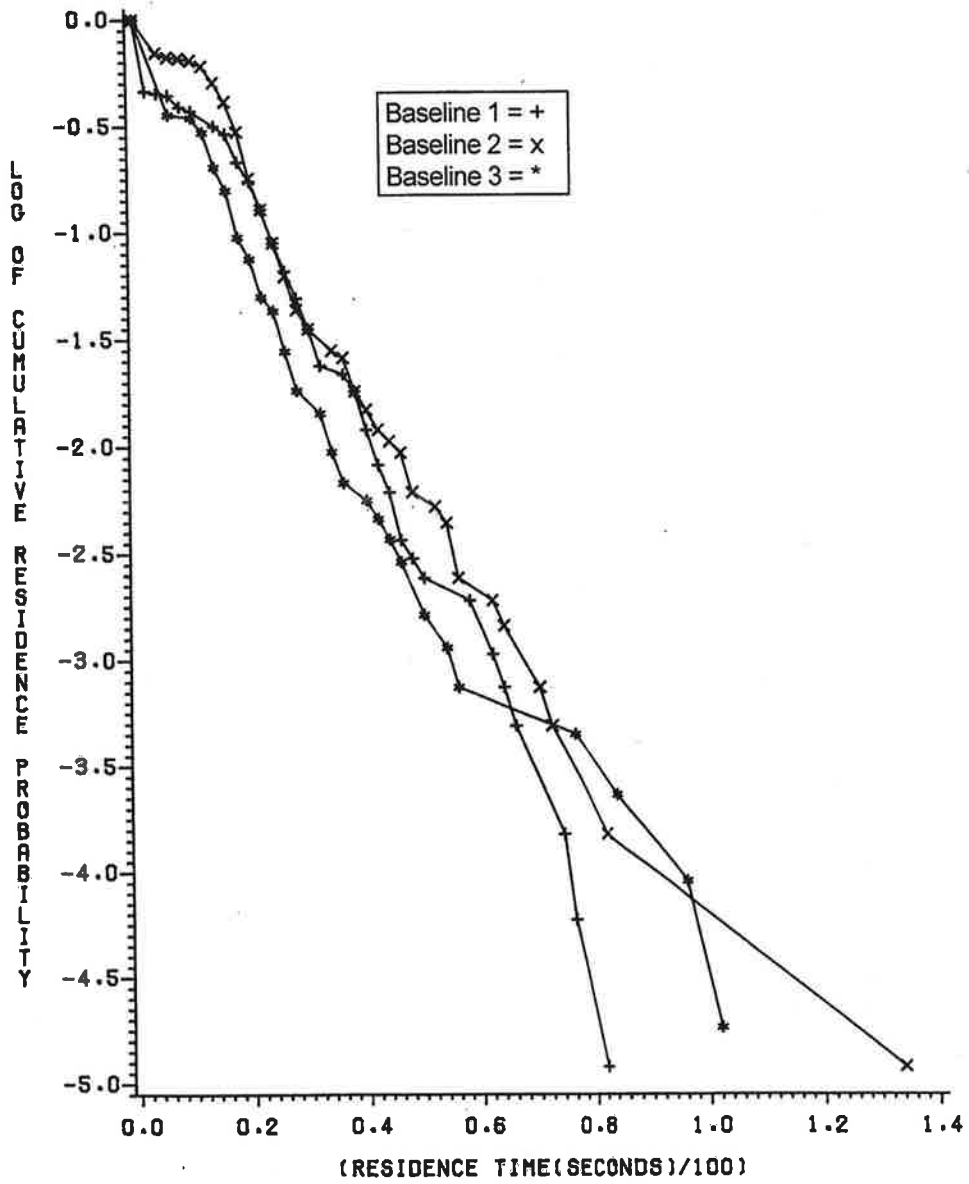


Figure 40. Kennedy DC-8 Cumulative Residence Probability vs. Time

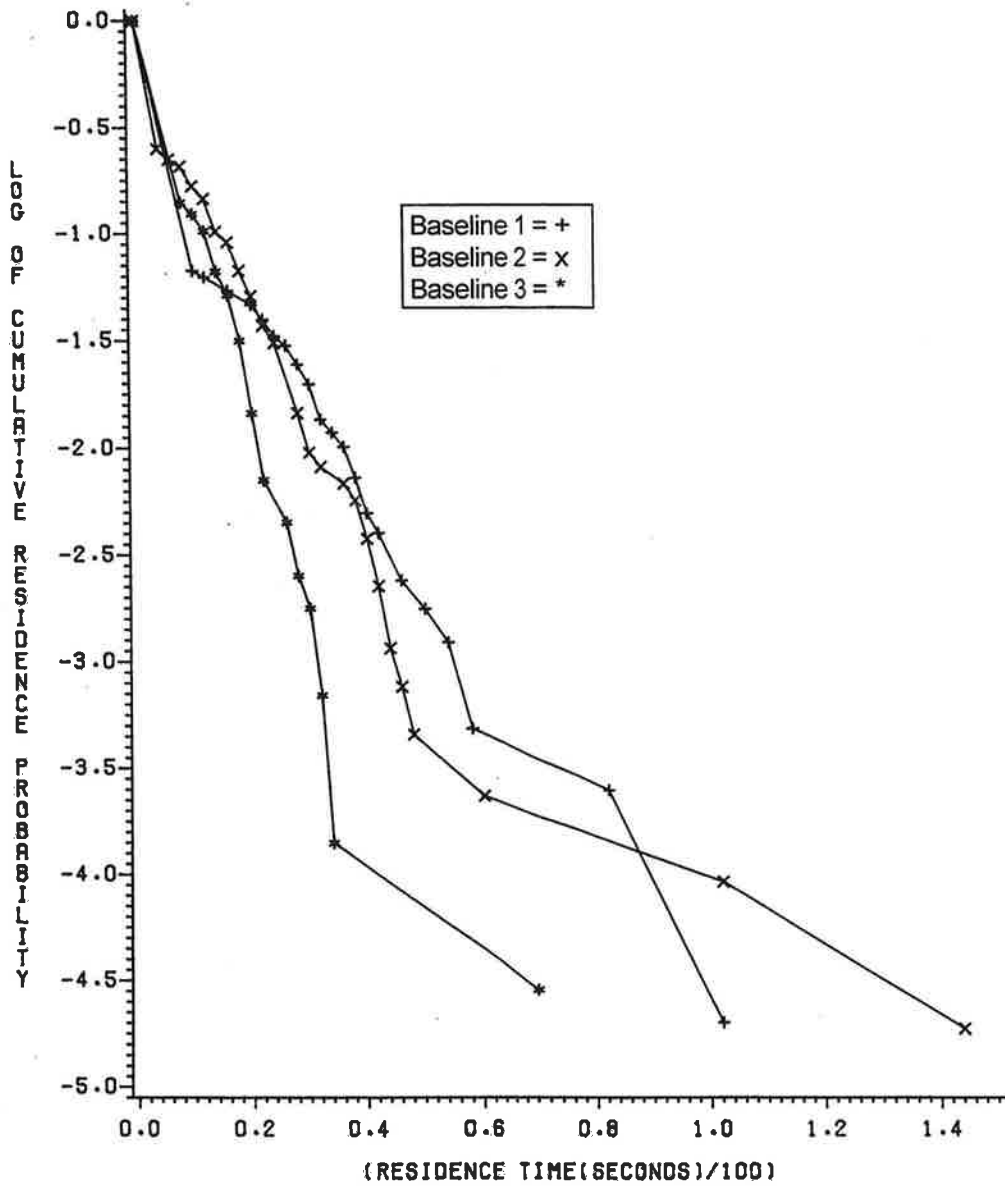


Figure 41. Kennedy DC-9 Cumulative Residence Probability vs. Time

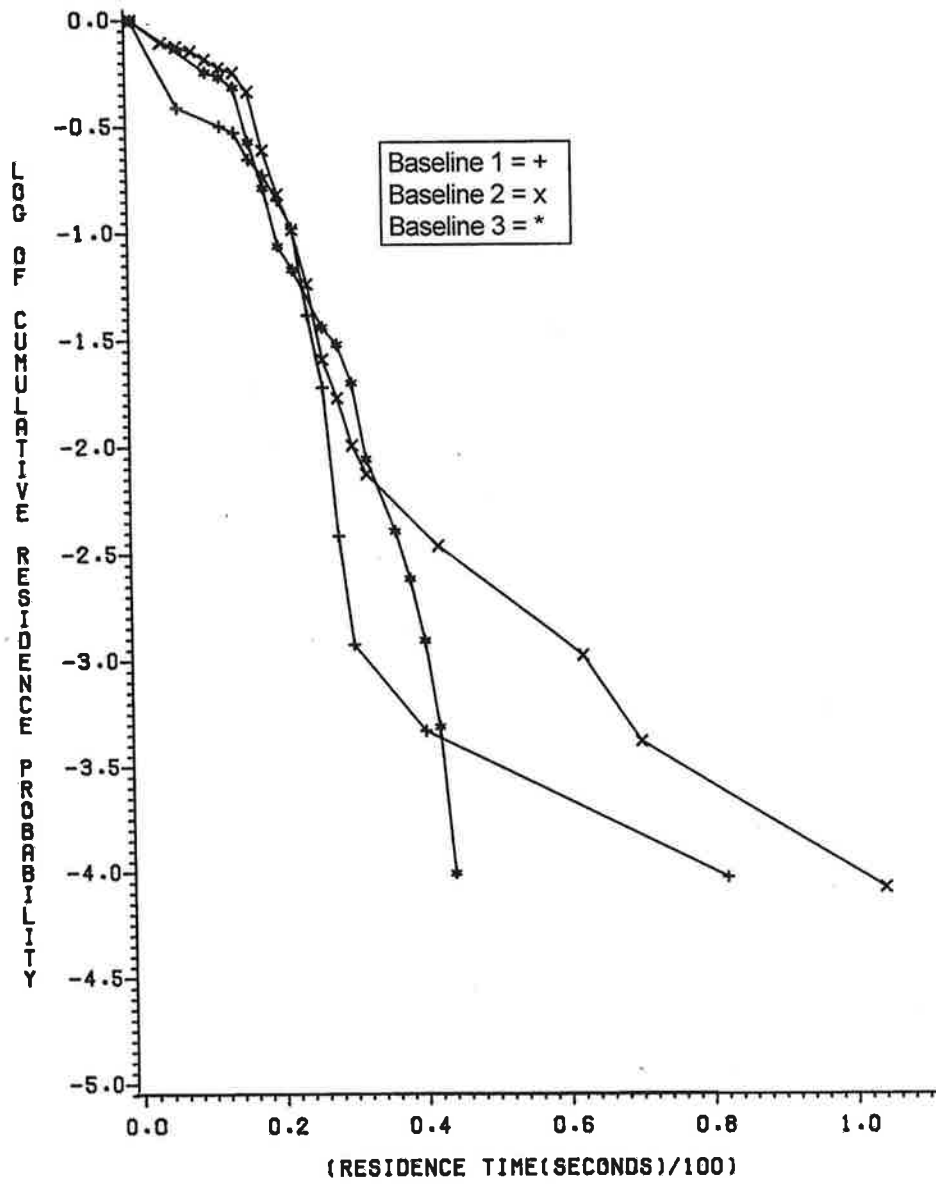


Figure 42. Kennedy DC-10 Cumulative Residence Probability vs. Time

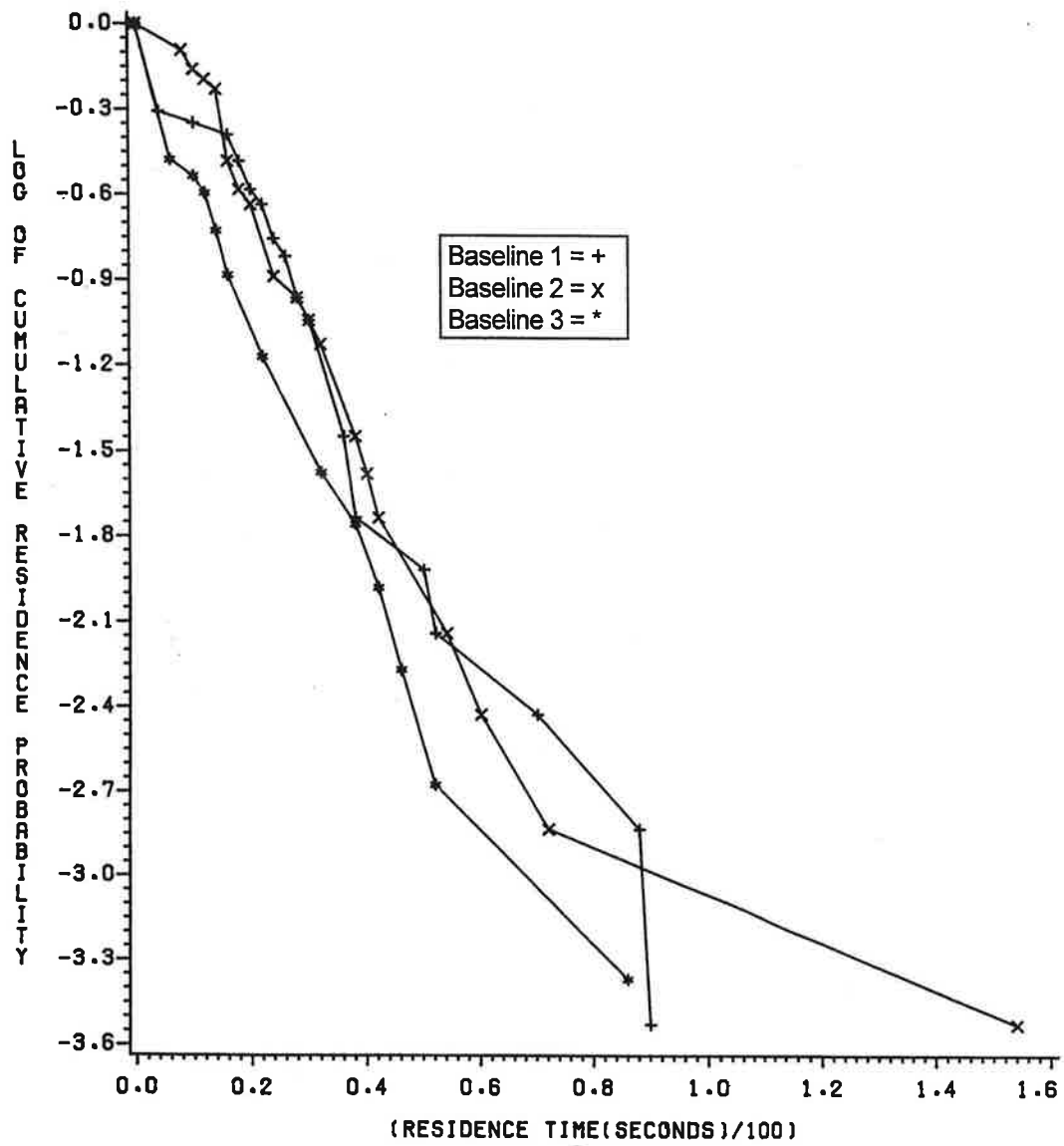


Figure 43. Kennedy L-1011 Cumulative Residence Probability vs. Time

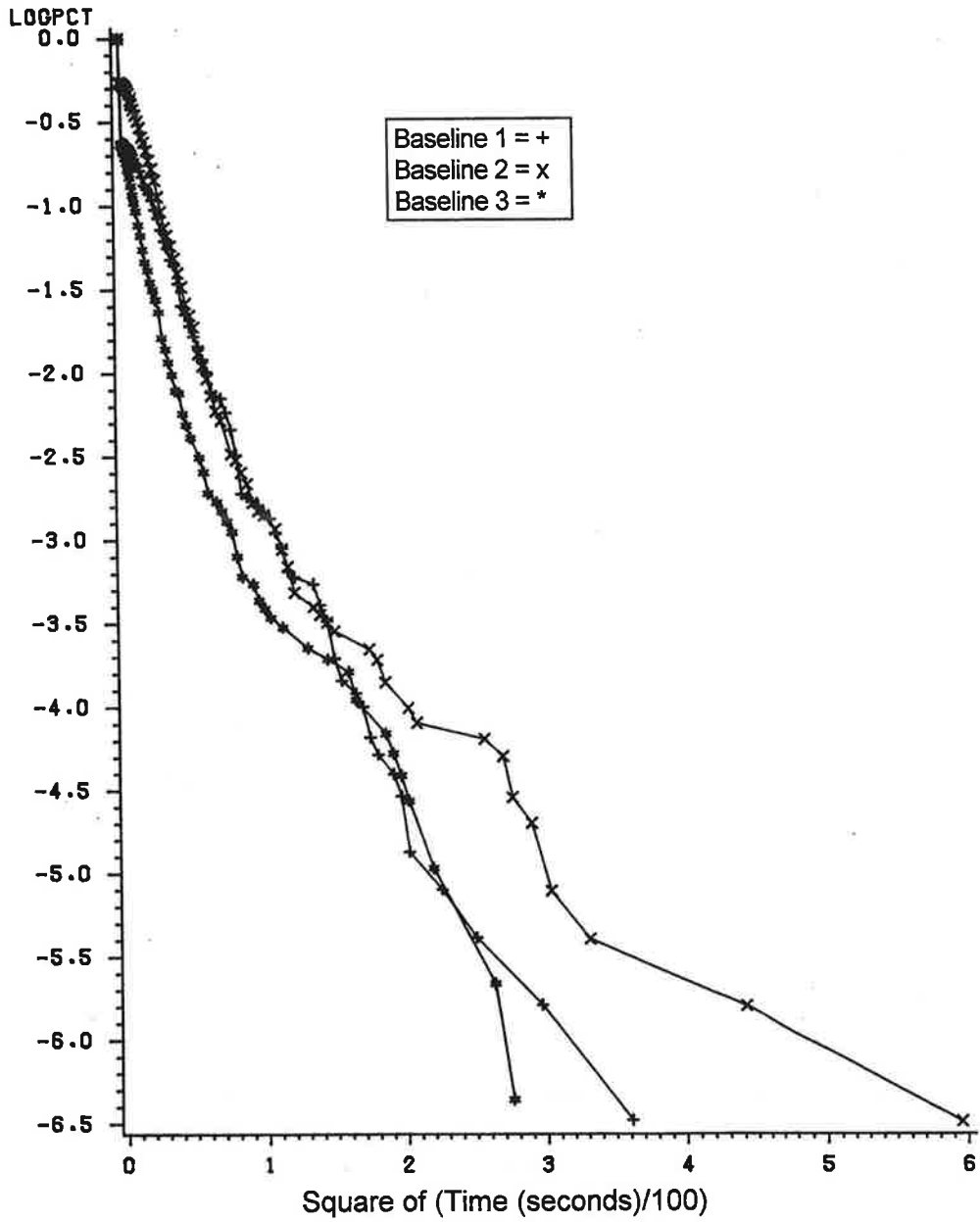


Figure 44. Kennedy B-727 Cumulative Survival Probability vs. Time

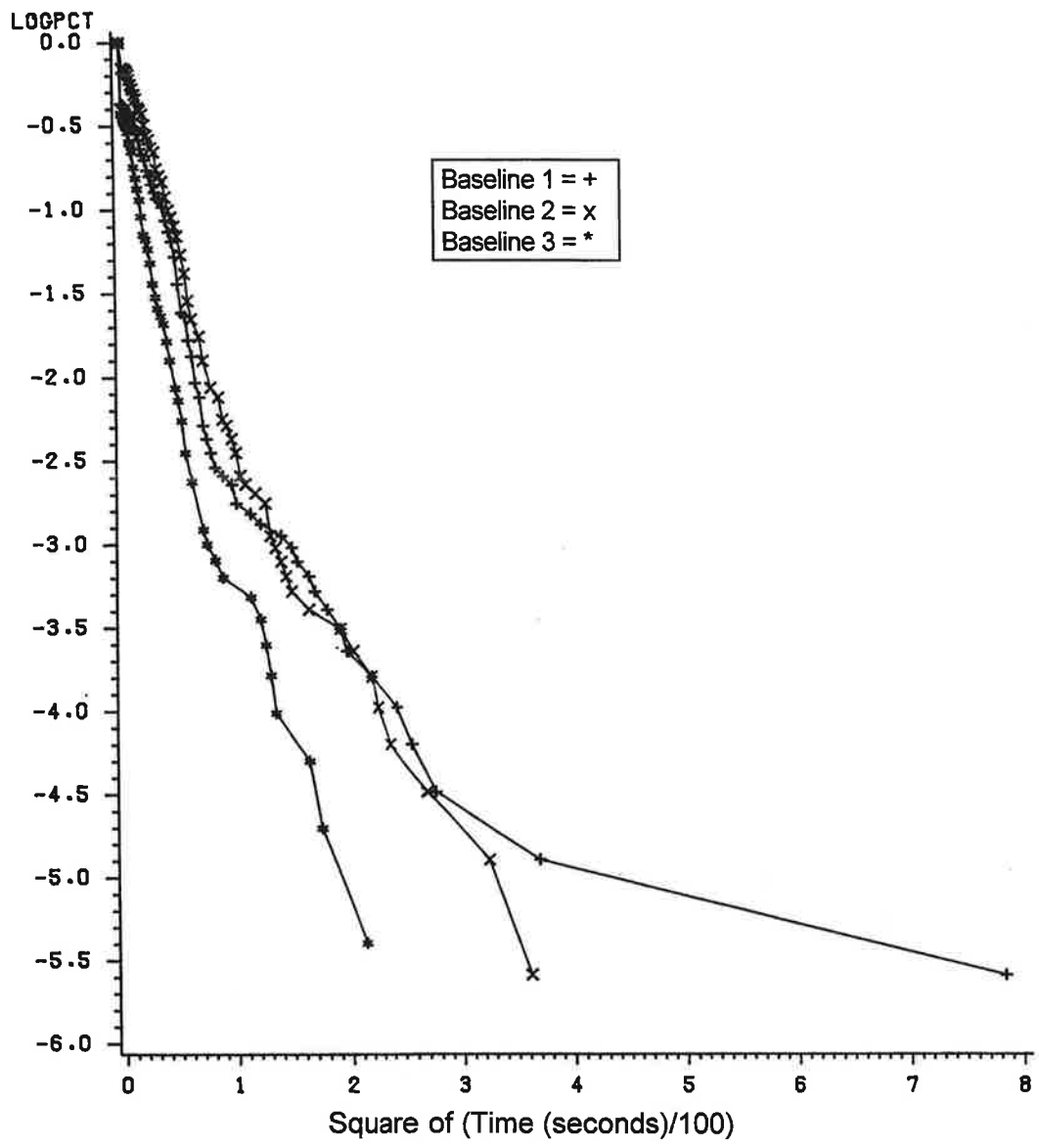


Figure 45. Kennedy DC-8 Cumulative Survival Probability vs. Time

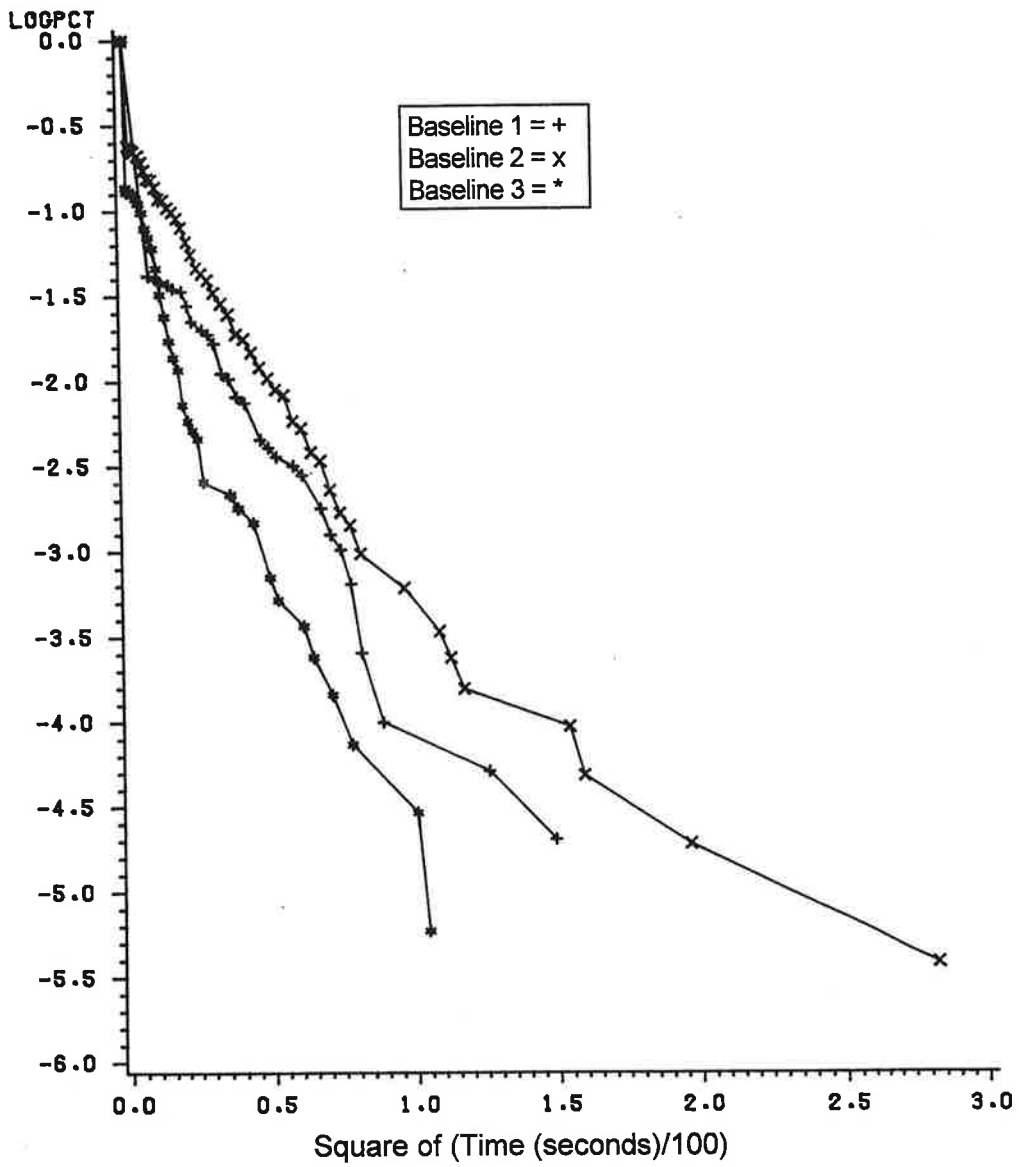


Figure 46. Kennedy DC-9 Cumulative Survival Probability vs. Time

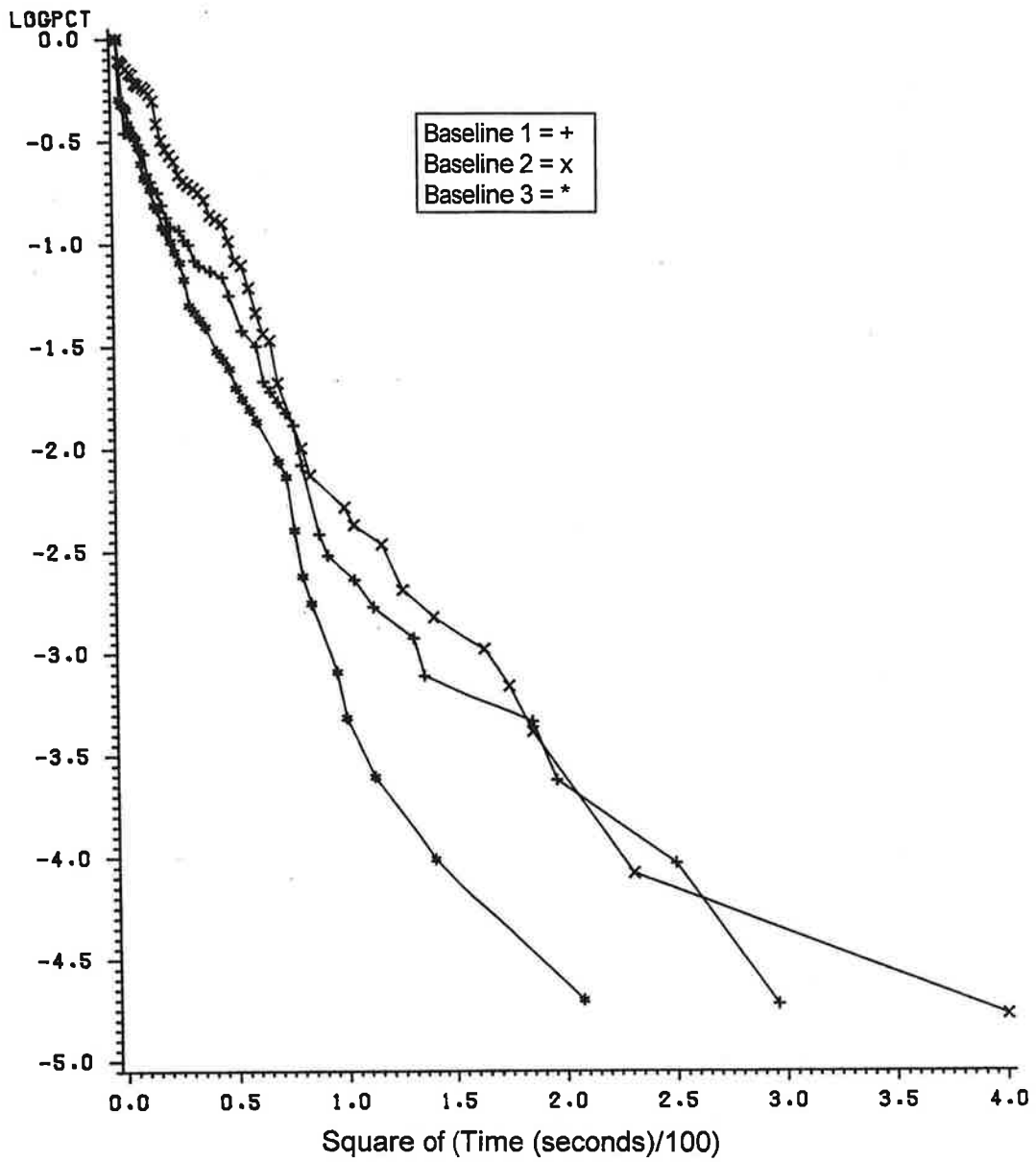


Figure 47. Kennedy DC-10 Cumulative Survival Probability vs. Time

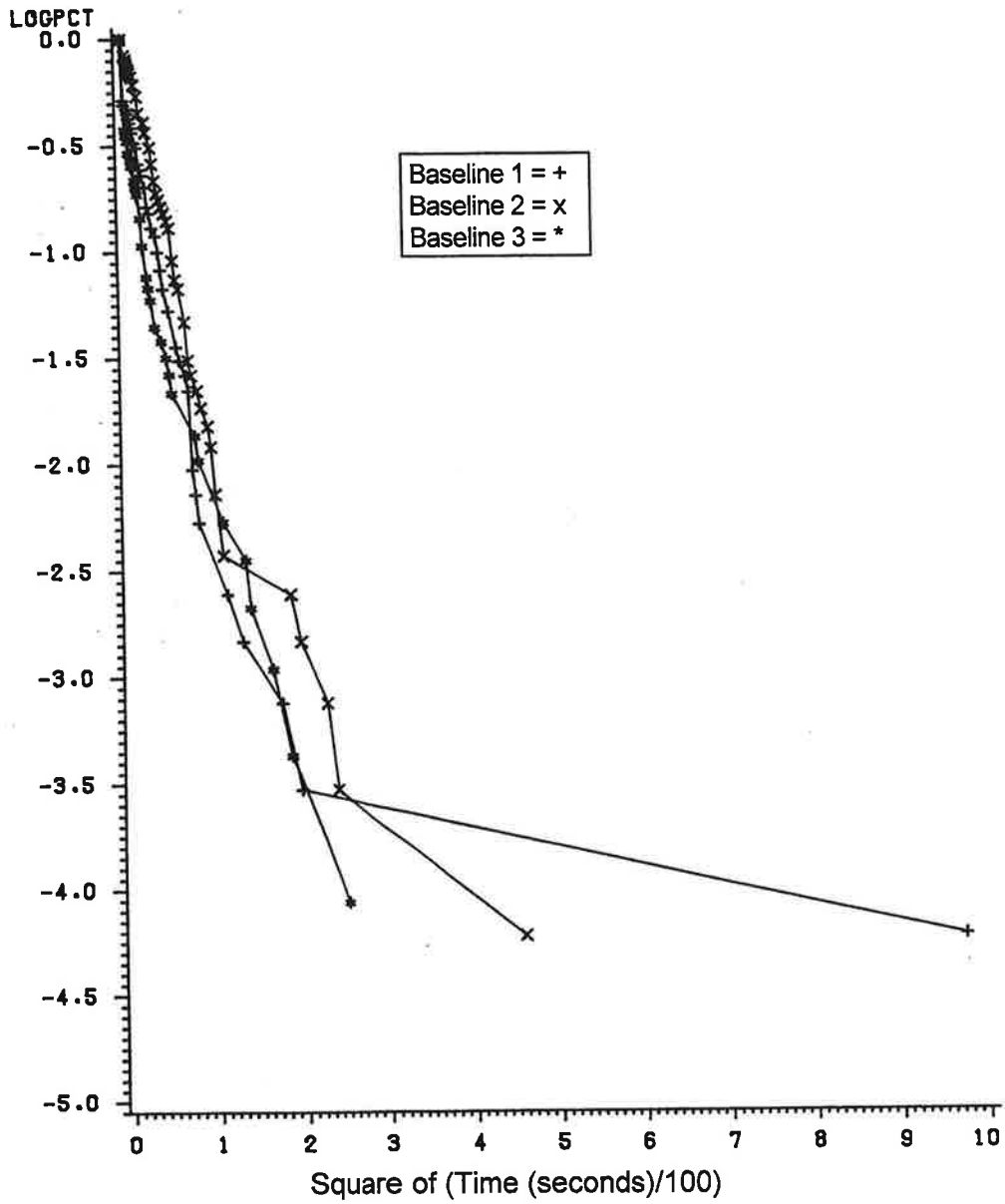


Figure 48. Kennedy L-1011 Cumulative Survival Probability vs. Time

Page intentionally blank

APPENDIX C - TAKEOFF DATA PLOTS

This appendix consists of distance plots (Figures 49-53) comparable to the plots in the main text. However, the plots contained in this appendix are for aircraft other than the B-707 and B-747. In addition, it should be noted that the takeoff process introduces complexities which make comparison with landing data analyses difficult (see discussion in Appendix A). For example, the flight pattern is less consistent. Data used to develop these plots are restricted as discussed in Section 4.4.

Of the aircraft included in this section, the B-727, B-737, and DC-9 are classified as Large and are lighter than the B-707. The L-1011 and DC-10 are somewhat lighter than the B-747, though in the same Heavy vortex weight class.

Initial choices of aircraft to represent the vortex classes were based upon the assumption that vortex persistence increases with aircraft weight. Thus, the B-747 and B-707 were chosen to represent the Heavy and Large classes, respectively. Comparing Figure 52 with Figure 10, it appears that vortices generated by the B-747 on landing have somewhat greater persistence than vortices generated by the DC-10 on departure. Comparing Figure 53 with Figure 10 it appears that vortices generated by the L-1011 on takeoff have somewhat greater persistence than vortices generated by the B-747 on landing. Comparing Figures 49, 50 and 51 with Figure 9 it appears that vortices generated by B-727, B-737, and DC-9 aircraft on takeoff have greater persistence than vortices generated by the B-707 on landing. However, noting the aforementioned differences between departure and landing conditions, the differences in vortex persistence were deemed insufficient to warrant change in the choice of aircraft to represent the Heavy and Large classes.

See Section B.4 for a discussion of the statistics of the plots. Note that takeoff Baseline 3 (off the end of the runway) had fewer cases than the other baselines for the smaller aircraft, presumably because their altitudes were frequently too high for the vortices to descend to the ground.

O'HARE DATA:

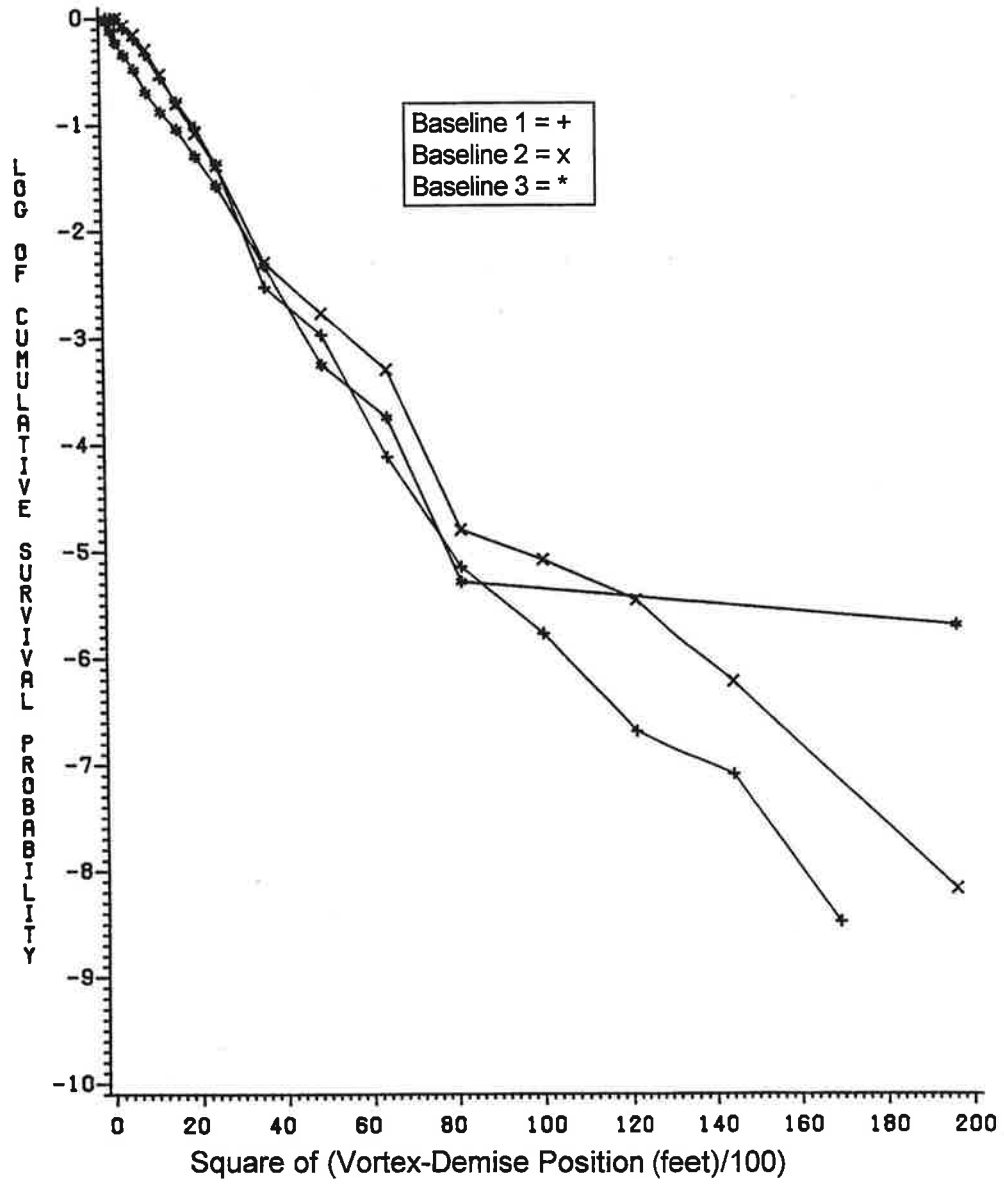


Figure 49. O'Hare B-727 Cumulative Survival Probability vs. Time

OHARE DATA:

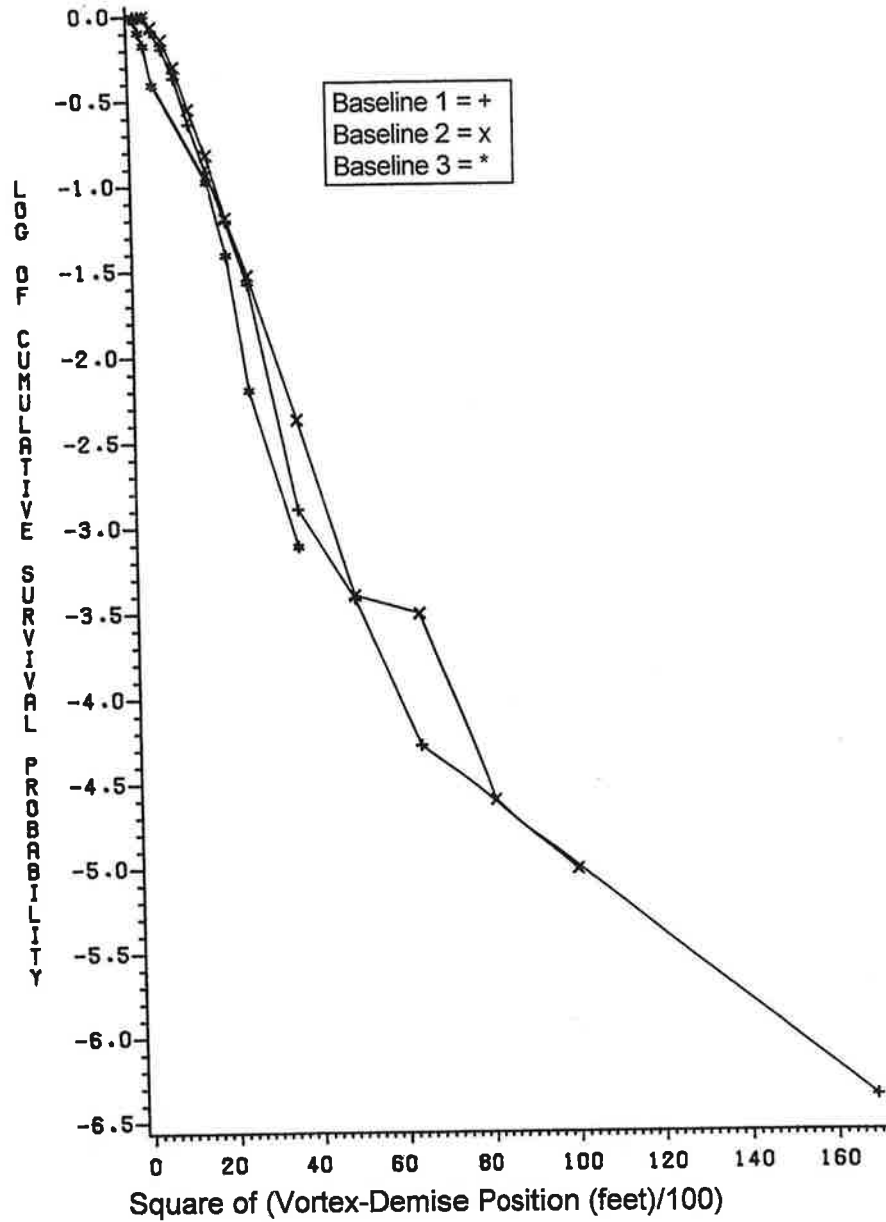


Figure 50. O'Hare B-737 Cumulative Survival Probability vs. Time

O'HARE DATA:

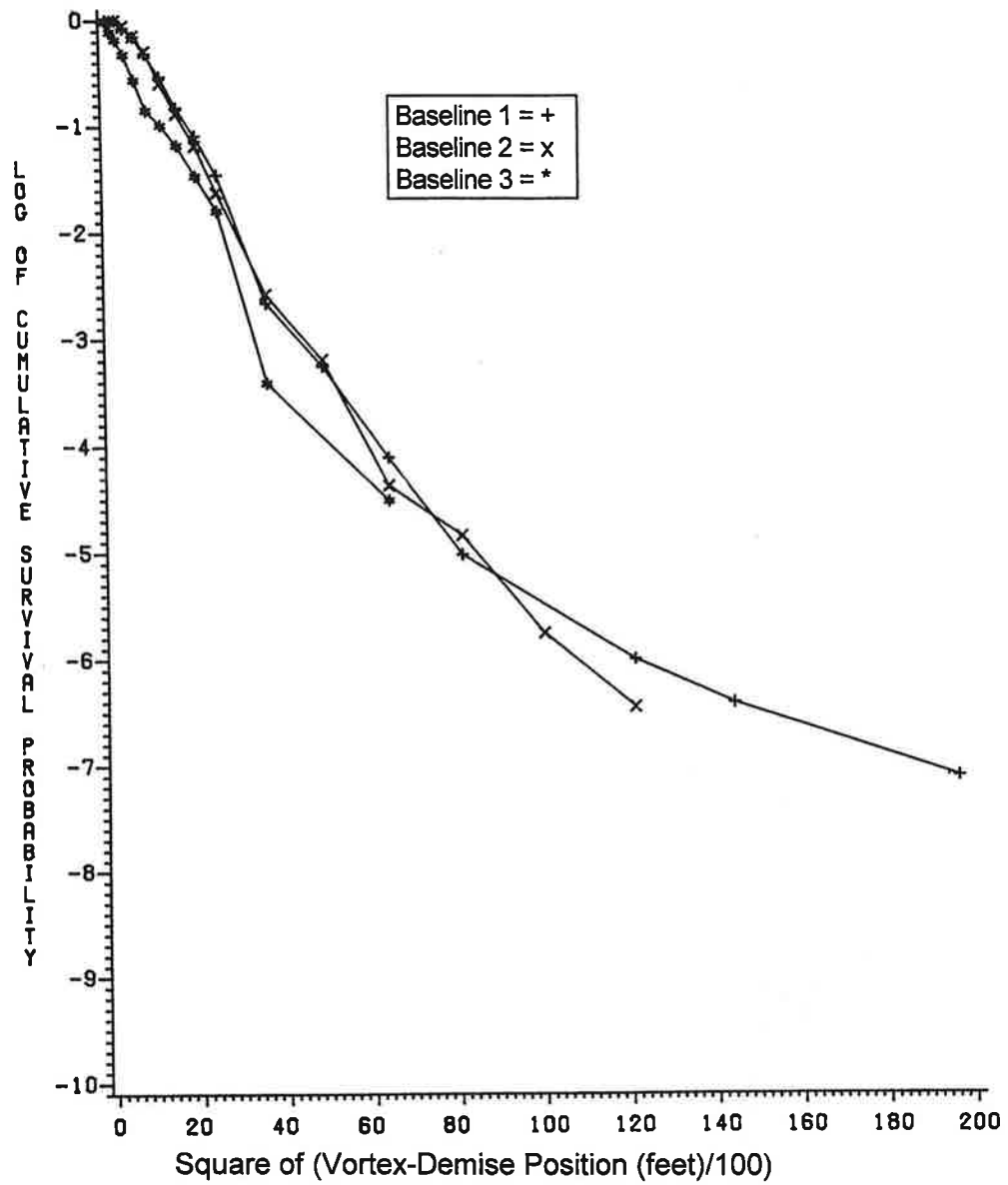


Figure 51. O'Hare DC-9 Cumulative Survival Probability vs. Time

OHARE DATA:

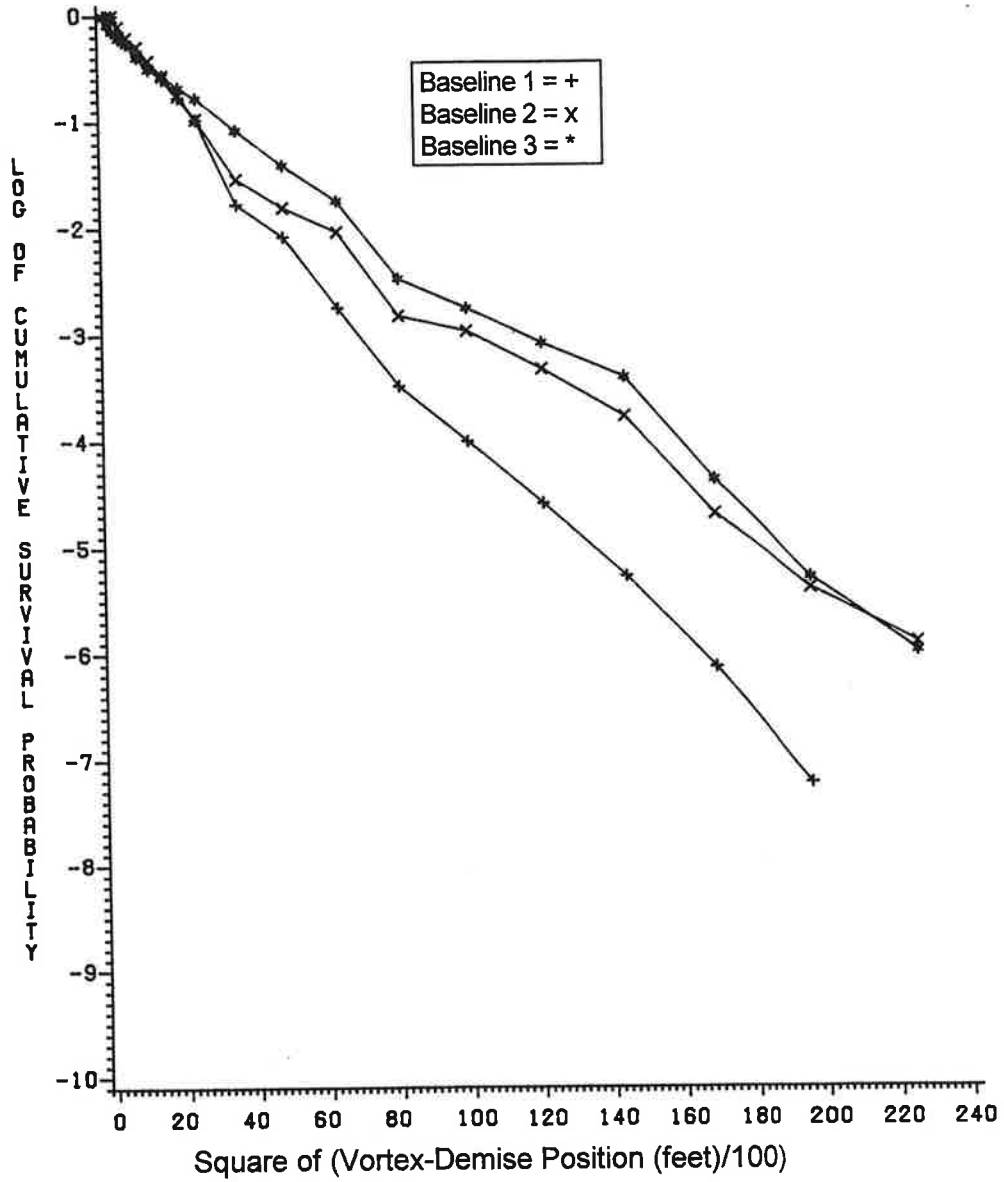


Figure 52. O'Hare DC-10 Cumulative Survival Probability vs. Time

O'HARE DATA:

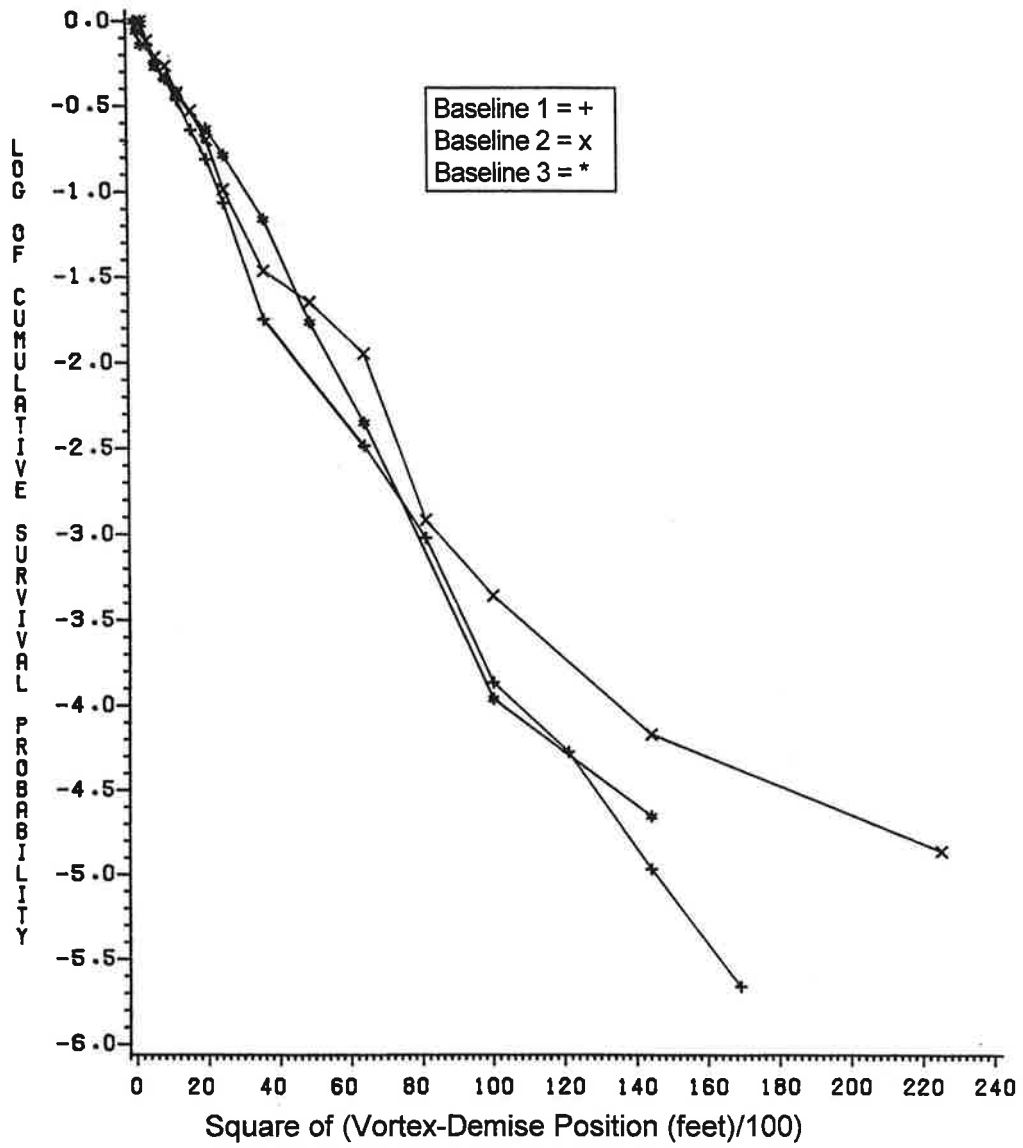


Figure 53. O'Hare L-1011 Cumulative Survival Probability vs. Time

REFERENCES

- ¹ Yarmus, J., Burnham, D., Wright, A. and Talbot, T., "Aircraft Wake Vortex Takeoff Tests at O'Hare International Airport," DOT/FAA/RD-94-25, August 1994, USDOT/Volpe National Transportation Systems Center, Cambridge, MA.
- ² Burnham, D.C. and Hallock, J.N., "Wind Effects on the Lateral Motion of Wake Vortices," DOT/FAA/AAR-99/88, November 1999, USDOT/Volpe National Transportation Systems Center, Cambridge, MA.
- ³ Hallock, J.N., Winston, B.P., Burnham, D.C., Sullivan, T.E., McWilliams, I.G. and Wood, W.D., "Joint US/UK Vortex Tracking Program at Heathrow International Airport, Vol. II: Data Analysis," FAA-RD-76-58,II, Sept. 1976, DOT/Transportation Systems Center, Cambridge, MA.
- ⁴ Hallock, J.N. and Eberle, W.R. (editors), "Aircraft Wake Vortices: A State-of-the-Art Review of the United States R&D Program," FAA-RD-77-23, Feb. 1977, DOT/Transportation Systems Center, Cambridge, MA.
- ⁵ Sullivan, T.E., Hallock, J.N. and Winston, B.P., "Analysis of Ground-Wind Vortex Sensing System Data from O'Hare International Airport," FAA-RD-80-133, Sept. 1980, DOT/Transportation Systems Center, Cambridge, MA.
- ⁶ Winter, H., "Research and Development for a Wake Vortex Warning System in Germany," in Proceedings of the Aircraft Wake Vortices Conference, DOT/FAA/SD-92/1.1, Washington, DC, October 29-31, 1991, pp. 3-(1-7).
- ⁷ See Reference 4, pp. 244-246.
- ⁸ Sullivan, T.E. and Burnham, D.C., "Ground Wind Vortex Sensing System Calibration Tests," FAA-RD-80-13, Feb. 1980, DOT/Transportation Systems Center, Cambridge, MA.
- ⁹ Air Traffic Control Handbook, FAA Order 7110.65L (current update 7/15/99).
- ¹⁰ Burnham, D.C., "Review of Vortex Sensor Development Since 1970," in Proceedings of the Aircraft Wake Vortices Conference, FAA-RD-77-68, June 1977, DOT/Transportation Systems Center, Cambridge, MA.
- ¹¹ Abramson, S. and Burnham, D.C., "Ground-Based Anemometer Measurements of Wake Vortices from Landing Aircraft at Airports," AGARD CP-584 Conference Proceedings, The Characterization & Modification of Wakes from Lifting Vehicles in Fluids, 20-23 May 1996, Trondheim, Norway, November 1996, pp. 13-(1-7).
- ¹² Hallock, J.N., Winston, B.P., Sullivan, T.E., and Burnham, D.C., "TSC Wake Vortex Data Base and Applications," Proceedings of the Aircraft Wake Vortices Conference, FAA-RD-77-68, June 1977, DOT/Transportation Systems Center, Cambridge, MA.

- ¹³ Sullivan, T., Hallock, J., Winston, B., McWilliams, I., Burnham, D., "Aircraft Wake Vortex Takeoff Tests at Toronto International Airport," FAA-RD-78-143, Feb. 1979, DOT/Transportation Systems Center, Cambridge, MA.
- ¹⁴ Burnham, D.C., and Hallock, J.N., "Chicago Monostatic Acoustic Vortex Sensing System, Volume II: Decay of B-707 and DC-8 Vortices," FAA-RD-79-103,II, Sept. 1981, DOT/Transportation Systems Center, Cambridge, MA.
- ¹⁵ Burnham, D.C., and Hallock, J.N., "Chicago Monostatic Acoustic Vortex Sensing System, Volume IV: Wake Vortex Decay," FAA-RD-79-103,IV, July 1982, DOT/Transportation Systems Center, Cambridge, MA.
- ¹⁶ Hallock, J.N., "Vortex Advisory System, Volume I: Effectiveness for Selected Airports," FAA-RD-80-62,I, May 1980, DOT/Transportation Systems Center, Cambridge, MA.
- ¹⁷ Hallock, J.N., "Vortex Advisory System Safety Analysis, Volume I: Analytical Model," FAA-RD-78-68,I, Sept. 1978, DOT/Transportation Systems Center, Cambridge, MA.
- ¹⁸ Burnham, D.C., "Effect of Ground Wind Shear on Aircraft Trailing Vortices," AIAA Journal, Vol. 10, No. 8, Aug. 1972, pp. 1114-1115.
- ¹⁹ Eberle, W.R., Brashears, M.R., Zalay, A.D., Shrider, K.R., and Love, D.A., "Aircraft Wake Vortex Characteristics from Data Measured at John F. Kennedy International Airport," FAA-RD-78-47, March 1978, Lockheed Missile & Space Company, Huntsville, AL.